RAPID DIFFUSION OF ZINC IN IRON

BY

JONATHAN S. DOHIE

A thesis submitted to
the Faculty of Graduate Studies
in partial fulfillment of the requirements for
the Degree of

MASTER OF SCIENCE

DEPARTMENT OF MECHANICAL AND MANUFACTURING ENGINEERING
UNIVERSITY OF MANITOBA
WINNIPEG, MANITOBA

THE UNIVERSITY OF MANITOBA

FACULTY OF GRADUATE STUDIES

*****

COPYRIGHT PERMISSION

"Rapid Diffusion of Zinc In Iron"

BY

Jonathan S. Dohie

A Thesis/Practicum submitted to the Faculty of Graduate Studies of The University of Manitoba in partial fulfillment of the requirement of the degree

Of

MASTER OF SCIENCE

ACKNOWLEDGEMENTS

To my advisor: Dr. Jack R. Cahoon,

To the technicians: Mike Boskwick, Don Mardis, Irwin Penner, and John Van Dorp,

To my family and friends,

I thank you.

Without your help and support, this work would have not been done.

ABSTRACT

Using semi-infinite amounts of pure zinc and pure iron as the diffusing media, the zinc diffusion coefficient into iron was experimentally derived at the temperatures of 400°C, 500°C, and 725°C. A new diffusion sampling technique, involving poured liquid metal, was developed for the production of the pure metal diffusion samples. The diffused material was examined for structure and chemistry using a Scanning Electron Microscope and Energy Dispersive X-ray Spectrometer. The zinc concentration gradient in the iron was measured, and the zinc diffusion coefficient was derived by comparing the result from a mathematical model to the experimental data. It was determined that diffusion of zinc in iron is not so-called "anomalous", but rather it follows normal diffusion behaviour in polycrystalline metals in that grain boundary diffusion dominates at temperatures below about 700°C, and bulk lattice diffusion dominates at temperatures above 700°C.

The structure of the pure metal diffusion couples were compared to heat treated commercial galvanized steel. After diffusion with zinc, large amounts of gamma phase particles were found in the grain boundaries of both pure iron and galvanized steel. The gamma phase particles in the grain boundaries caused severe embrittlement effects in the iron and steel.

TABLE OF CONTENTS

LIST OF SYMBOLS

All units used were System International

Units of Length

cm	centimeter, = $1/10^2$ of a meter
mm	millimeter, = $1/10^3$ of a meter
μm	micrometer, = $1/10^6$ of a meter
nm	nanometer, = $1/10^9$ of a meter

Units of Pressure

kPa	kilopascals, one thousand pascals

Units of Energy

kJ/mol	kilojoules per mole

Units of Concentration

at%	atomic percent

Element Symbols

Fe	iron
Zn	zinc
Al	aluminum
Mn	manganese
Si	silicon

Miscellaneous

~	about, approximately
≈	approximately equal to
FCC	face-centered cubic
BCC	body-centered cubic
HCP	hexagonal close-packed
VHN	Vickers Hardness Number
D_{Zn}	zinc diffusion coefficient

Units of Temperature

°C	degrees Celsius
K	degrees Kelvin (°C + 273.15)

Units of Mass

g	gram

Units of Diffusion

m^2/s	square meters per second

Units of Time

1 hour = 60 minutes = 3600 seconds

Greek Letters

ζ	zeta, a Fe-Zn phase
δ	delta, a Fe-Zn phase
δ_k	compact delta phase
δ_p	palisade delta phase
Γ_1	gamma-one, a Fe-Zn phase
Γ	gamma, a Fe-Zn phase
α-Fe	alpha-iron, solid solution of zinc in iron
η-Zn	eta-zinc, solid solution of iron in zinc
ε	epsilon, iron interface shift
Δ	delta, "change in"

LIST OF FIGURES

LIST OF TABLES

Chapter 1

INTRODUCTION

The reason for studying the iron-zinc system lies in the importance of galvanized steel. Galvanizing steel (zinc-coating steel) is one of the most popular methods of protecting steel from corrosion. Currently, steel products account for 90% of all metal usage, and a large portion of those steel products is galvanized to prevent corrosion. Examples of such galvanized steel products include: ductwork, nails, and other home hardware, fencing, highway guardrails, lamp posts, and other urban infrastructure, tension cables, automobile bodies, and high strength steel cables used in suspension bridges. The list of uses of galvanized steel will continue to grow in the coming years. In each of the new products, the limitations and thresholds of galvanized steel will be stretched. It is important to keep studying the iron-zinc system, and to learn all of its characteristics.

In the galvanizing process, liquid zinc is solidified on solid steel (iron) product. When molten zinc comes into contact with iron, interactions occur between the two metals. In the iron-zinc system, four different intermetallic phases exist, and all can form when zinc and steel interact. The iron-zinc intermetallic phases are brittle and their presence can result in the loss of the galvanize layer (zinc layer) during service. Since steel is the load bearing structural material, and zinc is the sacrificial corrosion protector of the steel, loss of the zinc coating can result in corrosion and possible failure of the steel structure. The formation and growth of the brittle intermetallic phases during the galvanizing process is determined by the interdiffusion of zinc and iron. Diffusion studies of the

iron-zinc system are required to understand the reactions that occur during the galvanizing process.

Several previous studies [1, 2, 3, 4] have shown that at temperatures in the range of 300°C to 620°C, zinc diffuses rapidly into iron. Some of the authors of these studies have called this "anomalous" diffusion of zinc in iron [1]. These studies were conducted using ordinary galvanized steel where the zinc layer measured only 0.1 mm thick or less. Other diffusion studies have used iron with zinc vapour sources. In all of these studies, the zinc layer, as well as some of the intermetallic phases, disappeared during the diffusion anneals. As a result, the boundary conditions in these studies were continually changing, therefore making analysis inconclusive.

This present investigation was conducted to study the nature of the diffusion of zinc in iron. It was decided to use semi-infinite amounts of both zinc and iron, which should have kept the boundary conditions essentially constant during the diffusion anneal. The use of large amounts of zinc and iron allowed the use of long diffusion anneals, which allowed the various intermetallic phase layers to become well developed and more readily structured. Polycrystalline iron was used to allow for grain boundary diffusion, should it have occurred to a significant amount. The diffusion studies were conducted at temperatures where the zinc was solid, and at temperatures where the zinc was liquid, to determine if liquid zinc penetration into the iron grain boundaries was a factor in the diffusion of zinc into iron. For the liquid zinc studies, the number of intermetallic phases formed were varied by changing the temperature of the diffusion anneal, which

determined if the nature of the intermetallic phases affected the diffusion of zinc into iron. The other objective of this work was to clarify the nature of the diffusion of zinc into iron during the galvanizing of steel, thus providing a better understanding of the galvanizing process.

For this investigation, diffusion between bulk pure zinc and iron was determined from three experimental temperatures: 400°C (solid Zn-solid Fe), 500°C, and 725°C (both liquid Zn-solid Fe). The diffusion couples were held at these temperatures for 96 hours. For comparison of the diffusion structures, and to check if the same effects occur in commercial product, galvanized steel strips were heat treated at two temperatures: 400°C and 500°C, for 96 hours. In all, a total of 85 experiments were conducted. Many of these, for various reasons, were not suitable for detailed analysis but were useful for perfecting the experimental technique. A review of the experiments performed in this investigation is presented in the documented experiment log in Appendix C.

The structure of the diffusion specimens were analyzed with a variety of optical microscopes and with a JEOL Scanning Electron Microscope (SEM). Composition analysis of the samples was measured with the Energy Dispersive X-ray Spectrometer (EDS) unit on the SEM. The zinc concentration gradient was measured in the bulk pure metal diffusion samples, and the experimental data was then compared with a numerical model to determine the zinc diffusion coefficient in the iron.

Chapter 2

LITERATURE REVIEW

2.1 The Galvanizing and Galvannealing Process

The majority of galvanized steel is produced by a continuous manufacturing process. Steel sheet, plate, or wire is passed through a zinc bath at speeds of up to 200 m/min. The composition of the zinc bath in the galvanizing process is zinc with <0.3 at% aluminum (Al additions are added to form an inhibition layer on the steel to prevent the iron-zinc compounds from forming). The temperature of the zinc bath with this composition is kept between 445-455°C. Zinc baths with different compositions (higher Al concentrations) require different temperatures. After coating, the galvanized product is either cooled by forced air or galvannealed (heated).

For the galvannealing process, galvanized steel is heated at 500°C to produce an alloyed coating made entirely of iron-zinc compounds. Galvannealing is a continuous process; the heating and cooling zones required for galvannealing are placed above the zinc pot. Good coating properties are dependent on the heating rate, hold time and temperature, and cooling rate.

2.2 The Iron-Zinc System

2.2.1 The Iron-Zinc Phase Diagram

The iron-zinc (Fe-Zn) equilibrium phase diagram has changed many times since it was first designed. The most recent iron-zinc phase diagram is that of Raghavan [5] (Figure 2.1), which is very similar to the diagram published by Burton and Perrot [6]. The iron-zinc phase diagram followed in this work is that of Raghavan [5]. Simplifications have been drawn into the phase diagram shown in Figure 2.1: there should be a eutectic or peritectic point, as well as a region for the solid solution of iron in zinc (η-Zn phase). Since these regions are so thin, and so close to 100% zinc, they cannot be drawn on a normal phase diagram. The solid solubility of iron in zinc is ~0.003 at%, so the η-Zn portion of the phase diagram is not depicted in the iron-zinc phase diagram shown in Figure 2.1.

2.2.2 Summary of the Iron-Zinc Phases

In the iron-zinc phase diagram there are six iron-zinc intermetallic phases relevant to this investigation. These phases are: alpha-iron, gamma, gamma-one, delta, zeta, and eta-zinc. A listing of some of the characteristics of these phases is given in Table 2.1. A brief description of the data shown in Table 2.1 is given below.

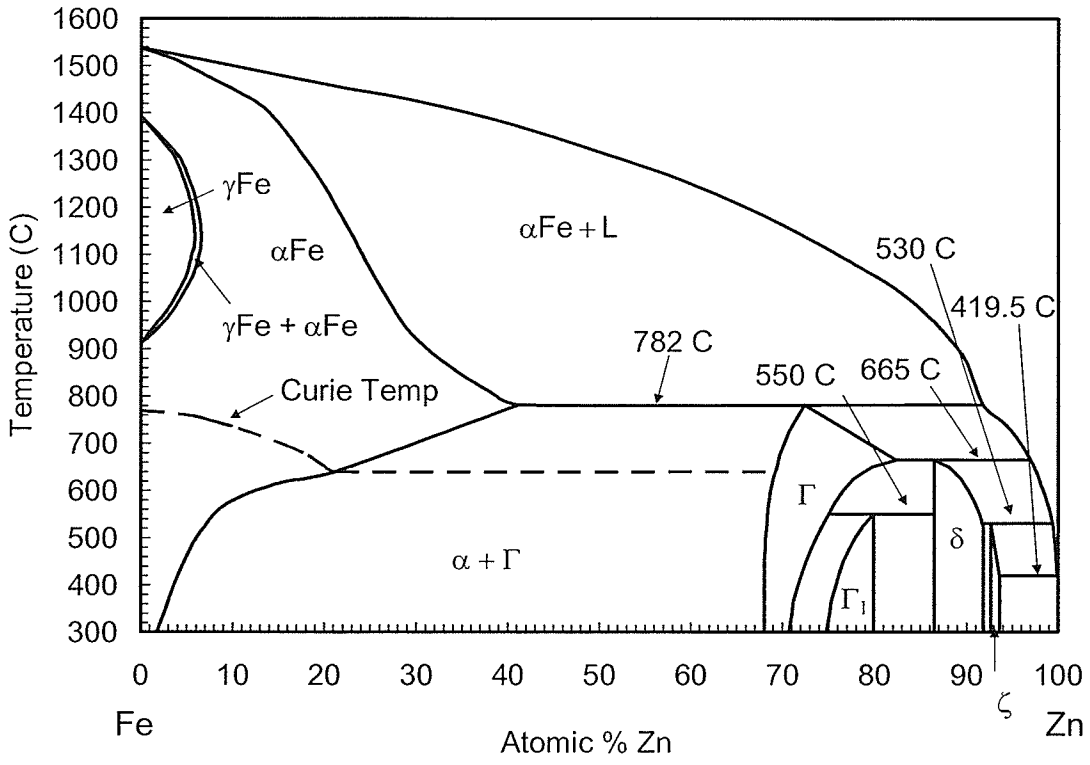

Figure 2.1: The iron-zinc equilibrium phase diagram [5].

Table 2.1: Characteristics and Properties of the Fe-Zn Phases

Phases	Formula [5]	Crystal structure [7]	Fe (at%) (at 450°C)	VHN (25 mg) [7]	VHN (25 g) [7]	ΔH	ΔG (450°C) (kJ/mol) [8]
α-Fe	Fe(Zn)	BCC	95	104	86		
Γ	Fe_3Zn_{10}	BCC	26 - 31.5	326	--	-10.9	-4.2
Γ1	$Fe_{11}Zn_{40}$	FCC	19 - 22	505	--	-11.7	-4.1
δ	$FeZn_{10}$	Hexagonal	8.2 - 13.5	358	273	-11.5	-3.5
ζ	$FeZn_{13}$	Monoclinic	6 - 7.2	208	118	-11.7	-2.8
η-Zn	Zn(Fe)	HCP	<0.003	52	41		

Alpha-Iron phase:

Depicted as α or α-Fe on the phase diagram, this phase is a solid solution of zinc in iron, or Fe(Zn). The alpha-iron phase can have a zinc concentration from 0 at% zinc to ~43 at% zinc, depending on the temperature. At room temperature, the solid solubility of zinc in iron is less than 2 at% zinc. There also occurs a paramagnetic transformation in the α-Fe region, depicted by the large dashed line in the phase diagram. Above this line, the rate of diffusion of zinc into iron is slower [9]. This transformation occurs at 770°C, at 0% zinc (pure iron).

Gamma phase:

Gamma phase (Γ) is the most iron-rich intermetallic found in the iron-zinc system. At 450°C, the composition of Γ phase is 26-31.5 at% iron. The Γ phase is formed by a peritectic reaction between α-Fe and liquid zinc at 782°C. The Γ phase has the same body centered cubic (BCC) crystal structure as α-Fe, but is over 3 times harder. The atomic formula for the Γ intermetallic phase is Fe_3Zn_{10}.

Gamma-one phase:

Reported in 1974 [10], gamma-one phase (Γ_1) is the second-most iron-rich intermetallic in the iron-zinc system. At 450°C, the composition of Γ_1 phase is 19-22 at% iron. The Γ_1 phase is formed by a peritectoid reaction between Γ and δ phases at 550°C. The Γ_1 phase has a face-centered cubic (FCC) crystal structure, and is about 5 times harder than α-Fe. The atomic formula for the Γ_1 intermetallic phase is $Fe_{11}Zn_{40}$.

Delta phase:

Delta phase (δ) is the second-least iron-rich intermetallic in the iron-zinc system. At 450°C, the composition of δ phase is 8.2-13.5 at% iron. The δ phase is formed by a peritectic reaction between Γ phase and liquid zinc at 665°C. The δ phase has a hexagonal crystal structure, and is approximately 3.5 times harder than α-Fe. The atomic formula for the δ intermetallic phase is $FeZn_{10}$. When the iron-zinc interphase is thick and fully developed, the δ phase layer subdivides into two structures: δ_k (compact δ phase) and δ_p (palisade δ phase).

Zeta phase:

Zeta phase (ζ) is the least iron-rich intermetallic in the iron-zinc system. At 450°C, the composition of ζ phase is 6-7.2 at% iron. The ζ phase is formed by a peritectic reaction between δ phase and liquid zinc at 530°C. The ζ phase has a monoclinic crystal structure, and is about 2 times harder than α-Fe. The ζ phase is the most ductile of the iron-zinc intermetallic phases, whereas Γ, Γ_1, and δ phases are brittle. The atomic formula for the ζ intermetallic phase is $FeZn_{13}$.

Eta-Zinc phase:

The eta-zinc phase (η-Zn) is a solid solution of iron in zinc, or Zn(Fe). At temperatures just below the melting point of zinc, the solubility of iron in zinc is less than 0.003 at% iron [6, 11]. Due to the low iron concentration of the η-Zn region, it does not appear in the iron-zinc phase diagram. The ζ – η-Zn two-phase region is shown in the bottom-right corner of the phase diagram in Figure 2.1 and likely involves a eutectic

reaction at about 0.0021 at% iron, about 0.05 K below the melting temperature of zinc [6]. The η-Zn phase has a hexagonal close packed (HCP) crystal structure.

2.2.3 The Iron-Zinc Reaction

When zinc contacts iron, both δ and ζ phases immediately form [7]. After a few seconds, the δ and ζ phases will form a continuous layer on the iron. A continuous layer of Γ phase will form after 30 seconds of contact. By heating the iron-zinc couple at low temperatures for long times, a layer of Γ_1 phase will form. Thus, the sequence of phase formation is: ζ, δ, Γ (after a short time), and Γ_1 (after a long time). At typical galvanizing temperatures (450-490°C), the phases that form are: α-Fe, Γ, Γ_1, δ, ζ, and η-Zn.

Shown in Figure 2.2 is the phase growth with time for an iron-electrodeposited zinc couple heat treated at 410°C. In this couple at 410°C, the ζ and δ phase layers immediately formed, followed by the formation of the Γ and Γ_1 phase layers after a delay. The thickness of the Γ and Γ_1 phase remained constant at 10 μm for very long diffusion times (>9 $\sqrt{h}$). The ζ phase had parabolic growth with time (shown by the straight line between 0 $\sqrt{h}$ and 6 $\sqrt{h}$), before levelling off at 7 $\sqrt{h}$ to a constant thickness of ~150 μm. The δ phase growth had two regimes: rapid growth followed by a levelling off (due to the compact δ phase growth, δ_k, achieving maximum thickness), and then rapid growth of the palisade δ phase (δ_p) for times greater than $6\sqrt{h}$. The growth of the two δ phase structures created an inflection point in the chart (the inflection point of the δ phase growth at

410°C occurred between 5-6 √h). Consequently, an inflection point was also formed in the total phase growth.

Each iron-zinc intermetallic phase has different growth characteristics depending on the temperature. At 450°C, ζ phase first grows rapidly, and then slows down, while δ phase first grows slowly, then rapidly. The Γ and Γ_1 layers grow only after long periods of time. Overall, the Γ and Γ_1 phases grow inward toward the iron, and the ζ phase is shifted outwards into the liquid zinc [12]. As the Γ and Γ_1 phases grow towards the iron, it is consumed by δ phase (therefore keeping the thickness of the Γ and Γ_1 phases constant at ~1 μm thick). The δ phase also consumes the ζ phase at the elevated temperature. The ζ phase is also consumed by the δ phase while cooling [13].

For short diffusion times, ζ phase dominates the intermetallic layer morphology [7]. For longer diffusion times, the δ phase dominates the layer morphology. With increasing temperature, the ζ phase thickness decreases, until at 500°C it no longer exists. With increasing temperature the δ phase grows parabolically until a maximum thickness is attained. This thickness is maintained, as outer portions break away, up to 665°C, when δ phase is no longer stable.

The formation of cracks in the intermetallic layer on the iron is another important feature of the iron-zinc system. The cracks run roughly parallel to the direction of diffusion (perpendicular to the iron interface). The cracks form in the δ phase layer, and extend to the ζ phase layer above, and to the Γ and Γ_1 phase layer below [7]. The cause of the

cracks is stress induced by the transformation of ζ phase into δ phase [14]. Cracks also occur at the ζ – η-Zn interface [10]. The interfacial cracks form from long diffusion times of iron-zinc couples (7 hours), when the Γ_1 phase grows. On further annealing of the resulting iron – ζ phase couple, the Γ and Γ_1 phase layers grow at the expense of the ζ phase layer.

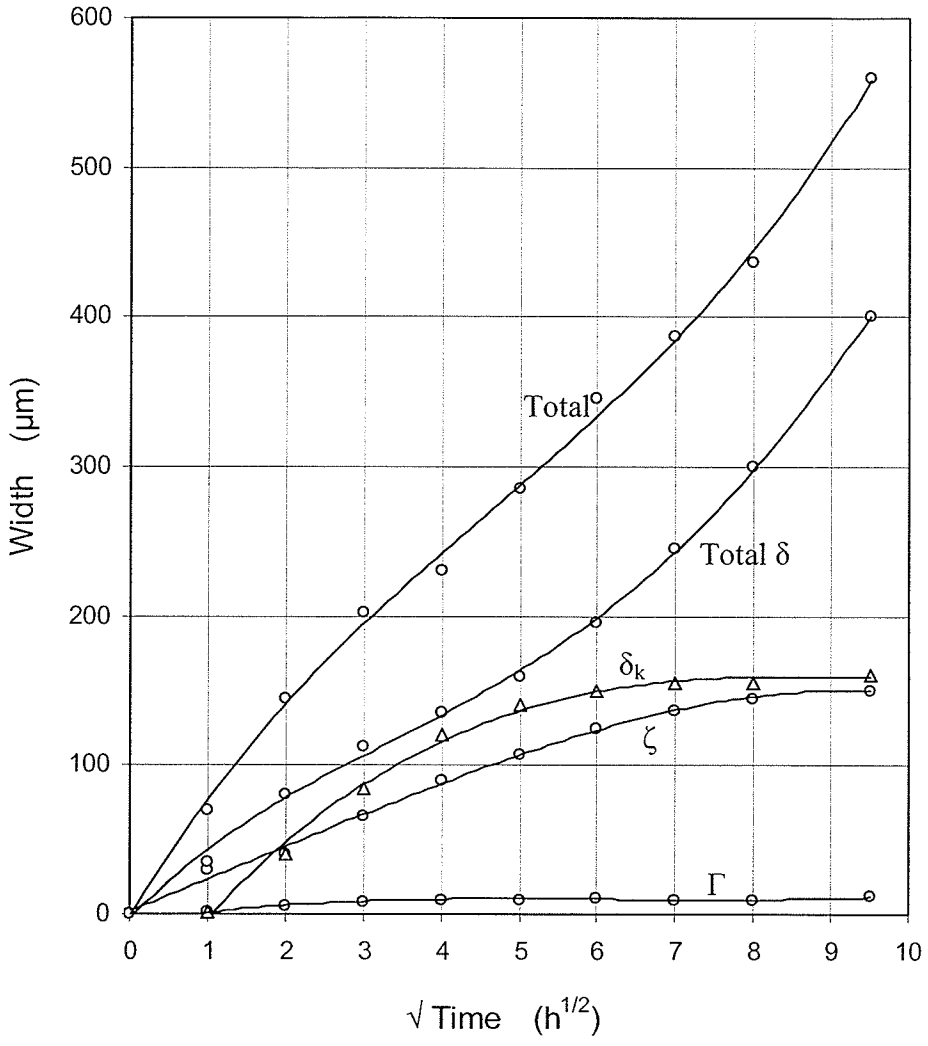

Figure 2.2: Width of the ζ, Γ, compact δ, total δ, and of the total phase layers vs. the square root of annealing time. Fe-electrodeposited Zn diffusion couples were annealed at 410°C (reproduced from Onishi et al. [12]).

2.3 Diffusion in the Iron-Zinc System

Most of the few studies on the interdiffusion in the iron-zinc system deal with Diffusion Induced Grain Boundary Migration (or DIGM – to be covered in the next section). The other studies investigated the behaviour of the iron-zinc reaction; however, some important information about the diffusion between iron and zinc can be obtained in all of these studies.

From the phase growth charts produced by Onishi et al. [12], the relative growth of the intermetallic phases was found to be similar between the temperatures of 300°C and 410°C. Based on the structures formed, if rapid grain boundary diffusion of zinc in iron occurs at 400°C, then it is certain to occur at temperatures as low as 300°C. It is important to note, however, that the work produced by Onishi et al. was from discs of pure iron (10 mm diameter by 2 mm height) electrodeposited with 700 μm of pure zinc. Since the specimens used by Onishi et al. will be the most like the specimens used in this investigation, the results obtained in this work should be similar.

Hillert and Purdy [2], in their work with DIGM, found in a sample produced at 580°C for 3 hours that zinc permeated into the iron almost entirely by grain boundary diffusion coupled with grain boundary sweeping. This same effect was also found in samples held at 600°C for 4 hours. In similar DIGM work done by Chongmo and Hillert [3], the same effect was found in samples that were produced at temperatures between 460°C and 780°C. Though both sets of researchers found evidence of rapid zinc diffusion (via grain

boundaries) across a range of temperatures, the sample technique used in both studies was solid iron – vapourized zinc. Hillert and Purdy used thin pure iron discs (3 mm diameter by up to 100 μm thick) that were sealed with a zinc vapour source. The samples used by Chongmo and Hillert were strips of pure iron foil (0.127 μm thick) sealed with a zinc vapour source.

The diffusion coefficient of zinc in BCC iron has been measured by Richter and Feller-Kniepmeier [9] between 575°C and 894°C. To determine the zinc diffusion coefficient in iron, Richter et al. used sections of single crystals of pure iron sealed with a zinc vapour source. Since the iron sample used was a single crystal (single crystals contain no grain boundaries), the work by Richter et al. measured the lattice diffusion coefficient of zinc in iron. Figure 2.3 is a plot of the zinc diffusion coefficients produced by Richter et al., in a chart of the logarithmic of D_{Zn} ($\log D_{Zn}$) versus the inverse of the temperature (1/T). From Figure 2.3, the diffusion coefficient of zinc in iron is shown to exponentially increase with temperature, and with zinc concentration in the iron. Figure 2.3 also shows the effect of the paramagnetic transformation in α-Fe: zinc diffusion decreases with the transformation (which occurs at a temperature greater than 770°C – the paramagnetic transformation temperature, or Curie temperature).

Work done on DIGM by Yu and Shewmon [4] found results that agreed with Hillert and Purdy [2]. They found the same effect with decarburized steel sheet, and high purity iron foils. The samples used by Yu et al. were similar to Hillert et al. [2] and Chongmo et al. [3]; 50 μm thick strips of decarburized steel, 50 μm thick strips of pure iron, and 10 mm

cubes of decarburized bulk steel sealed with a zinc vapour source were used, and were annealed at temperatures of 550°C – 630°C for varying times. The bulk steel samples did not show any effects of DIGM. It appears that grain boundary migration only occurs in very thin diffusion samples.

Other work by Shewmon et al. [1] studied the "anomalously" fast diffusion of zinc in iron. Shewmon et al. used samples of 0.6 mm thick galvanized steel heated at either 450°C for 12 to 196 hours, or 550°C for 3 to 192 hours. In samples annealed at 550°C for 12 hours, zinc concentration gradients were found that resembled "square waves". Due to the "square wave" shape of the zinc concentration gradient found in the strips of annealed galvanized steel, Shewmon et al. suggested that the D_{Zn} varied with zinc concentration in the iron, with D_{Zn} rapidly decreasing with a decrease in zinc concentration.

Shewmon et al. [1] also found in the annealed galvanized steel that the depth of zinc penetration was at least 10^2 times greater than that provided by lattice diffusion (using D_{Zn} values extrapolated from Richter et al. – Figure 2.3). Subsequently, by using the formula $x = 2*(D_{Zn}*t)^{0.5}$ (where x = penetration depth, D_{Zn} = the zinc diffusion coefficient, and t = diffusion time), the inherent zinc diffusivity in the samples was calculated to be 10^4 times greater than the lattice diffusivity. In these samples, it was also found that the diffusion of zinc occurred in an initial surge, and then finished in 48 hours at 450°C, and 12 hours at 550°C. Shewmon et al. concluded that the accelerated penetration (anomalously fast diffusion of zinc in iron) was probably due to DIGM.

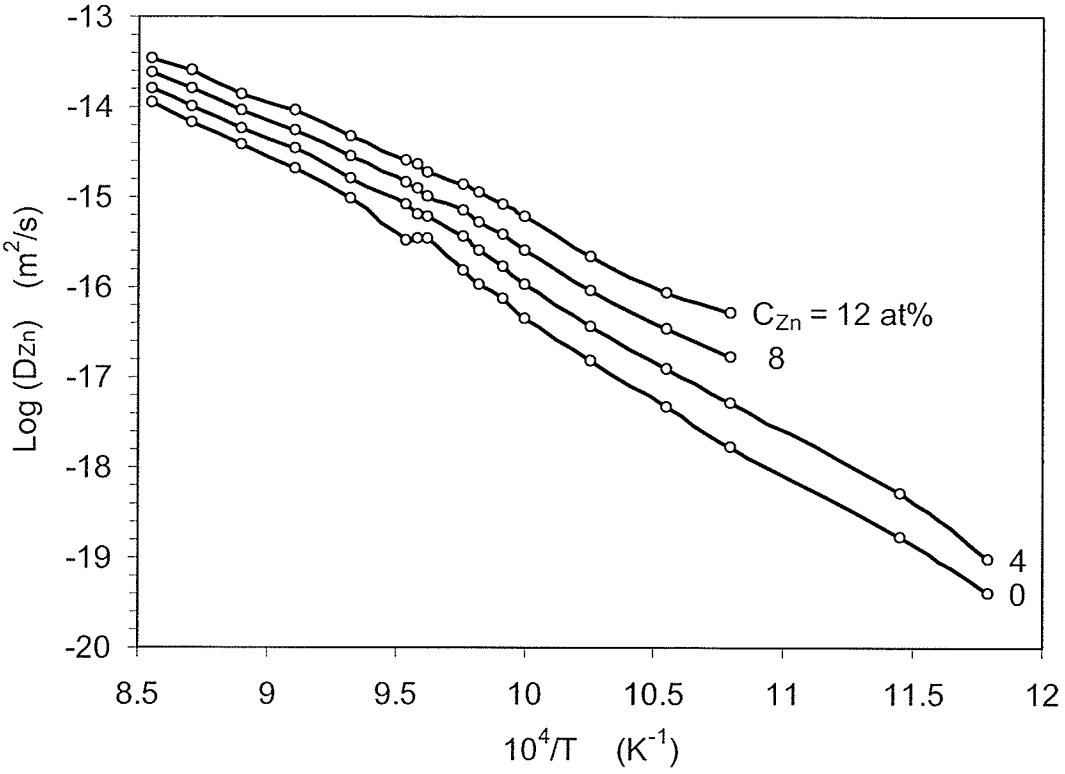

Figure 2.3: Arrhenius plots for zinc diffusion coefficients in iron (reproduced from Richter et al. [9]).

2.3.1 Principal Diffuser in the Iron-Zinc System

There is debate as to which metal is the principal diffuser in the iron-zinc system. Marder has stated that all phase transformations are governed by zinc diffusion into iron [7]. Marder also claimed that the iron diffuses outward into the zinc melt, but at a much slower rate than the zinc into the iron. These conclusions are backed up by results of Onishi et al. [12], in which Kirkendall marker shifts were analyzed. The markers were always found between ζ phase and η-Zn, which would mean that zinc is the principal diffuser.

This is in opposition to the earliest work with the iron-zinc system, by Rigg, who stated that iron is the principal diffuser [15]. This was also claimed in more recent work by Syahbuddin et al., that iron is the principal diffuser during early stages of diffusion [16]. This was based on the fact that ζ is the first phase to form, and not Γ phase. If zinc is the dominant diffuser, Γ phase would form first. Due to this ongoing debate, there needs to be more study and research into the iron-zinc system.

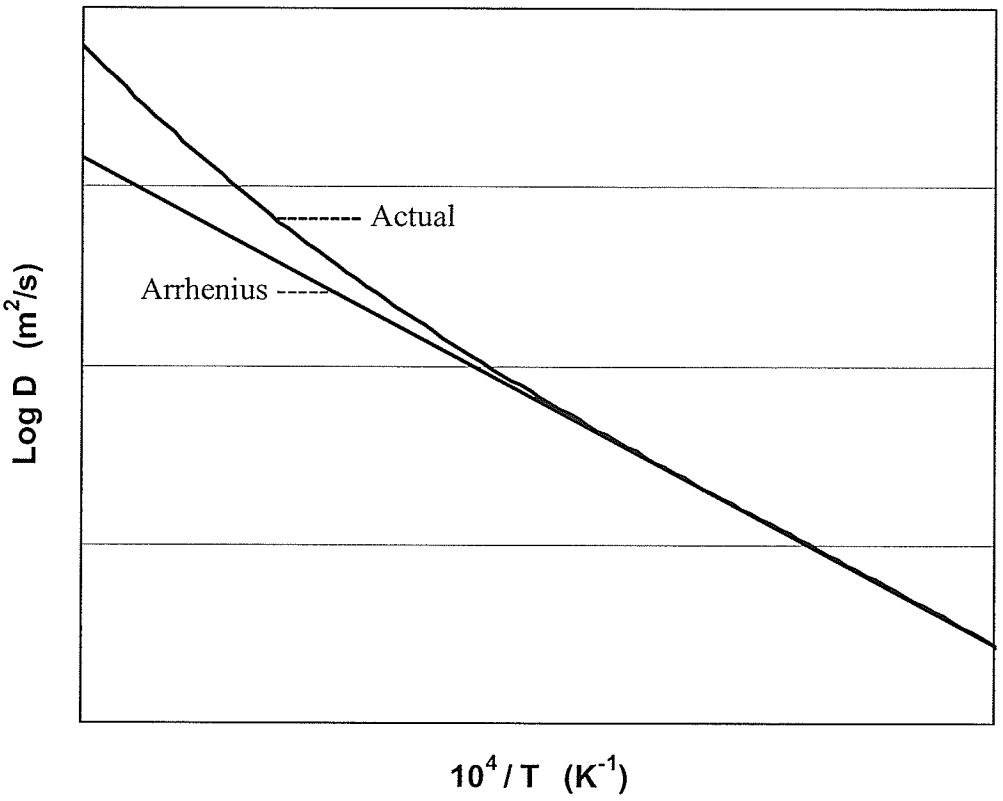

Figure 2.4: Arrhenius and actual relationship between the logarithmic of the diffusion coefficient and the inverse of temperature.

2.4 Mechanisms of Diffusion

2.4.1 Lattice Diffusion

Since iron and zinc have similar atomic radii (Fe: 0.124 nm, Zn: 0.133 nm), and ionic radii (Fe^{++}: 0.077 nm, Zn^{++}: 0.074 nm), it will be assumed for this investigation that lattice diffusion between the two materials is via a vacancy mechanism. It is unlikely that interstitial, interstialcy, or crowdian diffusion mechanisms contribute significantly to the lattice diffusion process. The lattice diffusion of zinc into iron follows the Arrhenius equation – Eq. (1.1).

(1.1) $$D = D_0 e^{-Q/RT}$$

Where: D = the diffusion coefficient (m^2/s)
Q = the activation energy (kJ/mol)
D_0 = the frequency factor (m^2/s)
R = the gas constant (8.31451 $kJ*K^{-1}/mol$)
T = temperature (K)

The activation energy and the frequency factor are material dependent constants in the Arrhenius equation, whereas the temperature is the only variable. From Eq. (1.1), the diffusion coefficient is temperature dependent; as the temperature increases, the diffusion coefficient exponentially increases. When the logarithmic of the diffusion coefficient (log D) is plotted versus the inverse of the temperature (1/T), the Arrhenius equation forms a straight line (shown in Figure 2.4). In the actual diffusion relationship, there exists a slight upwards curvature in the Arrhenius plot, which is caused by divacancy

formation in the crystal lattice (shown in Figure 2.4). The coupled vacancies, which exist in higher concentrations at higher temperatures, allow for faster movement of atoms, therefore faster diffusion, hence larger diffusion coefficients, and thus the curvature of the Arrhenius plot. The paramagnetic-ferromagnetic transformation in α-Fe will also affect the rate of zinc diffusion [17]. This transition occurs at 770°C in pure α-Fe.

2.4.2 Grain Boundary Diffusion

Grain boundaries are planar defects, usually ~0.5 nm thick [18], which occur between two adjoining crystal lattices. The grain boundary is slightly less dense than the crystal lattice, due to the excess volume in the boundary. The grain boundary is an ordered structure (though less so than the bulk metal) and therefore vacancies and interstitials can exist (the point defects have lower formation energy in the boundary than in the lattice).

The rapid atomic jumping along the grain boundaries in metals is by a vacancy mechanism (the formation energy for diffusion by an interstitial mechanism is too high [19]). The interstitial atoms are too difficult to from, and since there is only a single low energy interstitial site in the grain boundary structure, the interstitial atom will migrate to that particular site and get trapped [18]. Diffusion then cannot occur via an interstitial mechanism, and therefore atoms must move in the grain boundary solely by a vacancy mechanism.

In multicrystalline metals, diffusion is much faster along grain boundaries than through the crystal lattice. Grain boundary diffusion is most notable at temperatures much less than the melting point of the solvent. The effect of grain boundary diffusion is shown in the Arrhenius plot in Figure 2.5, which charts the relationship between the logarithmic of the diffusion coefficient (log D) and the temperature relative to the solvent metal melting temperature (T_m / T). From Figure 2.5, the average data for diffusion in a face-centered cubic lattice (FCC lattice) is much lower than the average data for the grain boundary diffusion in FCC metals (FCC – grain boundaries). At a temperature of half the melting temperature in an FCC metal (T_m / T = 2.0), the grain boundary diffusion coefficient is 10^7 times greater than the lattice diffusion coefficient.

The grain boundary diffusion in body-centered cubic metals (BCC – grain boundaries) is similar to the grain boundary diffusion in FCC metals (FCC – grain boundaries). The relationship between log D and T_m / T is similar, with the diffusion coefficient in BCC metals approximately an order of magnitude less than in the FCC metals. It is expected that a similar relationship exists between BCC lattice diffusion and FCC lattice diffusion, and that there is the same large orders of magnitude difference between BCC grain boundary diffusion and BCC lattice diffusion. It is assumed that these relationships all hold for zinc diffusion in BCC α-Fe.

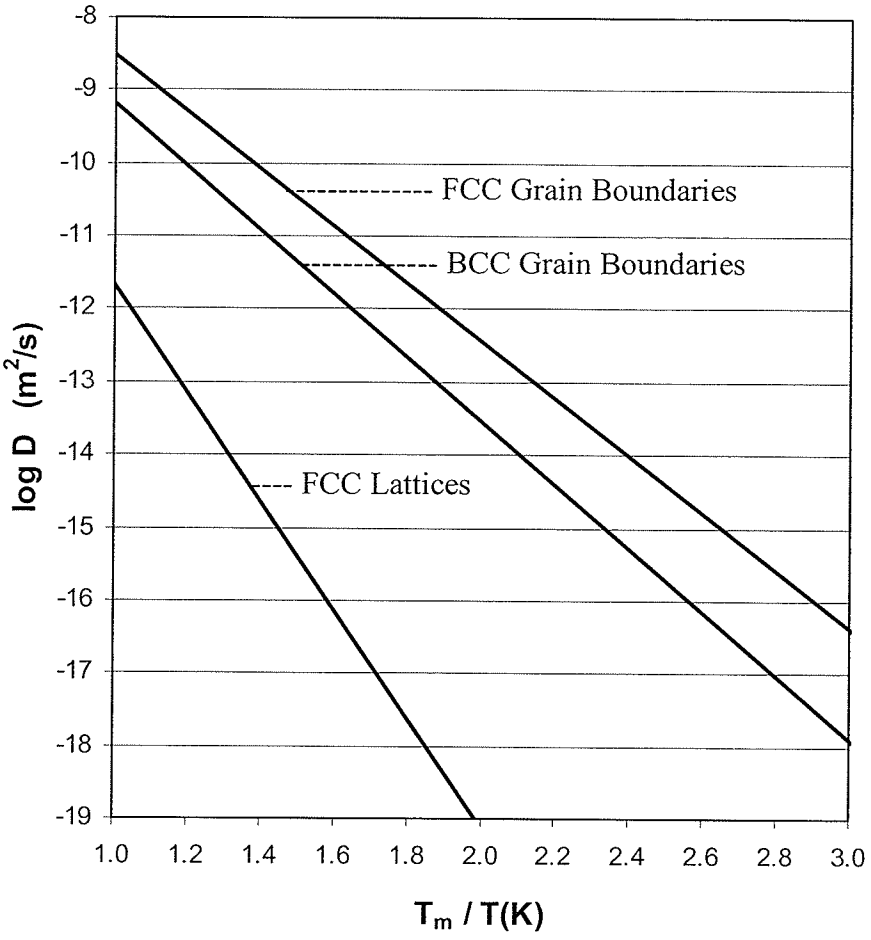

Figure 2.5: Diffusivity spectrum for metals (reproduced from Balluffi [19]). Curves represent averaged data, and a reduced reciprocal temperature scale is used in an effort to normalize the data.

It has been claimed that diffusion along a moving boundary is much faster than along stationary boundaries. Hillert and Purdy concluded that diffusion along migrating boundaries is 10^4 times greater than along stationary boundaries [2]. Other researchers have found that D_0 is 10^4 times larger and Q is 50% greater for moving boundaries. Peterson has stated that this data is not trustworthy since: i) the results were compared between impurity diffusion in a moving boundary to self-diffusion in a stationary boundary in a pure metal, and ii) the researchers didn't state the boundary type [18]. In addition, other researchers have found results that contradict the claim that grain boundary diffusion is faster along migrating boundaries than along stationary boundaries. It is unlikely that diffusion rates are orders of magnitude greater along a moving grain boundary than along a stationary grain boundary [19].

2.4.3 Diffusion Induced Grain Boundary Migration

In steep concentration gradients, diffusion along grain boundaries can cause the boundaries to move, and to cause the formation and growth of new grains. When the boundary moves, it leaves behind a solute enriched layer [17]. This mechanism is called diffusion induced grain boundary migration, or DIGM. Large amounts of solute can be swept behind the boundary, producing a higher solute concentration in the solvent than would be found with both lattice and grain boundary diffusion. The increased amount of solute transported in the metal will greatly increase the diffusion coefficient. DIGM is most evident at lower temperatures, but can occur at temperatures up to the melting point.

Diffusion induced grain boundary migration has been observed in all binary alloys where it has been studied. One of the systems that easily shows DIGM is the iron-zinc binary alloy system; consequently there have been numerous studies of DIGM in this system [2, 3, 4, 20, 21, 22]. Thin iron or steel sheet (~50 μm thick), exposed to zinc vapour at temperatures of 350-800°C, will show the effects of DIGM [4].

Most of the studies of DIGM in the iron-zinc system concerned the effect seen in thin foils (DIGM is most noticeable in thin foil). Bulk samples of iron do not show DIGM [4]. Thick samples of iron do not undergo DIGM because the grains in the interior anchor the grains at the surface that would have moved [21]. DIGM appears only at the edges of thick samples because of the lack of constraint in the grains. Thus, it will be assumed that DIGM does not occur, or has negligible effect, in the bulk iron samples used in this investigation.

Chapter 3

EXPERIMENTAL PROCEDURE

3.1 Materials

The materials used for the solid-liquid diffusion couple experiments were the following.

1) Iron (99.95% pure), obtained from Electronic Space Products International (ESPI) in the form of a 3.175 mm diameter, 610 mm long rod.
2) Zinc (99.99% pure), obtained from Alfa Aesar in the form of 8 mm diameter, 2 mm thick pellets.

Galvanized steel specimens were obtained from a commercial sheet, which was 0.7 mm thick. Using the EDS unit on the SEM, the composition of the steel was measured to be:

Fe	99.23 at%
Mn	0.45 at%
Si	0.33 at%

There was also some carbon present, but this was not analyzed.

Likewise, the composition of the zinc coating on the steel was measured to be:

Zn	98.32 at%
Fe	1.14 at%
Al	0.55 at%

In the as-received condition, no interdiffusion between the iron and the zinc could be measured and was therefore considered negligible.

Tapered alumina crucibles were used for all solid-liquid diffusion experiments. The alumina crucibles (99% pure) were obtained from Almath Crucibles Ltd. The dimensions of the crucible (designation code TW36) were: 36 mm outer diameter (max), 29 mm inner diameter (max), and 45 mm in height.

Ceramic iron specimen holders were machined from 25.4 mm diameter machineable ceramic rod, obtained from Cotronics Corporation. The composition of the machineable ceramic was alumina silicate (Rescor 902 trade name). The iron holders were required in the experiments since they held the diffusing face of the iron rod upwards, and allowed only uni-directional diffusion by preventing zinc from contacting the other surfaces of the iron rod. An iron holder had to be machined for each sample since it was later destroyed during sample sectioning. The iron holders were precisely machined to fit the bottom of the TW36 crucible. The holders were machined dry, to avoid adding more water to the already wet machineable ceramic. After machining, the iron holders were baked at 700˚C for 48 hours to eliminate the trapped water. A ceramic iron specimen holder is shown in Figure 3.1, and a crucible with the metal samples and a ceramic holder is shown in Figure 3.2.

3.2 Iron Preparation

For use in the iron-zinc diffusion couple experiments, segments of iron 9 mm long were cut off the rod stock. It was determined that a 9 mm long segment of iron would provide conditions for a semi-infinite diffusion couple, where the boundary conditions would

remain the same. To avoid cold working the iron, and changing the microstructure, the iron rod was cut by using a Hansvedt Electro-Discharge Machine (EDM). After the iron rod was cut, the segments were pre-heat treated, prior to the diffusion anneal.

For pre-heat treatment, four 9 mm long iron rod segments were placed two abreast in a machineable alumina crucible (Figure 3.3). A machineable alumina lid was placed over top, to contain the iron rod segments. The white, coffin-like assembly was then wrapped in tool steel to reduce oxidation during heat treatment. The pre-heat treatment process consisted of heating this assembly in a box furnace (air atmosphere) at 725°C for 90 minutes, followed by air cooling. The pre-heat treatment process standardized the iron segments, as the microstructural effects of solidification and/or forming were eliminated. The elongated grain structure in the as-received material was changed to an equiaxed grain structure with grain size of 13 ± 3 μm (Figure 3.4). This small grain size was desirable since it would accentuate any grain boundary diffusion of zinc in iron.

A heat treated iron rod segment was first ultrasonically cleaned in ethanol to remove any loose iron oxide and other dirt. One end of the iron segment was then sanded and polished to 600 grit silicon carbide (SiC) paper. After sanding and polishing, no more than 1 mm was removed from the original 9 mm length. The iron oxide on the other surfaces was kept intact, to serve as a barrier to zinc diffusion. The iron segment was then lightly forced into the center hole of the iron holder, with the exposed metal end protruded 1 mm above the top face of the holder.

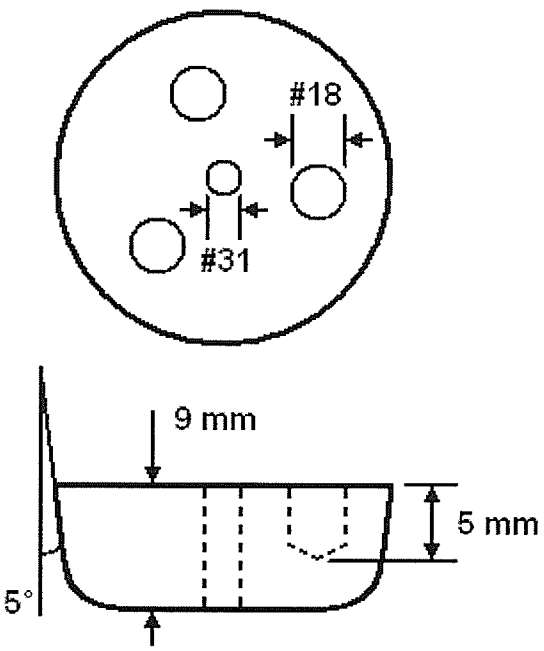

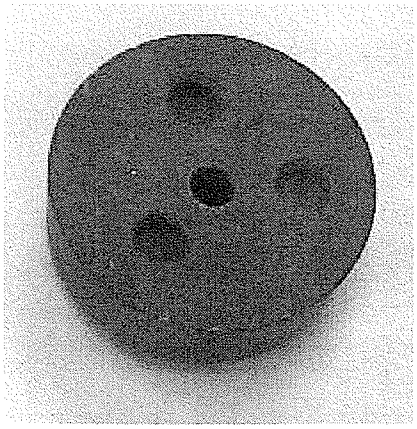

1) The top face of the holder was ground to 320 grit SiC paper.
2) #31 bit: 3.05 mm diameter.
3) #18 bit: 4.305 mm diameter.

Figure 3.1: Schematic of the machineable ceramic iron holder. The iron holder was machined so that there was a 1 mm space next to the crucible wall (there was no set diameter). The bottom edge was hand ground (in the lathe) to fit the bottom of the TW36 crucible.

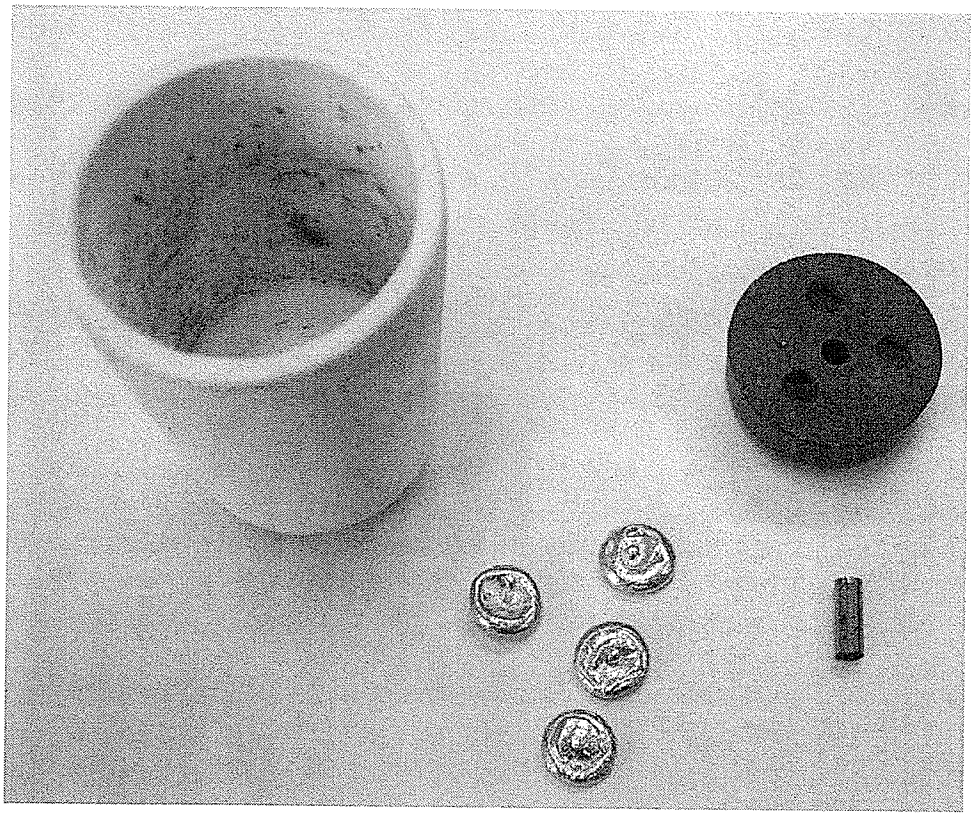

Figure 3.2: Pure metal sample material. Clockwise from top left: TW36 alumina crucible, machineable ceramic iron holder, 99.95% pure iron rod segment, and 99.99% pure zinc shot.

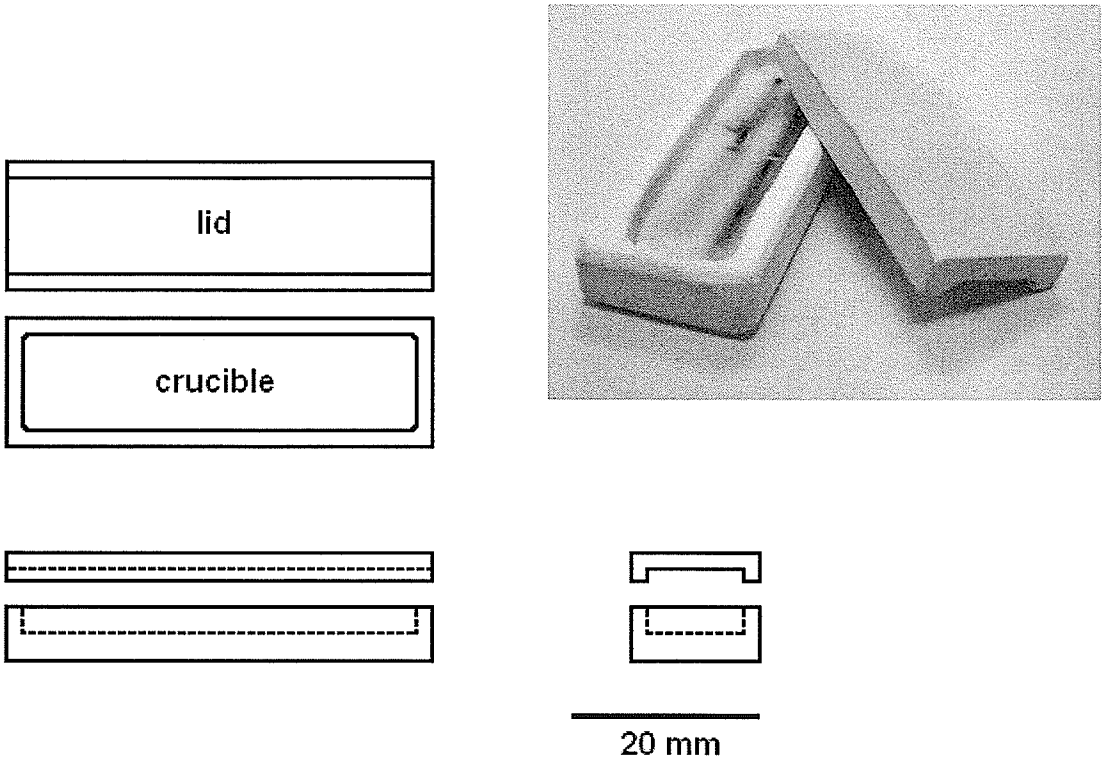

Figure 3.3: Machineable alumina crucible and lid.

(a)

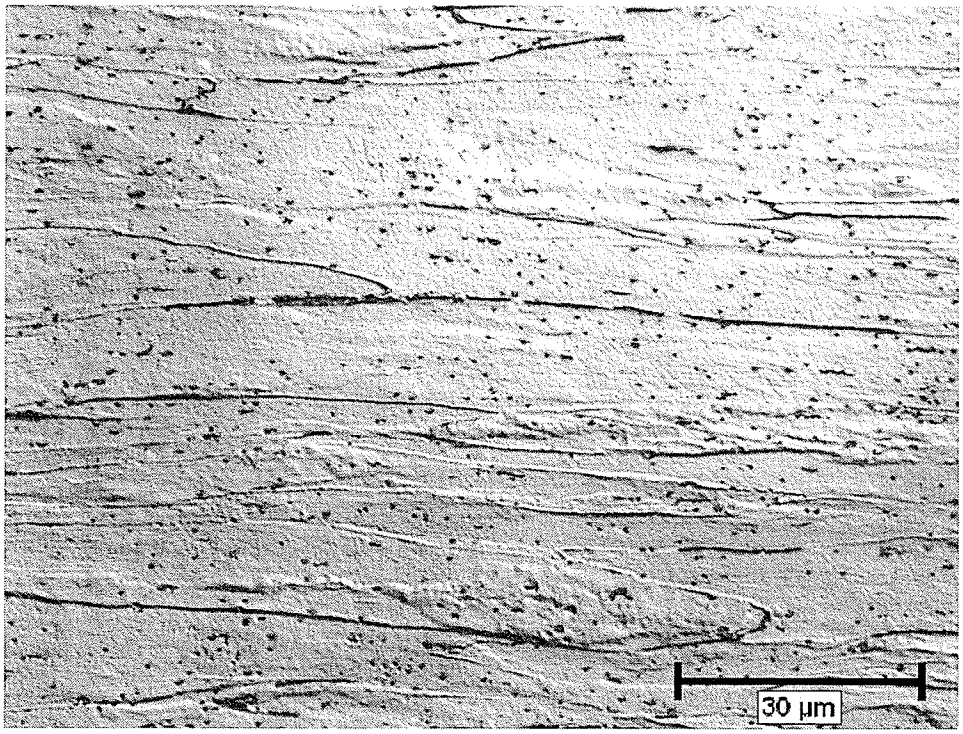

(b)

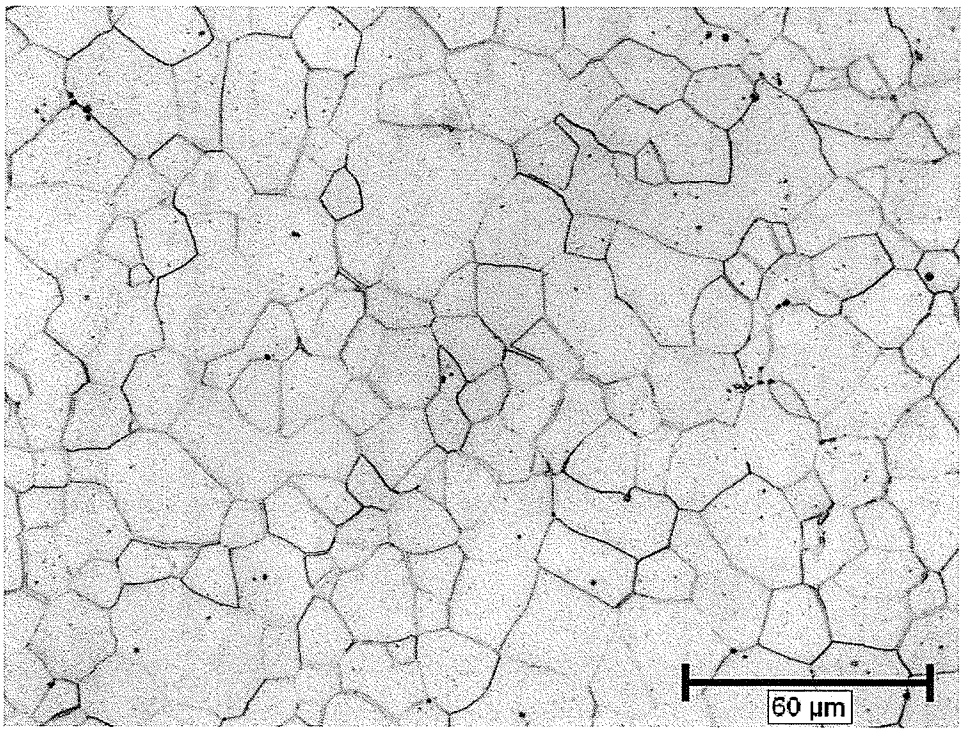

Figure 3.4: Grain size of the pure iron; (a) before pre-heat treatment (*Mag 1000x*), (b) after pre-heat treatment (*Mag 500x*).

3.3 The Pure Metal Diffusion Methods

Two methods were employed for the production of the iron-zinc diffusion couple samples: the vacuum chamber method, and the poured liquid metal method. The vacuum chamber method comprised of placing the iron specimen and holder at the bottom of the TW36 crucible, with the zinc pellets poured over it (about 80-90 g), filling the crucible to the top. The sample crucible was then lowered into the vacuum chamber, and the vacuum chamber was sealed, evacuated, flushed with argon 10 times, and left with 34 kPa argon pressure.

The loaded chamber was then placed in a vertical furnace, and heated at 725°C for 3 hours (in order to liquefy the zinc and make contact with the iron). The chamber was then cooled down to the diffusion experiment temperature, and held for 96 hours. The chamber was then air cooled, the sample crucible extracted, and the sample / ingot removed from the crucible. The equipment used for the vacuum chamber method is shown in Figure 3.5. The results from using the vacuum chamber method were inconsistent and therefore the poured liquid zinc method was developed.

Poured liquid metal method

The poured liquid zinc method involved melting 90-110 g of zinc pellets in a crucible pre-heated to 525°C in a pot furnace, under an atmosphere of flowing argon. Once the zinc was molten, the room temperature iron holder was dropped into the pre-heated, empty, TW36 crucible. The molten zinc was then immediately poured over top the iron

holder, and the crucible was filled up to 1-2 mm from the rim (~70-90 g of zinc). The lid to the furnace was re-placed, and the assembled sample was held at 525°C for 15 minutes to allow for proper contact between the iron and zinc (a lower melt temperature / shorter heating time might be adequate for proper contact between the zinc and the iron, but testing would be required to determine these).

The sample was then removed from the pot furnace, the zinc was solidified (for samples performed at 400°C), and the sample crucible was placed into a pre-heated box furnace (air atmosphere) at the experiment temperature (400°C, 500°C, or 725°C). The sample was then held at the experiment temperature for 96 hours, then removed from the furnace and air cooled. The pot furnace used for the poured liquid zinc technique is shown in Figure 3.6 (with the TW36 crucible), and a resultant specimen shown in Figure 3.7.

It was deemed that at least 50 g of zinc would provide a situation for a semi-infinite diffusion couple, where the boundary conditions would remain the same during the diffusion anneal. An extra amount of zinc shot (40-60 g) was melted for each sample in order to fill the TW36 crucible, and to allow for error, oxidation, and residual zinc in the melting pot. In addition, it was calculated that at least 50 g of zinc was required to counteract the buoyancy force of the machineable ceramic iron holder. A buoyancy force was created because the lighter density machineable ceramic holder was designed to sit at the bottom of the crucible, underneath the higher density molten zinc pool. The actual mass of zinc required was ~20 g, but a factor of safety of 2 to 4 times was employed.

As long as the zinc pool remained above the iron holder, the mass of the zinc pool would force the iron holder to the bottom of the crucible.

3.4 Sample Sectioning

Once out of the crucible, the whole sample/ingot was cut by being placed end-to-end in a vise (to compress the diffusion zone). Once in the vise, a hacksaw was used to cut the zinc casting off of the diffusion zone (Figure 3.8a). The cutting line was made 5-6 mm above the top face of the iron holder. Holding the diffusion zone end-to-end in the vise, the hacksaw was then used to bisect the sample, the cutting line made about 1 mm offset from the iron center hole (Figure 3.8b). The sample was then flipped 180°, and the back portion was cut off (the cutting line was about 2 mm from the iron center hole).

The front cut surface was then faced on a water-cleaned disc grinder until a 1 mm wide rectangle of iron appeared (Figure 3.8c). The sample was then re-clamped, and 5 mm were cut off the left and right sides. At this point, the sample was in the shape of a cube with dimensions of about 15 mm tall by 6 mm thick by 13 mm wide, with the length of the iron rod oriented to the tall axis. The sample was then re-clamped from the iron-end to the zinc-end, and the remnants of the machineable ceramic holder were carefully chiselled away. It was important to remove all of the machineable ceramic, otherwise it would break out while polishing, and ruin the finish of the specimen. The all-metal diffusion zone was then placed in the bakelite mount mold, with the flattened, cut surface of the iron facedown.

3.5 Mounting and Polishing

The pure metal diffusion samples were mounted in bakelite, forming a mount that was 31.8 mm in diameter and ~15 mm in height. The mounted sample was then carefully ground on a water-cleaned disc grinder (180 grit silicon carbide disc) until 3 mm of the diameter of the iron rod was revealed (Figure 3.8d). The sample was then polished through a gradually finer series of silicon carbide papers (220, 320, 400, 600), and then fine polished using colloidal diamond paste on a cloth wheel (6 μm, then 1 μm). After the 1 μm polishing wheel, the cross-section surface of the sample was ready for optical and SEM examination.

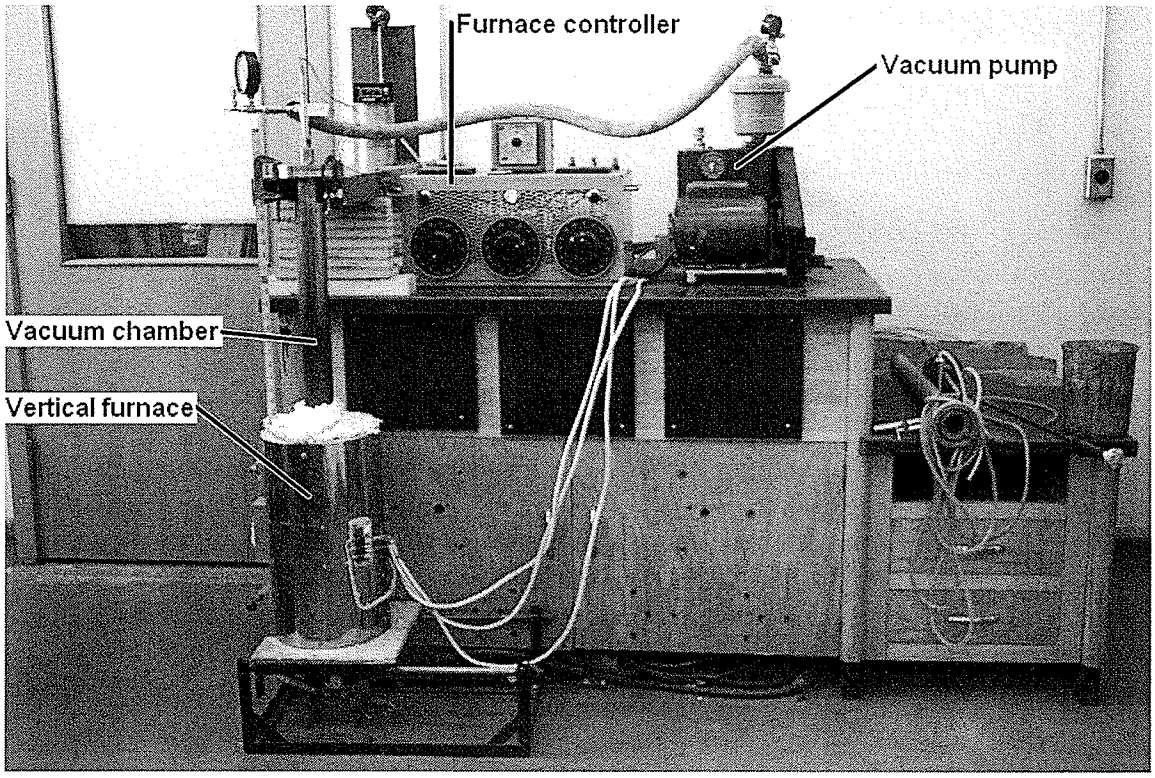

Figure 3.5: Vacuum chamber apparatus.

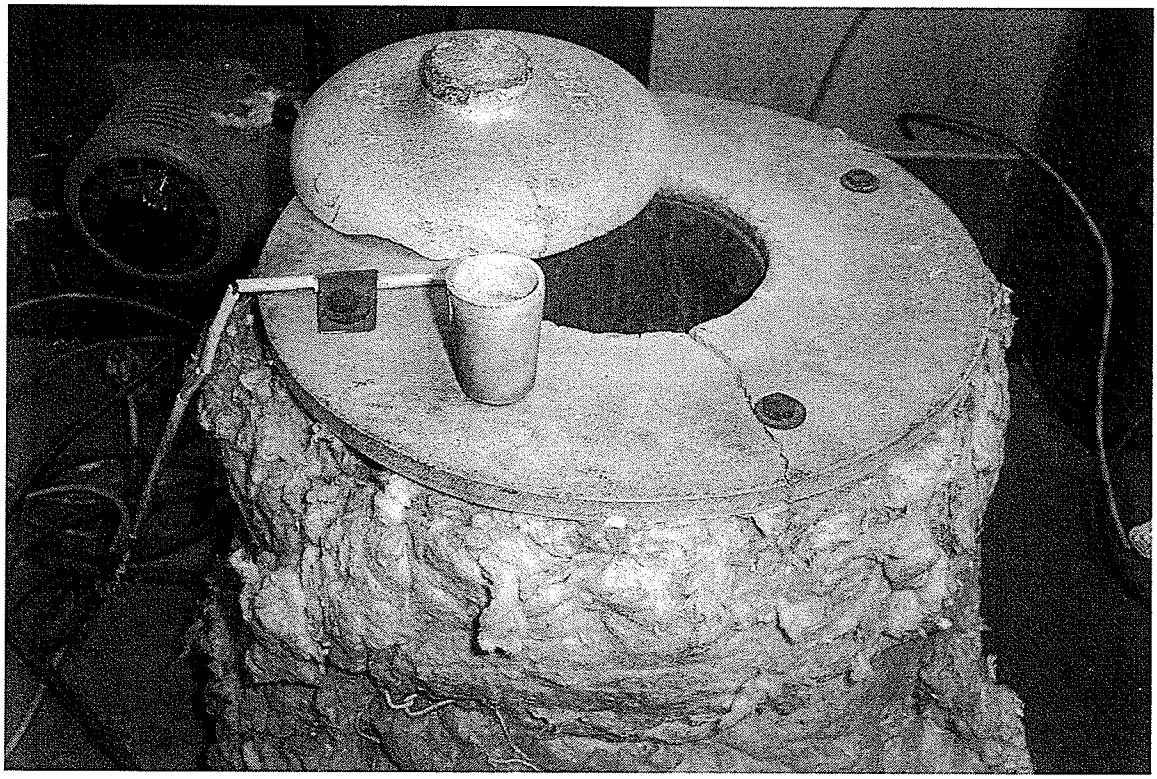

Figure 3.6: Pot furnace (with the TW36 crucible).

Figure 3.7: Poured liquid zinc sample, as removed from the TW36 crucible.

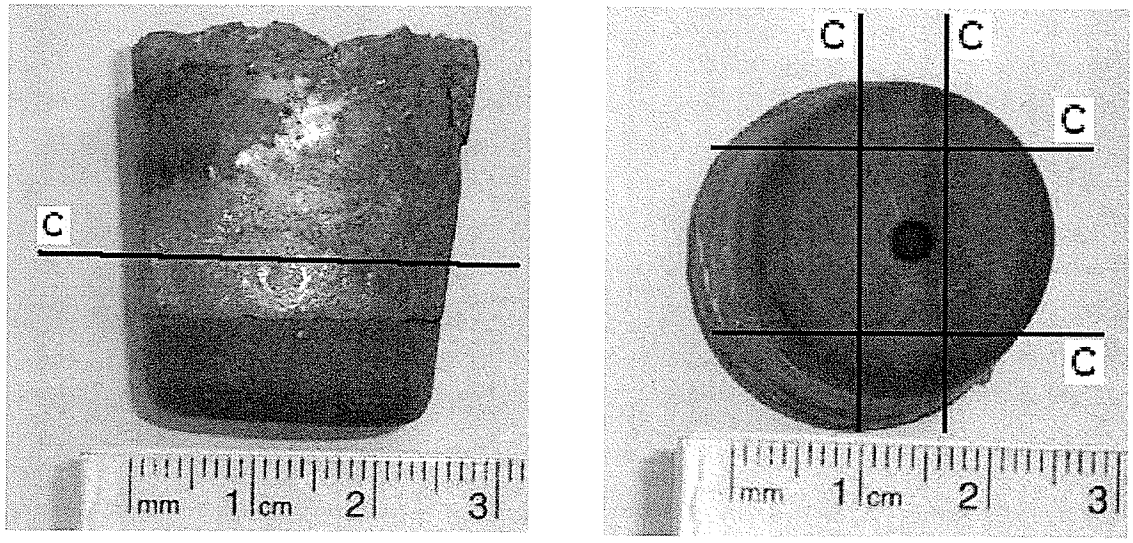

(a) (b)

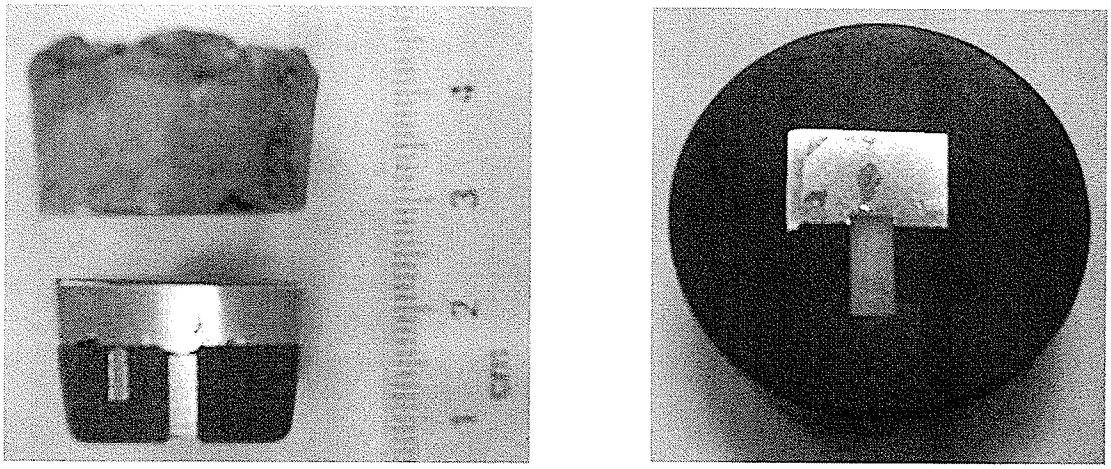

(c) (d)

Figure 3.8: Pure metal sample sectioning; (a) side view, (b) bottom view, (c) cut sample showing diffusion zone, (d) mounted sample. Cut lines are marked by a black line, and labelled with a C.

3.6 Etching the Iron-Zinc Couples

Samples of iron-zinc pure metal diffusion were always etched using Nitol (nitric acid and ethanol), since only the microstructure of the iron was important. The concentration and duration used in the etching procedure varied from sample-to-sample, due to the randomness and irregularity of the diffusion structure. Concentrations between 2-5% nitric acid, and durations between 1-3 minutes were used to develop the microstructure of the iron for each sample. The mounted samples were submerged upside down in a pool of Nitol, and gently oscillated for intervals of 30-45 s until the microstructure was developed. After each interval, the sample was dried, and the degree of etch was checked using an optical microscope. If the etch was unsatisfactory, another interval in the Nitol was performed.

The etched iron microstructure slowly developed from the bottom of the iron rod to the top (due to the galvanic protection from the zinc). Eventually a satisfactory etch of the iron-zinc interface was generated. The long duration in the Nitol etchant severely damaged/overetched the rest of the polished surface (the zinc matrix, the iron-zinc intermetallic phases, and the areas of the iron rod furthest away from the iron-zinc interface).

3.7 Galvanized Steel Samples

Strips of galvanized steel for heat treatment experiments were cut from the sheet metal stock by using a mechanical shear. The 0.7 mm thick sheet was cut into strips ~6 mm wide by ~25 mm long. After cutting, the strips were left with a cold worked edge.

Prior to use in each experiment, the as-cut galvanized steel strip was wiped clean with ethanol. The strip was then placed flat in a machineable alumina holder (Figure 3.3), wrapped in tool steel (to reduce oxidation), and then placed in a pre-heated box furnace (air atmosphere) at either 400°C or 500°C for 96 hours. After the diffusion heat treatment, the strip was removed from the furnace and air cooled.

Mounting, polishing, and etching

Before mounting and polishing, the heat treated galvanized steel strip was backed on either side by two non-heat treated galvanized steel strips. The three strips were then held together with a plastic clip (Figure 3.9). The plastic clip was used to hold the strips upright in the mounting equipment, and allow the diffusion cross-section to be polished. The backing strips of galvanized steel preserved the narrow diffusion zone from edge rounding/undercutting during polishing, and were composed of a material that would not ruin the polish or contaminate the sample.

For polishing and analyzing, the strips were held in a bakelite mount. The mount was required, since the thin, 0.7 mm by 25 mm cross-section of the strip had to be ground and

polished. The mount was formed in a 31.8 mm diameter mold, and was ~15 mm in height. Using a water-cleaned disc grinder with 180 grit paper, the exposed metal face of the mounted sample was then carefully ground down ~2 mm. At the 2 mm depth, the revealed cross-section of the galvanized steel was far removed from any edge effects, and was assumed to be representative of the rest of the strip.

Once the appropriate cross-section depth was obtained, the mounted strip was then carefully hand-polished through a set of gradually finer silicon carbide grit papers (220, 320, 400, 600), and then fine polished with colloidal diamond (6 μm and then 1 μm). After the 1 μm polishing wheel, the cross-section surface of the sample was ready for optical and SEM examination.

After the initial as-polished analysis, the galvanized steel samples were etched using methods similar to those used on the pure metal samples. Again, Nitol was used to develop the microstructure of the steel. A 2% nitric acid, 98% ethanol solution was used, and the samples were etched for a period of 40-60 s. To avoid over-etching, the mounted samples were held in the etchant using 10 s intervals. The samples were submerged upside-down in a pool of the etchant for 10 s, dried, and checked using an optical microscope. If the sample needed to be further etched, the process was repeated until the steel microstructure developed.

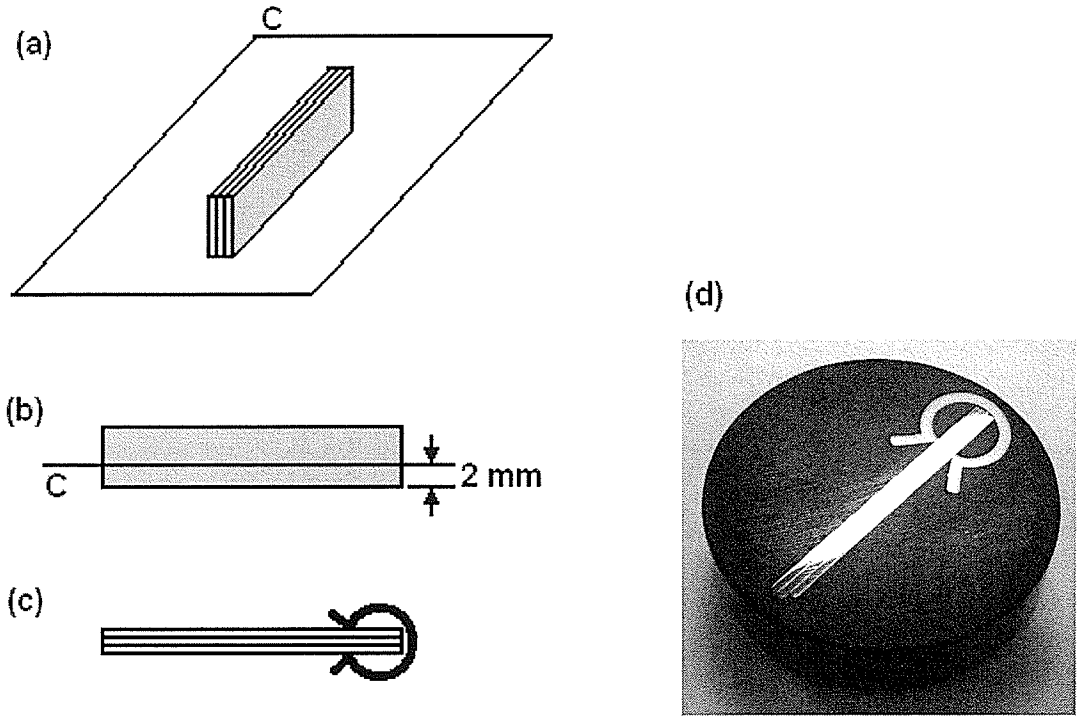

Figure 3.9: Galvanized steel sectioning; (a) cutting plane in the backed sample, (b) side view of cutting plane, (c) top view of backed and clipped sample, (d) mounted backed and clipped sample. C denotes the cutting plane.

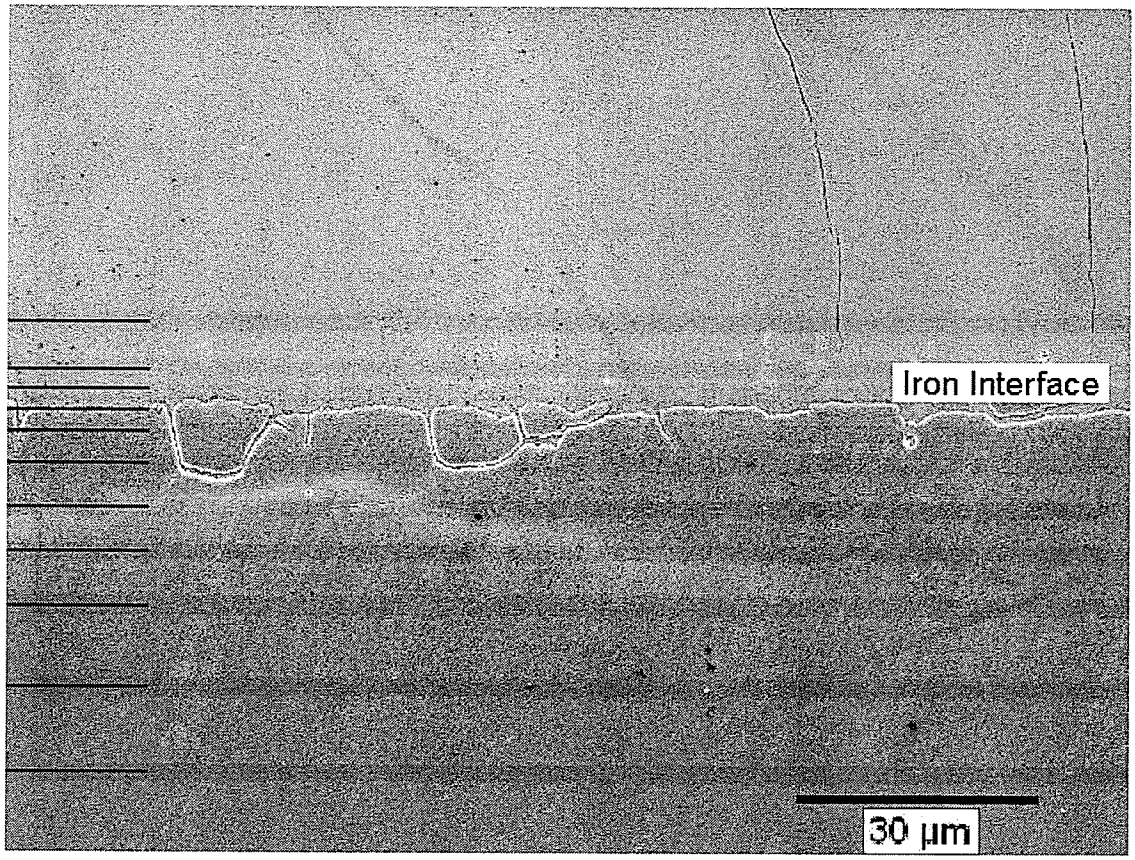

Figure 3.10: Coarse concentration gradient reading (*Mag 1000x*).

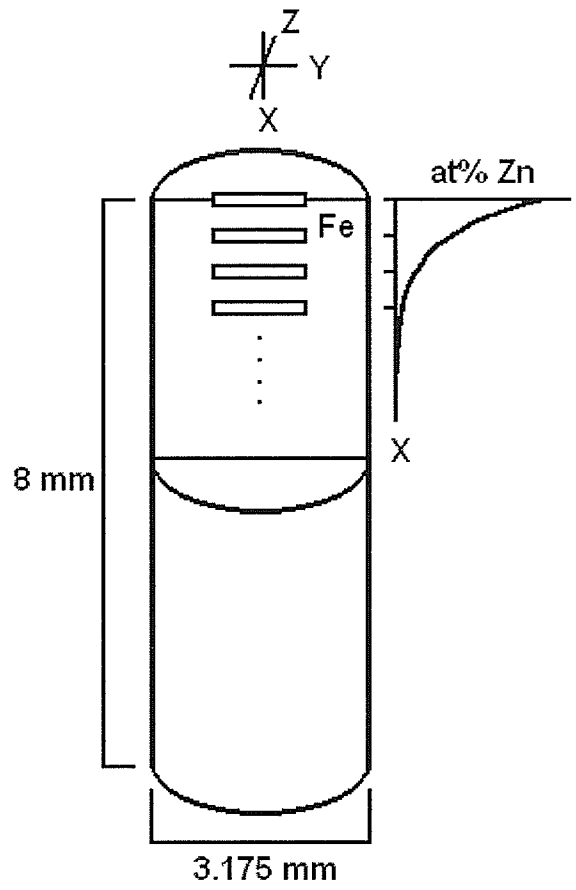

Figure 3.11: Iron rod cross-section, with concentration gradient diagram.

3.8 Scanning Electron Microscopy and EDS Chemical Analysis

High magnification examination and composition analysis were performed on a JEOL 5900 scanning electron microscope (SEM). All samples were always analyzed using 20 kV accelerating voltage, in either secondary electron imaging or backscattered electron imaging modes. The working distance was set at 12-14 mm.

Semi-quantitative energy dispersive x-ray spectrometer (EDS) analysis was performed on the JEOL 5900 SEM, which had an Oxford EDS detector and analysis system, with INCA standardless correction software. Atomic compositions of scanned areas were produced by using a live time of 60 s with a deadtime of 22-26%. Only composition percentages of iron and zinc were used, all other elements were removed from the composition list. The deviation in the atomic percent composition was usually ± 0.2 at%, and upwards to ± 0.4 at% at the α-Fe – Γ interface. All EDS composition analysis was performed on samples that were in an as-polished, unetched state.

3.9 Concentration Gradient Procedure

The concentration gradient was a reflection of the change in the amount of zinc across the iron-zinc interphase, and with depth into the iron rod. Scanned iron interface regions were performed close to the middle of the iron rod, which eliminated 2-dimensional diffusion effects. Multiple readings of the same sample were taken at positions of 1/5 to 1/2 the diameter of the iron rod.

The zinc concentration gradients in the sample were read on the SEM using the following method. The magnification was usually set at 750x, but some readings used 500x, while others used 1000x. The scanned sample region was set up so the iron side was on the bottom, with the iron interface parallel to the bottom edge of the screen (Figure 3.10). The scanned sections used to measure the concentration were thin rectangles 2-4 μm in height, by the width of the imaging screen (widths of: 285 μm for 500x, 190 μm for 750x, and 143 μm for 1000x). The scanned sections are shown as the darker grey, parallel rectangles in Figure 3.10 (black lines mark the locations). Portions of at least 10 grains were included in each scanned section, so an adequate distribution of grains was measured.

The first scanned section was set at the α-Fe – Γ interface. The position of this section was shifted across the interface, and the scan repeated, until a zinc concentration of 68-70 at% was measured. After this composition was obtained, this position was set as the zero distance, and further scanned sections were measured from this position using the onscreen callipers (Figure 3.10). With respect to the iron rod and interface, the concentration gradient readings were performed close to the diameter of the rod, in the x-y plane (Figure 3.11). The thin sections for composition analysis were repeated at regular intervals along the x-direction of the rod.

The position steps in the gradient were kept constant from one sample to the next, but the step distance varied on the location in the interphase. The steps were every 5 μm (sometimes 2.5 μm) across the α-Fe – Γ interface, every 10 μm in the area 20 μm to

50 μm depth in the iron, and every 20 μm at depths greater than 50 μm (Figure 3.10). The scanned sections were repeated until 0% zinc concentration was found in consecutive recordings. At each scanned step on the sample, atomic %, weight %, and the step distance were recorded. This information was then used later to plot the concentration gradient, and to determine the zinc diffusion coefficient in iron.

Chapter 4

RESULTS

This chapter begins with a presentation of the results obtained in the pure metal diffusion samples produced at 400˚C, 500˚C, and 725˚C. The as-polished structures in these samples will be described first, followed by a description of the etched microstructures. The zinc concentration gradient measured in the iron with the SEM and EDS will then be presented, followed by the results of the iron diffusion at each of the experiment temperatures. With data from these sections, the calculation of the zinc diffusion coefficient in the iron will be presented. The as-polished and etched structures found in the galvanized steel samples heat treated at 400˚C and 500˚C are then described. Finally, the results of the effect of zinc diffusion in galvanized steel are presented.

4.1 Iron-Zinc Diffusion Couples

The samples produced in this investigation were always analyzed first unetched, to prevent contamination and erroneous composition readings from the EDS unit. Several microstructural features in the samples were only visible in the as-polished, unetched state, whereas other features were only apparent after etching. In the bulk pure iron-zinc diffusion samples produced in this investigation, the large amount of zinc (coupled with the long duration of the heat treatment) created a diffusion structure that was different than what has been previously reported. Though the structures were different, they were still consistent with that which might be expected from the iron-zinc phase diagram (Figure 2.1).

4.1.1 As-Polished Structure

Diffusion at 400°C

The structure of the diffusion zone from experiments conducted at 400°C contained intermetallic phases and structures as described throughout the literature [7, 8, 10, 12, 16]. In the samples produced at 400°C, the boundary conditions possibly changed from pure Zn – pure Fe to ζ(δ) phase – pure Fe at some point during the 96 hour diffusion anneal. The structure produced when 99.99% pure zinc diffused with 99.95% pure iron at 400°C for 96 hours, was as follows (from Figures 4.1, 4.2, and 4.3). The interface shown in Figures 4.1, 4.2, and 4.3 was formed by using the poured liquid zinc method.

From the pure iron side to the pure zinc side:

1) Iron (α-Fe) with 13 ± 3 μm sized equiaxed grains (Figure 4.1 – the layer at the bottom of the micrograph).
2) A two-phase region consisting of outer grains of the iron "broken up" by Γ phase (Figure 4.1 – Γ is the dark grey/black phase in the micrograph). The Γ phase formed in amongst the grain boundaries, thereby separating the outer grains from the bulk of the iron rod.
3) A discontinuous, pillar-like layer of Γ intermetallic phase (5-20 μm thick).
4) A continuous layer of Γ_1 intermetallic phase (30-50 μm thick). This phase appears as the lighter grey layer in Figure 4.1, and the outline of the layer is shown in Figure 4.2.
5) A continuous layer of δ intermetallic phase (~200 μm thick). The top of this layer, near the δ – ζ interface, was riddled with voids (Figure 4.2). Cracks were also found running perpendicular to the iron interface (Figures 4.2 and 4.3). The cracks propagated through the entire thickness of the δ and Γ_1 phases, similar to what was reported by Marder [7].
6) A discontinuous layer of ζ intermetallic phase (possibly 0-10 μm thick). The thickness, or even the existence, of the ζ phase layer was inconclusive. Based on readings by the SEM, locations at the top of the intermetallic layer shown in Figure 4.3 were found that were close to the composition of the ζ phase. These readings were not accurate, as there might have been pick up of the η-Zn (>99 at% Zn) found directly above the intermetallic layer, thus throwing off the composition reading. The ζ phase is depicted in Figure 4.3 as the irregular,

broken top of the intermetallic layer (the white/light grey area of the micrograph); however, this could be just an extension from the δ phase below. Large voids were also found around the interface between the ζ(δ) phase and the η-Zn phase above it (Figure 4.3). It might be possible that there was a cracked interface between the ζ(δ) phase and the η-Zn, similar to what was reported by Bastin et al. [10], but this was also inconclusive. As shown in Figure 4.3, a voided area (space) existed between the intermetallic layer, and the η-Zn phase.

7) Above the ζ(δ) phase layer; homogeneous, continuous η-Zn phase/pure zinc. The η-Zn phase/pure zinc appeared as the darker, mottled phase in Figures 4.2 and 4.3. The cause of the mottled surface was zinc dendrites.

The structure listed above was typical of the samples produced by the poured liquid metal technique. In comparison, the vacuum chamber technique created a different form to the structure (Figure 4.4). The samples produced by this method had a large liquid diffusion component. In Figure 4.4, evidence of liquid diffusion is shown by the thick, δ and ζ phase dominated, continuous intermetallic layer on the iron, and the large δ and η-Zn two-phase region above this layer. Samples created in the vacuum chamber also had large barriers to diffusion in the interphase (voids, iron and zinc oxides), which are shown by the large black spots in the top half of Figure 4.4. The results from the vacuum chamber technique were less conclusive, consistent, and absolute, than the results produced via the poured liquid metal technique.

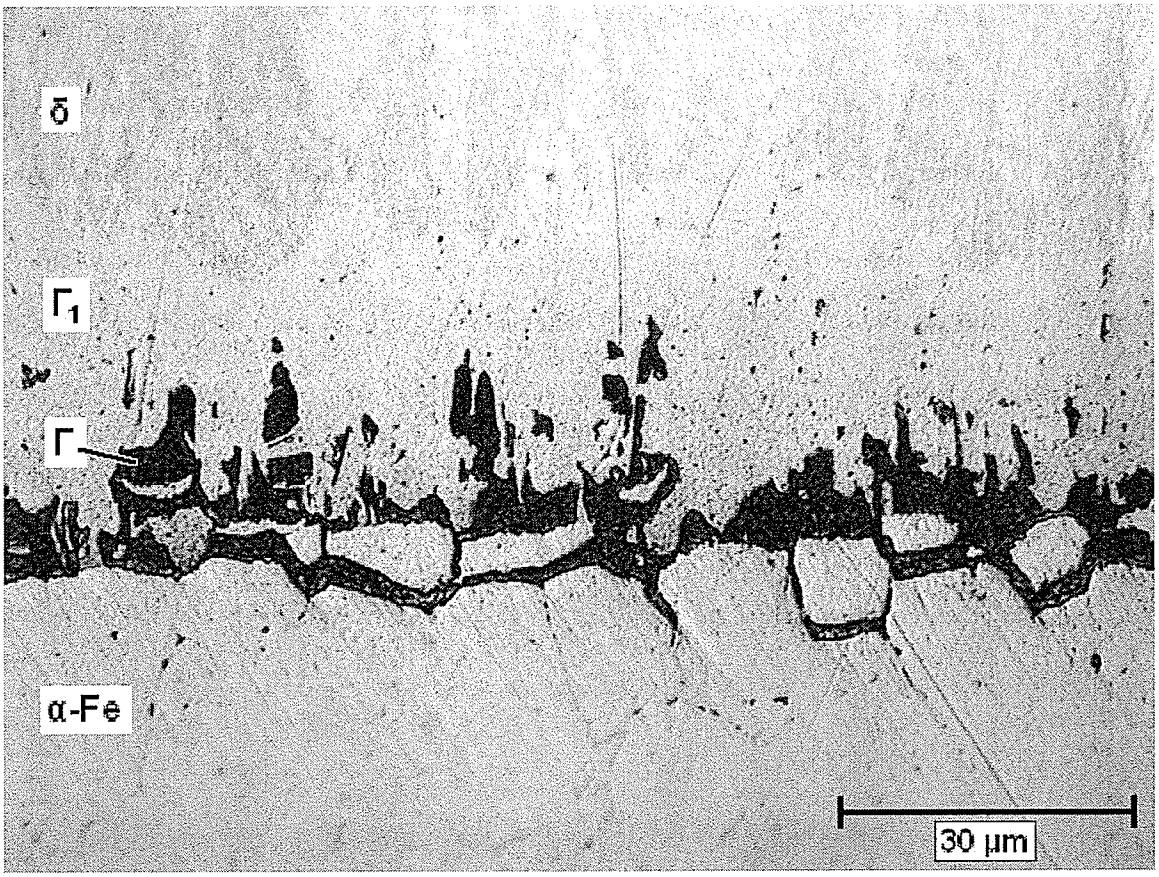

Figure 4.1: Iron-zinc interface formed at 400˚C, for 96 hours (*Mag 1000x*).

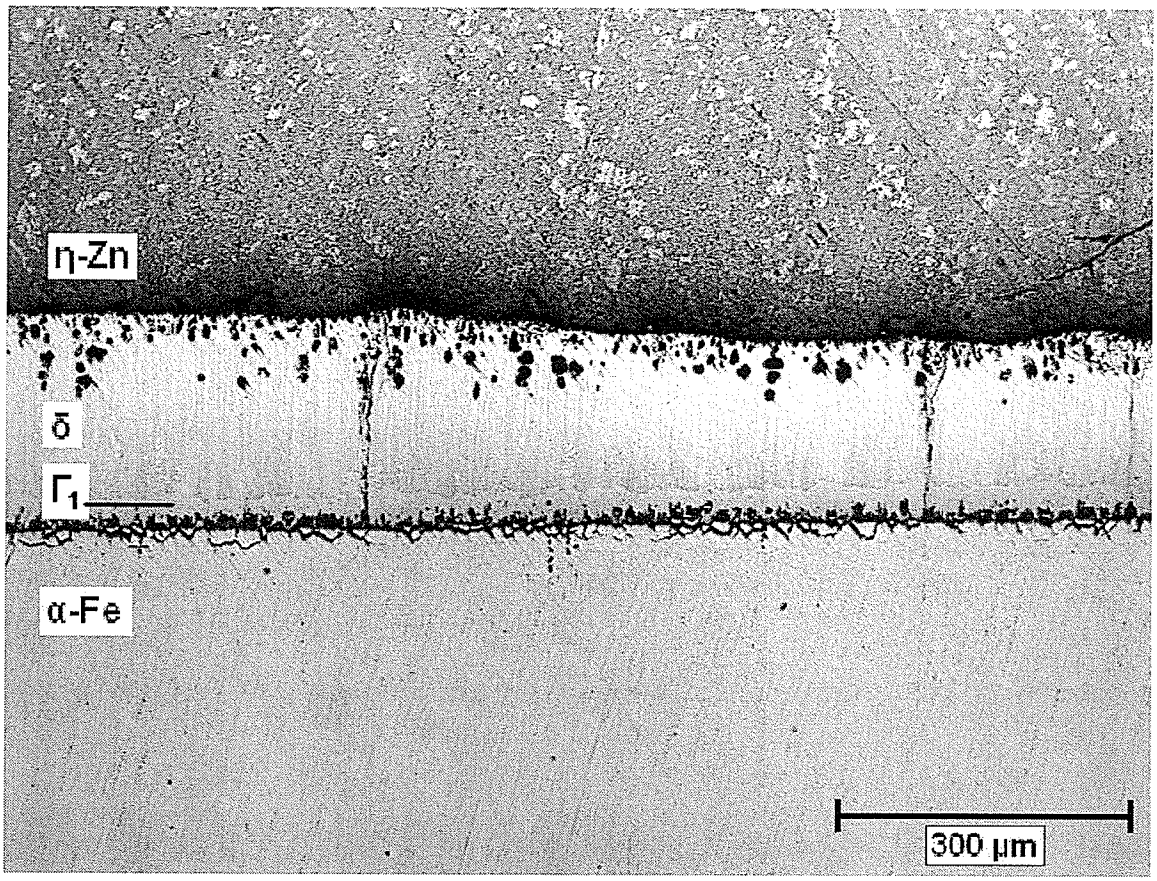

Figure 4.2: Iron-zinc interphase formed at 400˚C, for 96 hours (*Mag 100x*).

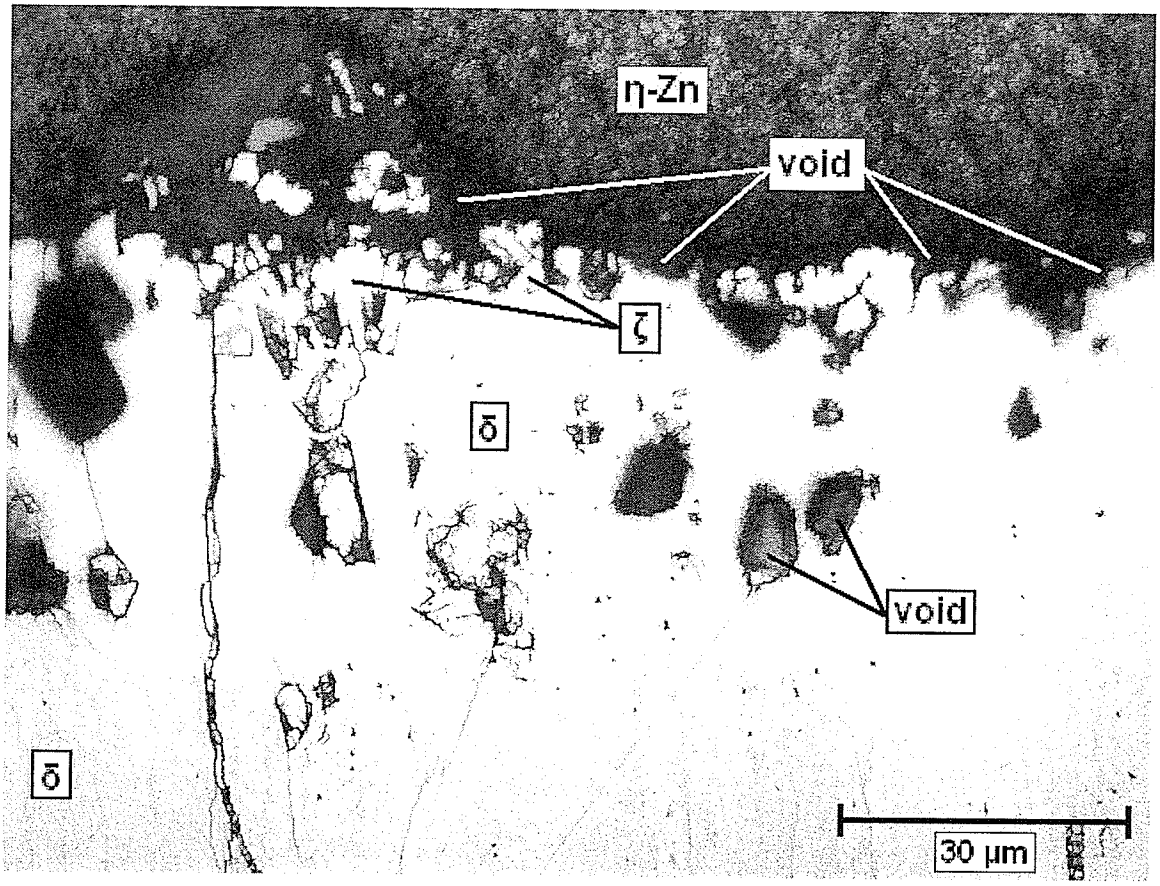

Figure 4.3: Structure at the η-Zn interface, 400˚C for 96 hours (*Mag 1000x*).

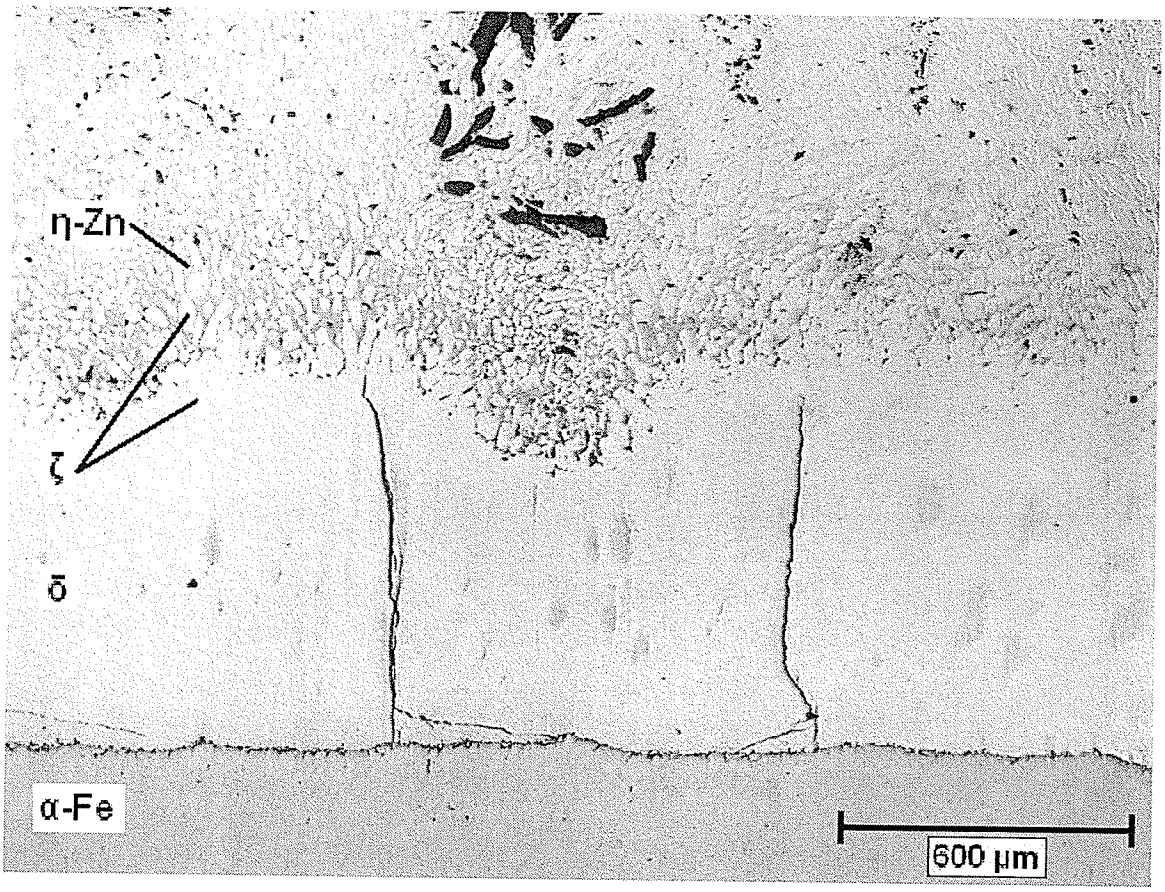

Figure 4.4: Iron-zinc interphase formed at 400˚C, for 96 hours, using the vacuum chamber method (*Mag 50x*).

Diffusion at 500°C

The structure produced at 500°C was in the same layered form as the structure produced at 400°C. This was the only similarity as the phases that formed, the phase morphologies, and the phase thicknesses, were all different. In the samples produced at 500°C, the boundary conditions remained the same (pure Zn – pure Fe) during the entire 96 hour diffusion anneal. For 99.99% pure zinc poured on 99.95% pure iron, and subsequently heated at 500°C for 96 hours, the structure produced was as follows (from Figures 4.5 and 4.6). The interphase shown in these figures was formed by using the poured liquid metal technique.

From the pure iron side to the pure zinc side:

1) Iron (α-Fe) with 13 ± 3 μm sized equiaxed grains (the dark grey layer at the bottom of Figure 4.5).
2) A sparse, discontinuous, pillar-like layer of Γ phase (1-10 μm thick). There was less Γ phase formation after 96 hours at 500°C, when compared to the amount formed in samples heated at 400°C for 96 hours.
3) A continuous layer of Γ_1 intermetallic phase (10 μm thick). A faint outline of the Γ_1 phase can be seen 10 μm above the dark iron layer, in Figure 4.5. Again, less Γ_1 phase formed after 96 hours at 500°C, than at 400°C.
4) A thick, continuous layer of δ intermetallic phase (~300 μm thick). The δ phase layer ended in a large, globular shaped interface with the η-Zn phase (Figure 4.6). No voids were found in the δ phase layer, at the δ – η-Zn interface, or in the

δ – η-Zn two-phase region. Numerous thick cracks propagated throughout the δ phase (Figures 4.5 and 4.6). The δ – η-Zn interface was not cracked.

5) Above the δ phase layer; homogeneous, continuous η-Zn phase / pure zinc. The η-Zn phase / pure zinc layer appears at the top of the micrograph in Figure 4.6, past the large globular particles of δ phase.

Only small rectangular / rhombic-shaped particles of ζ-phase were found in the pure metal samples heated at 500°C for 96 hours (Figures 4.7 and 4.8). In Figure 4.7, a single (but relatively large) ζ phase particle was found at the extreme end of the δ – η-Zn two-phase region. This ζ phase particle formed as a result of liquid diffusion of iron into the zinc melt, and could have only formed while cooling (the samples were air cooled, which equates to a slow cooling rate). The same growth mechanism accounted for the formation of the group of ζ phase particles shown in Figure 4.8. These particles were found ~2.5 mm from the δ – η-Zn interface shown in Figure 4.6. No ζ phase was found in the intermetallic layer on the iron; the ζ phase could not form on the iron at 500°C.

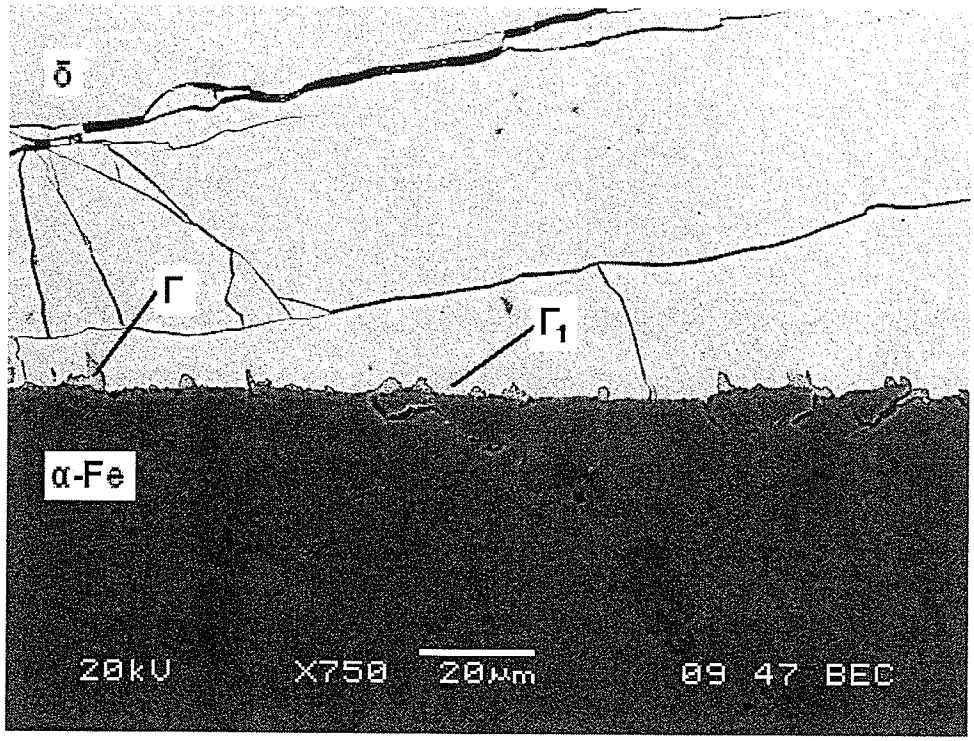

Figure 4.5: Iron-zinc interphase formed at 500˚C, for 96 hours (*Mag 750x*).

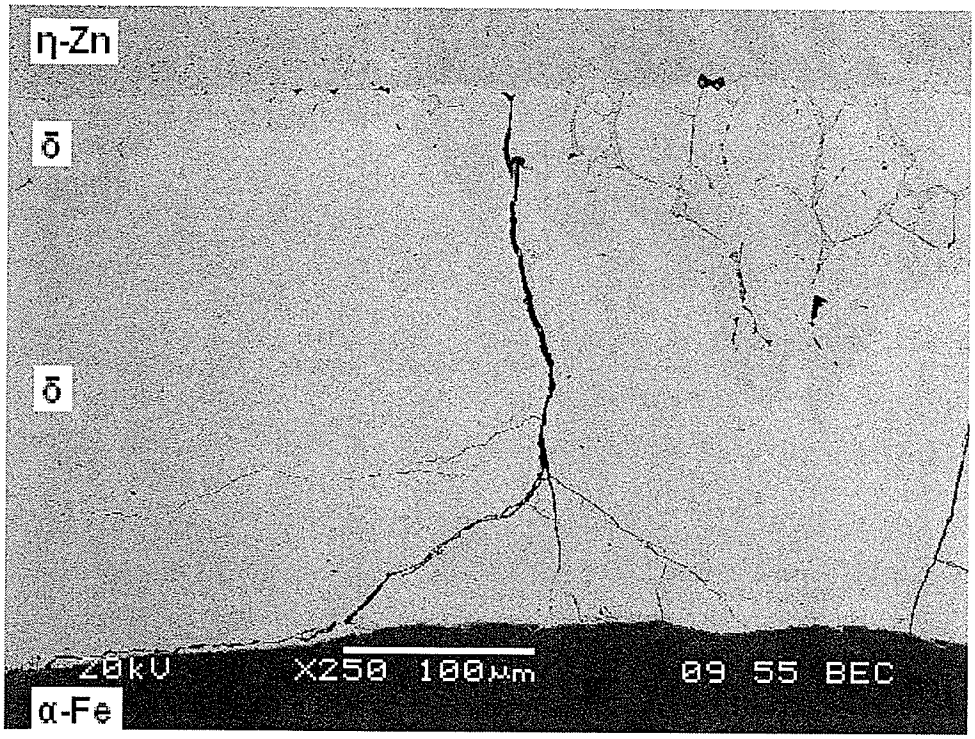

Figure 4.6: Iron-zinc interphase formed at 500˚C, for 96 hours (*Mag 250x*).

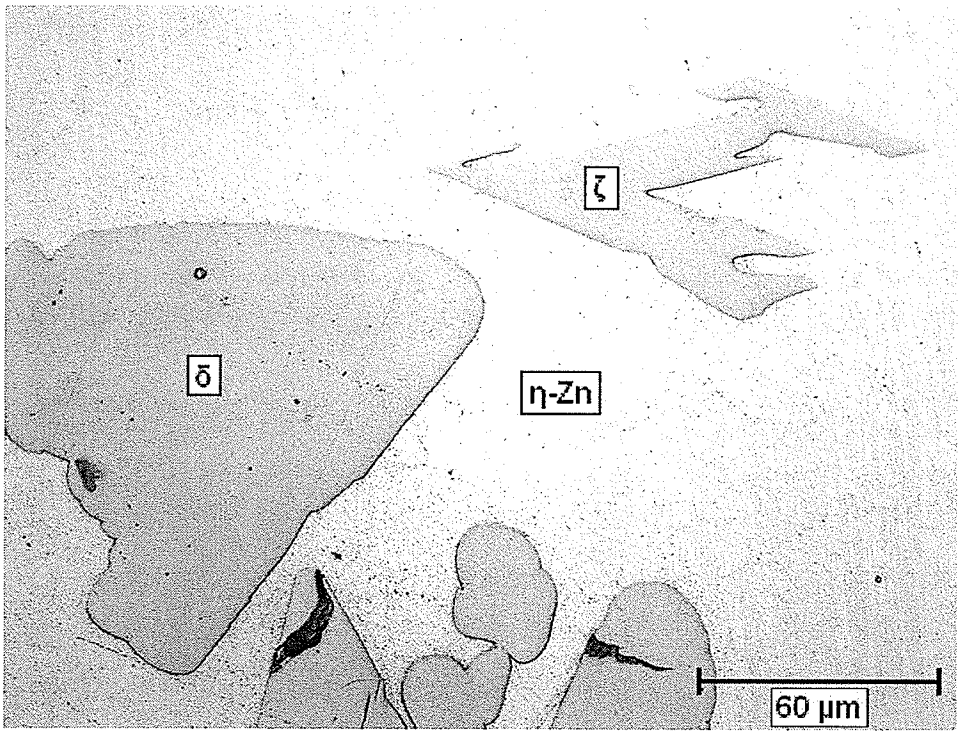

Figure 4.7: ζ phase particle at the δ – η-Zn two-phase region (*Mag 500x*).

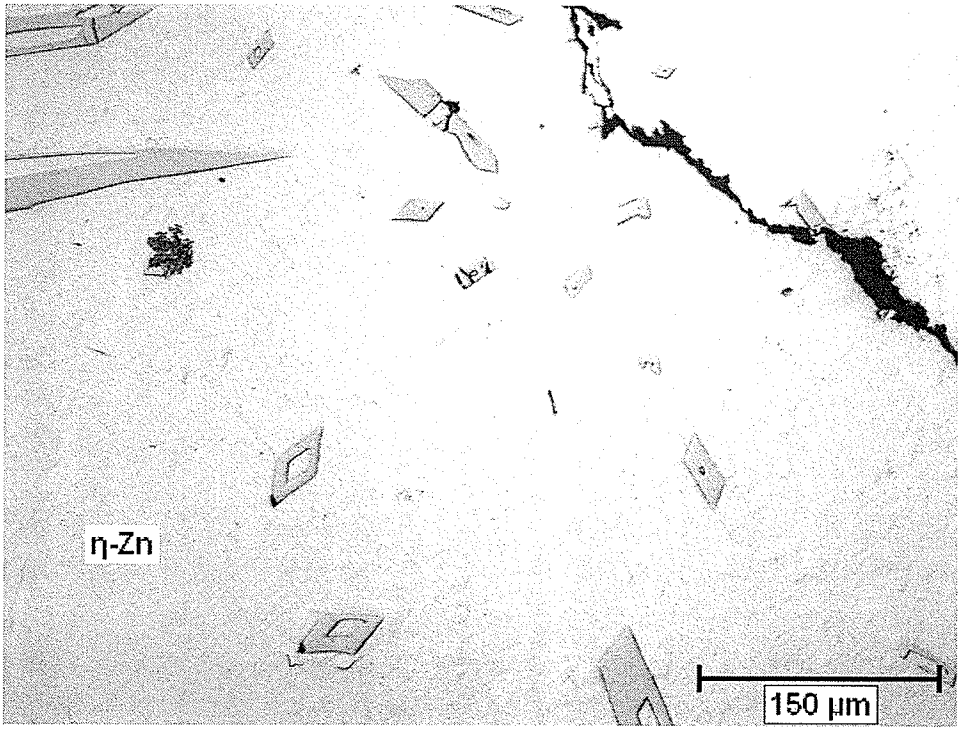

Figure 4.8: ζ phase particles formed at 500°C, for 96 hours (*Mag 200x*).

Diffusion at 725°C

The structure formed by diffusion at 725°C was much different than the structure formed at 400°C or 500°C. Due to the large liquid diffusion reaction at 725°C, the phases that formed, and the shape and thicknesses of the phases, were much different than what was found in the samples produced at 400° and 500°C. Most of the structure in these samples formed during the slow temperature decrease that occurred when cooling the molten zinc to room temperature. In the samples produced at 725°C, the boundary conditions remained the same (pure Zn – pure Fe) during the entire 96 hour diffusion anneal. The phases that formed when a 99.99% pure zinc pool on top of a 99.95% pure iron rod held at 725°C for 96 hours, was solidified, was as follows (from Figures 4.9, 4.10, 4.11, 4.12, and 4.13).

From the pure iron side to the zinc side:

1) Iron (α-Fe) with 13 ± 3 μm equiaxed grain size (Figure 4.9 – the layer at the bottom of the micrograph).
2) A very thin, discontinuous, pillar-like layer of Γ phase on the iron (1-5 μm thick). There were some layered and globular structures of Γ phase found on the iron as well (the solid, dark grey coloured phase in Figure 4.9).
3) A discontinuous, crystal-shaped layer of Γ_1 intermetallic phase (5-15 μm thick). The quantity of Γ_1 phase was much greater than Γ phase, as shown by the large, mottled, darker grey areas in Figure 4.9.
4) A thin, continuous layer of crystal-shaped δ phase (75-125 μm thick). No voids were found in this layer, though δ phase particles broke out while polishing

(the large black voids in Figure 4.10). There were no cracks found in this layer, and no crack was found between the δ phase and η-Zn phase.

5) A large δ – η-Zn two-phase region above the continuous intermetallic layer. This phase was several millimetres thick (4-5 mm). The δ phase particles were small and numerous closer to the iron, and then gradually changed to large, widely spaced particles further away (Figure 4.11). The δ phase particles are shown by the darker grey, irregular-shaped phase in Figure 4.11. Some of the δ phase particles had a six-sided / hexagonal shape (ex. the large particle at the top of the micrograph collage in Figure 4.11).

6) A transition region between δ – η-Zn and ζ – η-Zn. As shown in Figure 4.12, this region was ~2 mm thick. In this region, both ζ and δ phase particles formed in amongst each other in the η-Zn matrix. In Figure 4.12, the ζ phase can be identified by the smaller, darker grey, rectangular / rhombic-shaped particles, and the δ phase can be identified by the larger, darker grey, irregular / six-sided / hexagonal-shaped particles. The δ – η-Zn / ζ – η-Zn transition region was located ~6 mm above the iron interface.

7) A thick ζ – η-Zn two-phase region found in the rest of the polished area of the sample (several millimetres thick). The two-phase region had large ζ phase particles (some were 2-3 mm long), which were surrounded by large η-Zn regions (Figure 4.13). The ζ phase particles are the darker grey, rectangular / rhombic-shaped phase in Figure 4.13. The ζ phase particles shown in Figure 4.13 were found ~12 mm from the iron interface.

No pure zinc was found in the polished sections from samples heated at 725˚C, though ζ phase eventually disappeared. This was confirmed in the polished face of the cut off section of the zinc ingot (the large ζ phase particles were only found in the center of the polished face of the zinc casting, in an area directly above the iron rod – the other areas of the polished face could then be assumed to be pure zinc). The interphase displayed in Figures 4.9, 4.10, 4.11, 4.12, and 4.13 came from a sample produced by the poured liquid metal technique. The best results came from using this technique.

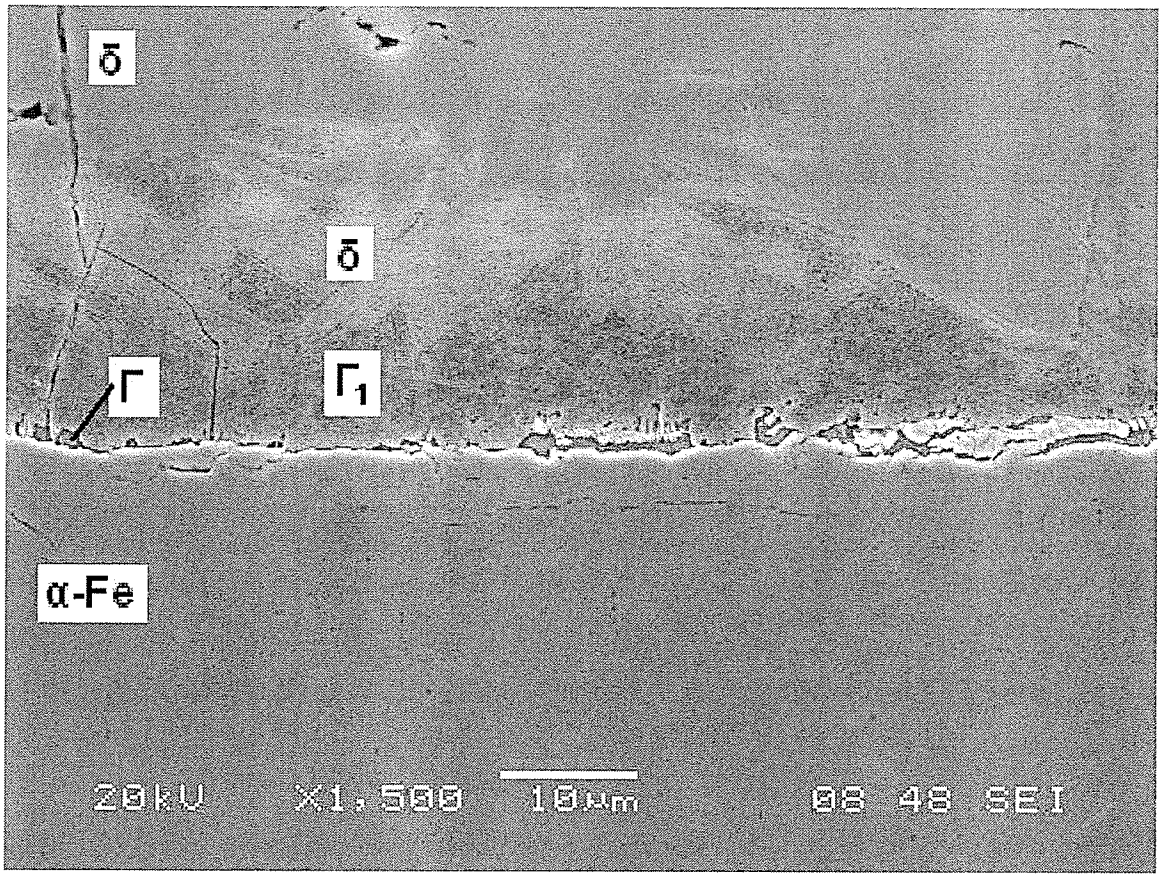

Figure 4.9: Iron-zinc interface formed when cooling from 725˚C (*Mag 1500x*).

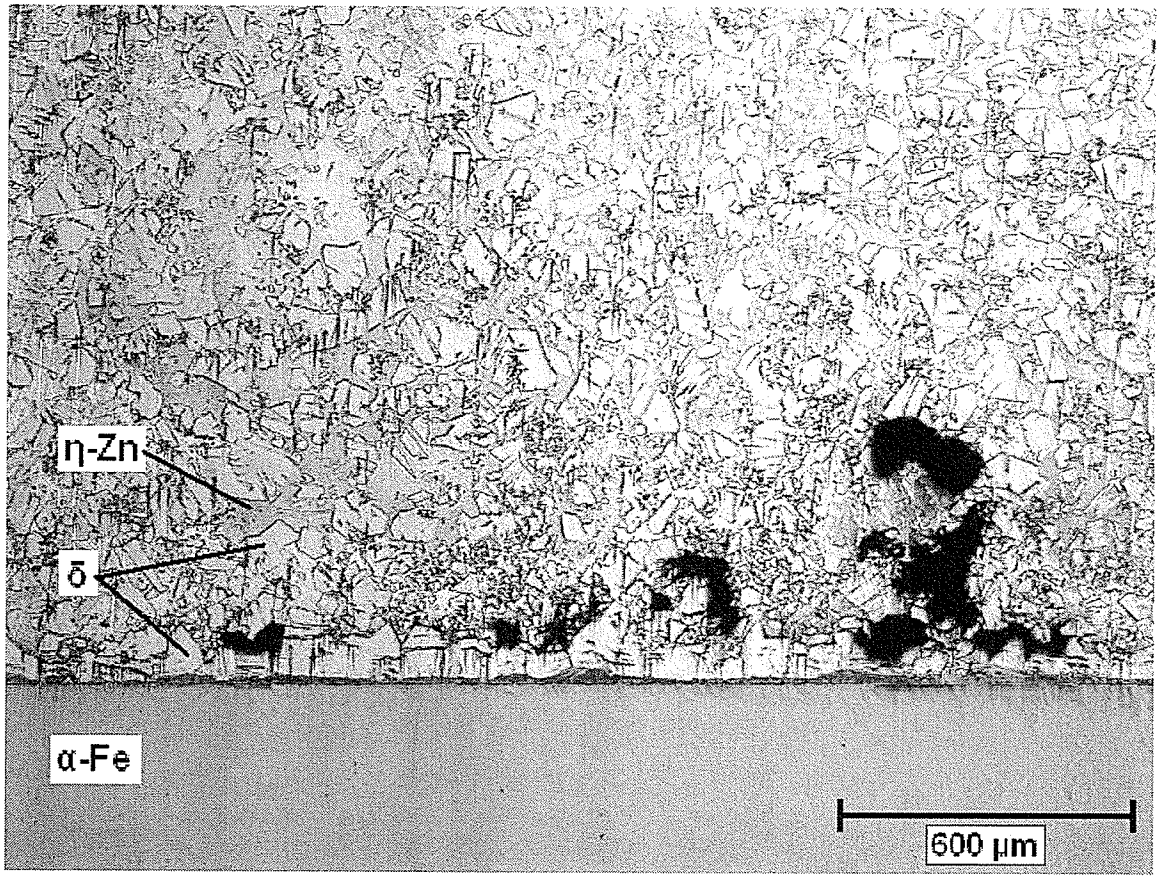

Figure 4.10: Iron-zinc interphase formed when cooling from 725°C (*Mag 50x*).

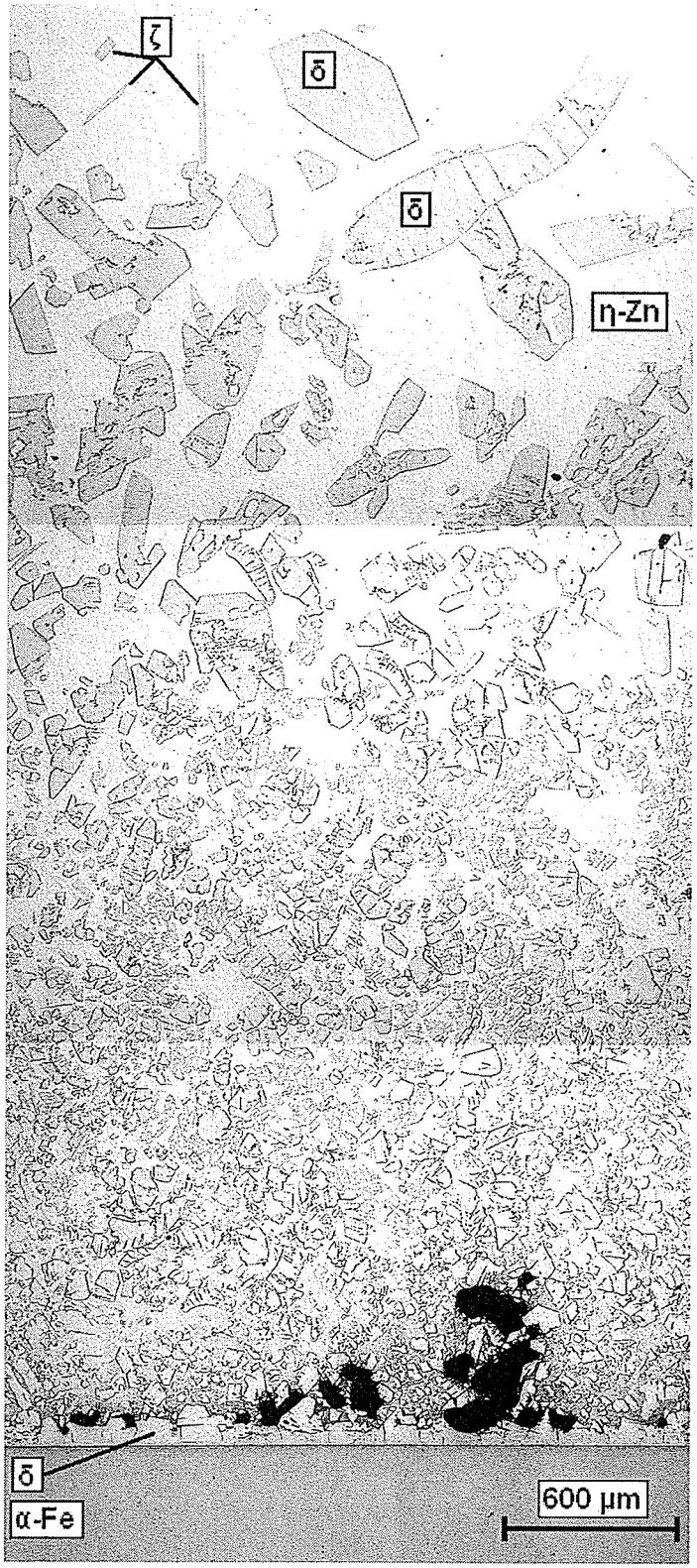

Figure 4.11: δ phase transition formed when cooling from 725˚C (*Mag 50x*).

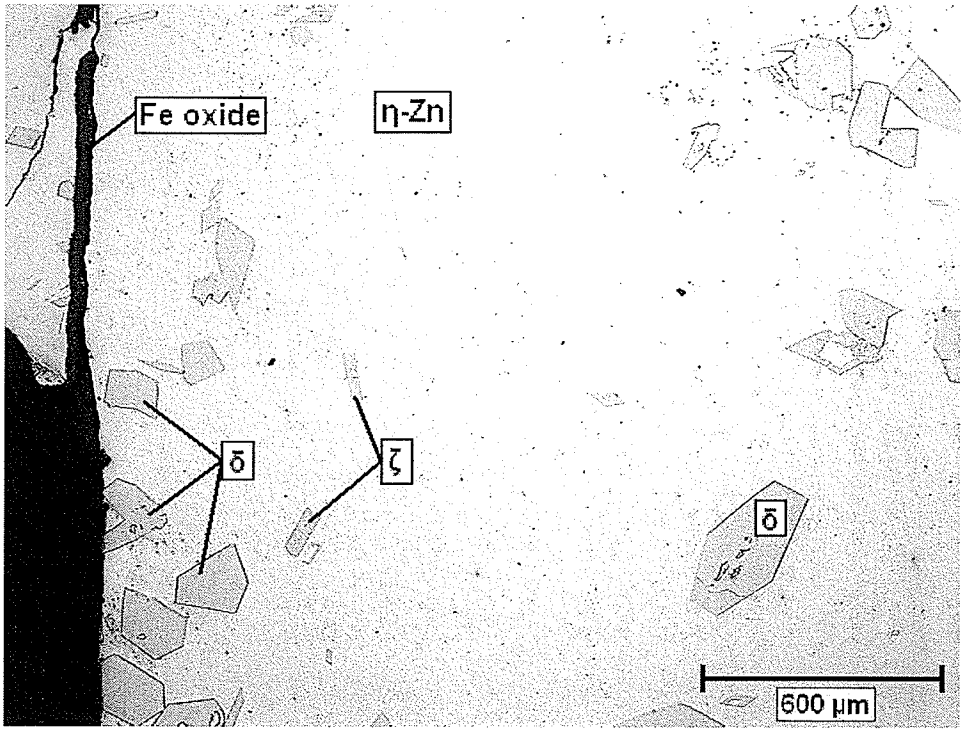

Figure 4.12: δ to ζ phase transition formed when cooling from 725°C (*Mag 50x*).

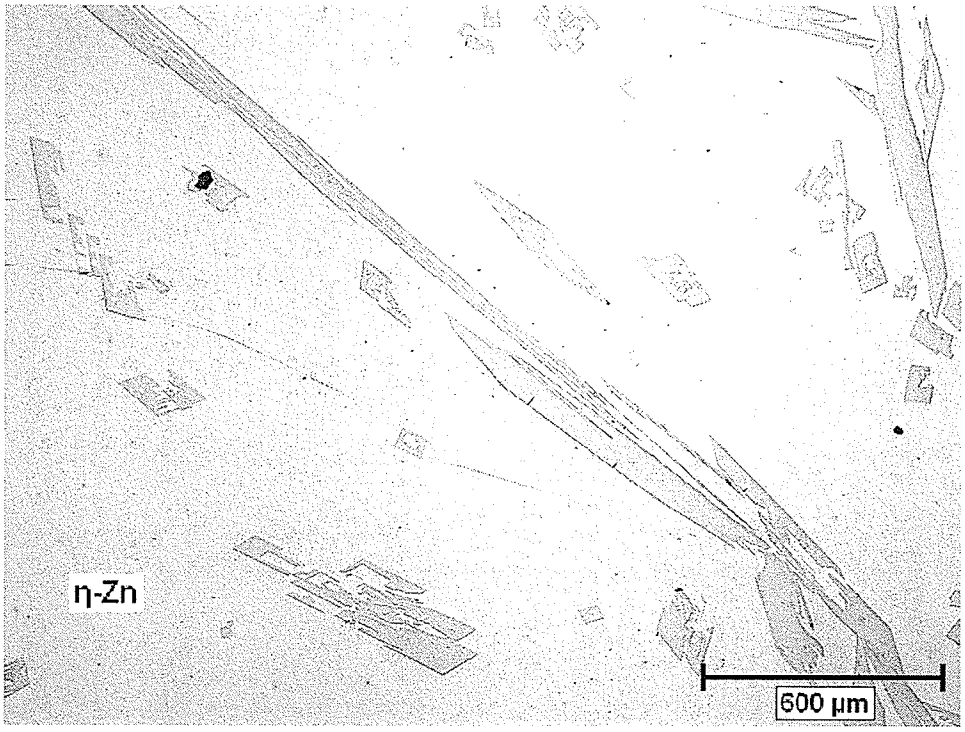

Figure 4.13: ζ phase particles formed when cooling from 725°C (*Mag 50x*).

4.1.2 Etched Iron Microstructure

The results of etching were inconsistent due to the different and irregular microstructures formed in each sample. The etching was aggravated by the galvanic effect of the zinc, which protected the first 50-100 μm of the iron, therefore making it difficult to create a good etch of the most important diffusion region. In spite of these nuisances, the samples were satisfactorily etched, and the results were conclusive.

Diffusion at 400°C

Samples of 99.99% zinc – 99.95% iron, heated at 400°C for 96 hours, had thin ribbons of a second phase in the grain boundaries of the first 3-6 grains (40-80 μm depth) from the interface (Figure 4.14). In Figure 4.14, the iron interface was the dark grey band at the top of the micrograph, while small grey globs of a second phase in the grain boundaries were clearly defined. The second phase was determined to be Γ, as the ribbons in the grain boundaries were an extension of the α-Fe – Γ interphase, shown in the as-polished state in Figure 4.15.

A high magnification of the iron interface is shown in Figure 4.15, with the iron grains represented by the large black masses, the Γ phase represented by the darker grey colour, and with the lighter grey Γ_1 phase filling the rest of the micrograph. The pillar-like shapes of Γ phase can be seen on the iron grains, with this same phase enveloping the grains, and leading down into the grain boundaries. Since no other phase was present in this area, Γ is the only zinc-iron phase that forms in the grain boundaries of iron.

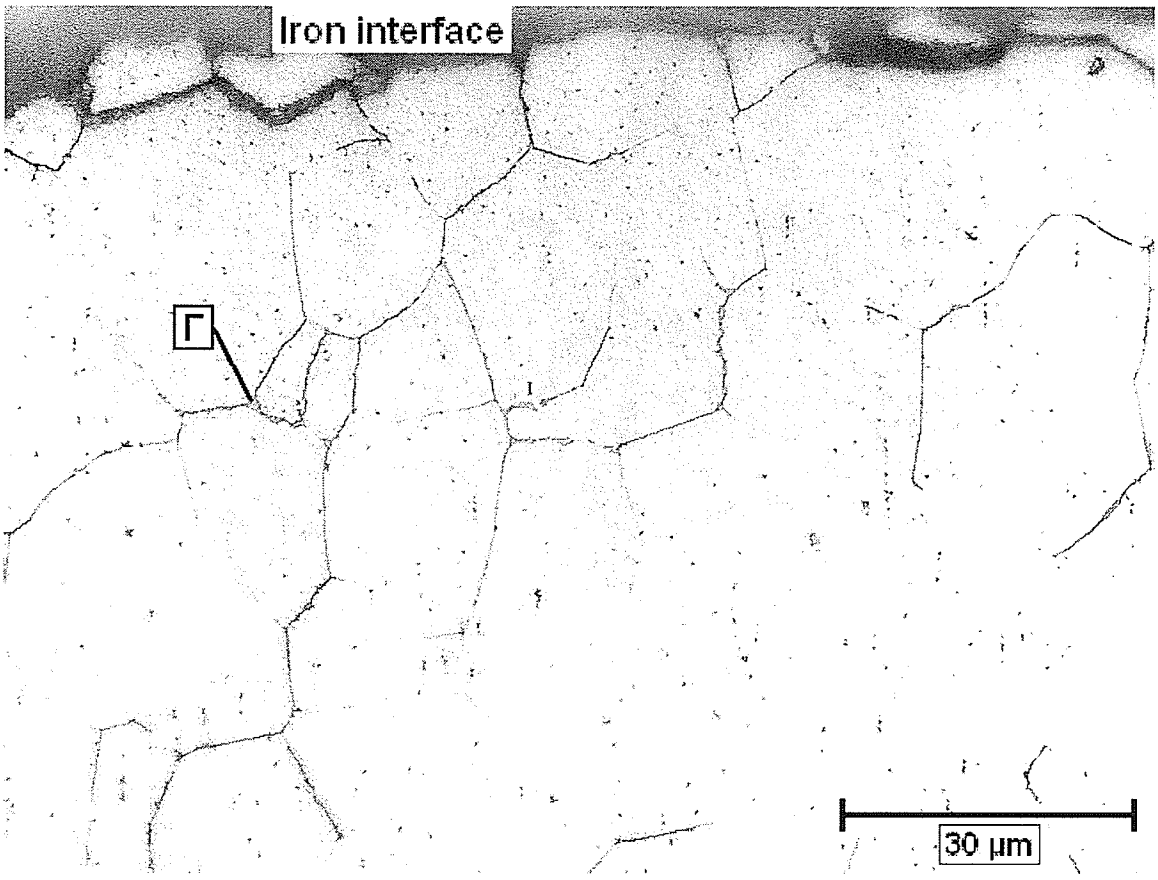

Figure 4.14: Etched iron microstructure, formed at 400˚C, for 96 hours (*Mag 1000x*).

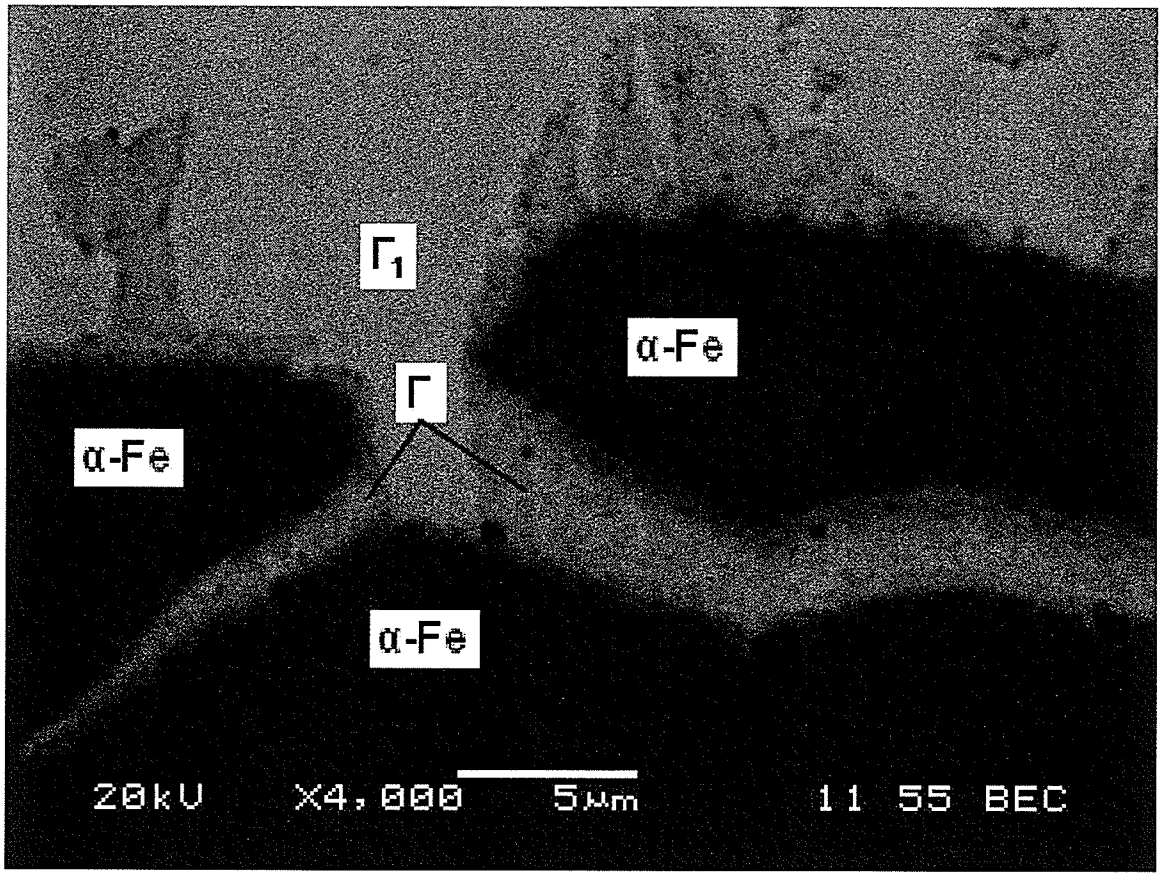

Figure 4.15: Γ phase in the grain boundaries of the iron, formed at 400˚C, for 96 hours (*Mag 4000x*).

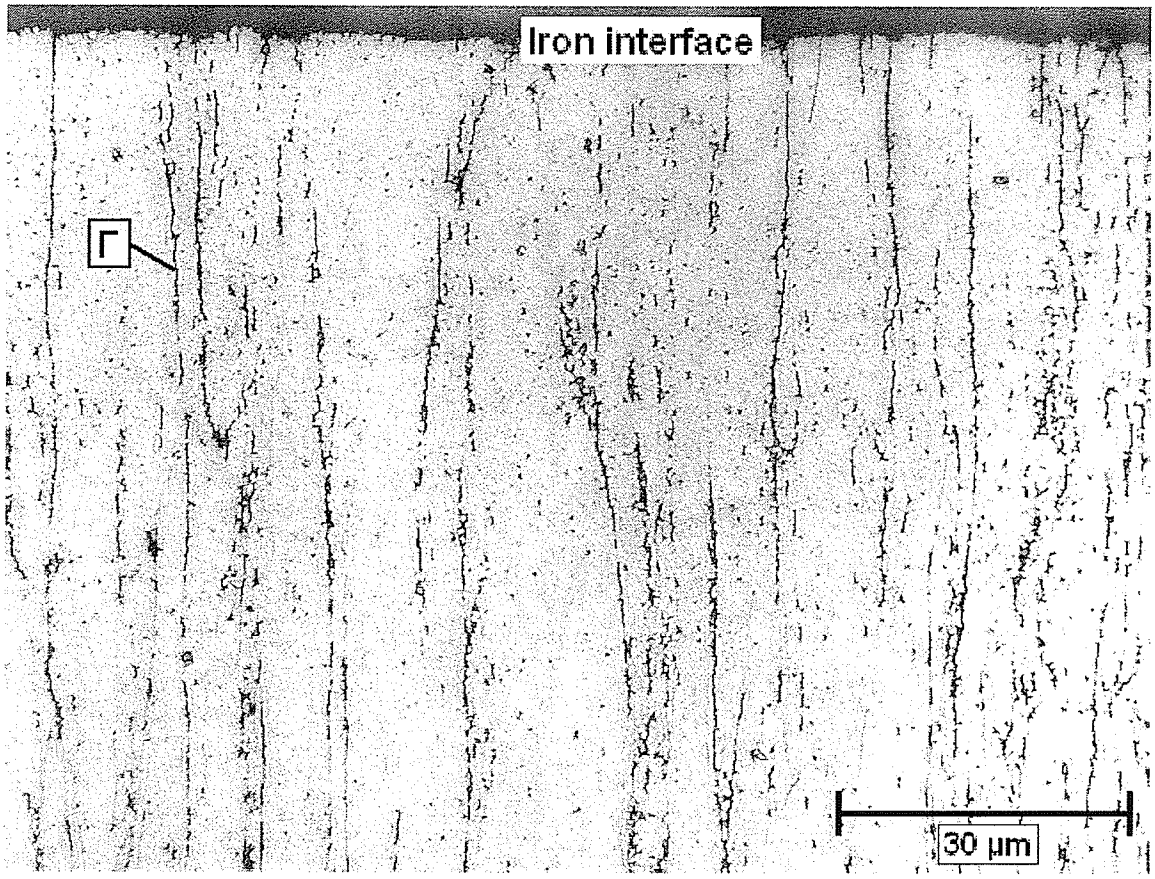

Figure 4.16: Etched non-pre-heat treated iron microstructure, formed at 400˚C, for 96 hours (*Mag 1000x*).

A micrograph of etched iron from a pure metal diffusion sample produced with using non-pre-heat treated iron is shown in Figure 4.16. Since the iron did not undergo a pre-heat treatment prior to the experiment, the elongated grains in the as-received iron allowed zinc to diffuse far into the iron. Shown in Figure 4.16, thin black ribbons of Γ phase formed in the parallel grain boundaries of the iron, and the ribbons extended, nearly linearly, greater than 100 μm into the iron. Comparing Figure 4.16 to Figure 4.14, the Γ phase formed deeper in the non-pre-heat treated iron with elongated grains than in the pre-heat treated iron with equiaxed grains.

Diffusion at 500°C

For samples of 99.99% zinc – 99.95% iron, heated at 500°C for 96 hours, the Γ phase in the grain boundaries took the form of thin ribbons, some thicker ribbons, and some large globs of 2-3 μm size (Figure 4.17 – the darker grey phase leading from the iron interface at the top of the micrograph). These features were found as far as 40-80 μm deep into the iron (3-6 grain diameters). It could be possible that the higher heat at 500°C allowed the Γ phase to form larger shapes within the grain boundary. Even though the Γ phase was in larger shapes, the overall amount of Γ phase was less than that observed for samples at 400°C. Per sample, only 2-3 regions were found with Γ phase in the grain boundaries, whereas for each sample created at 400°C, the Γ phase was found all across the diameter of the iron rod.

Diffusion at 725°C

For samples of 99.99% zinc – 99.95% iron, heated at 725°C for 96 hours, there was no detectable Γ phase in the iron grain boundaries (Figure 4.18 – the iron interface is at the top of the micrograph). There was no evidence of Γ phase, even as far as 80 μm depth into the iron. If Γ phase existed in this area, it would have to be in a very thin or small shape. The only place where Γ phase showed signs of existing was in the first grain boundaries away from the interface (~5 μm into the iron, or about half a grain diameter). There might have been some very small Γ phase particles in amongst the grain boundaries, but nothing was conclusive.

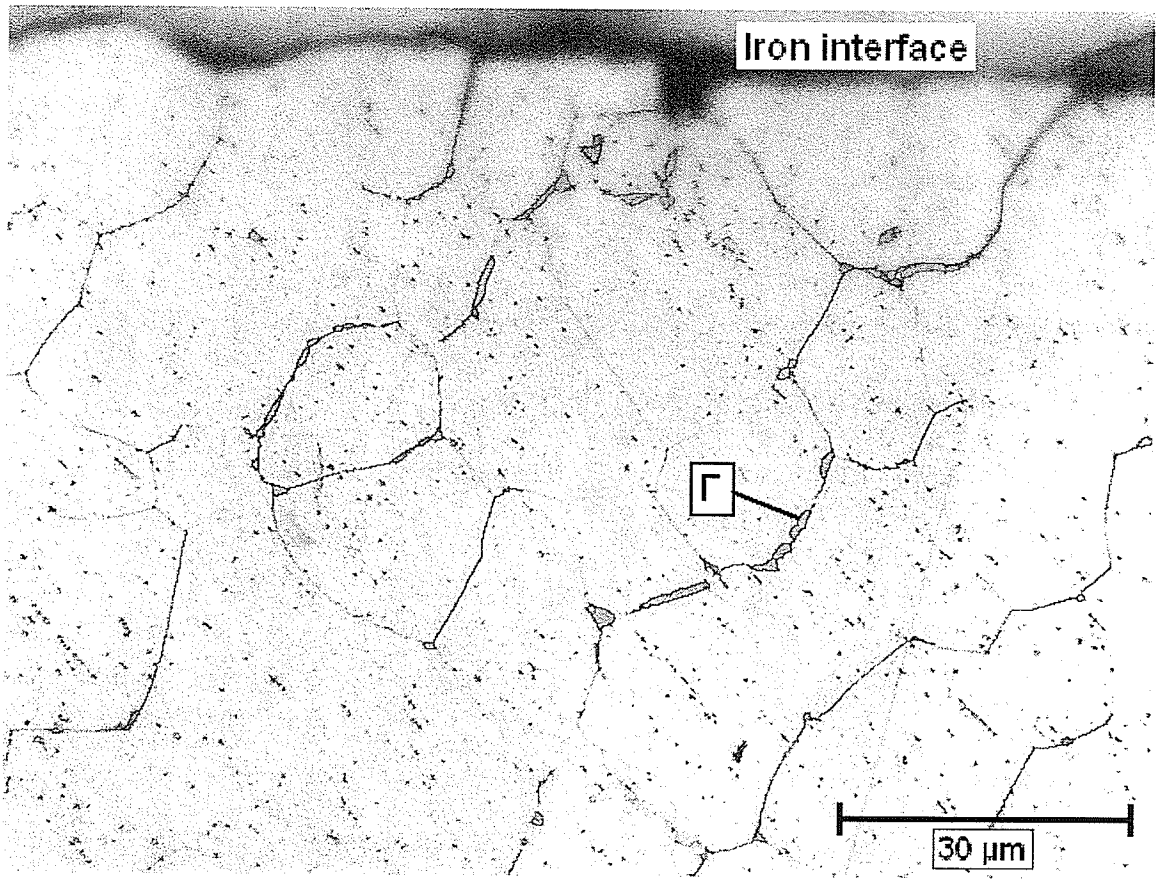

Figure 4.17: Etched iron microstructure, formed at 500˚C, for 96 hours (*Mag 1000x*).

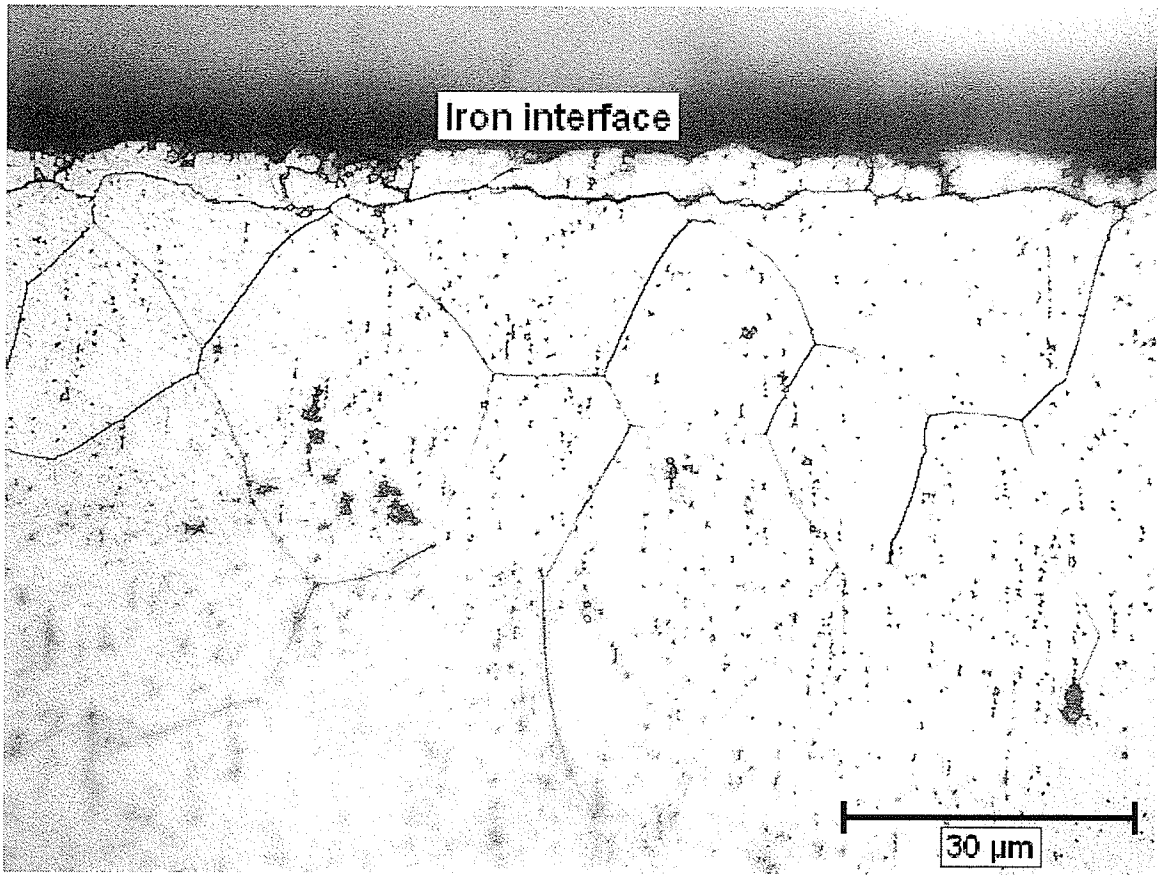

Figure 4.18: Etched iron microstructure, formed at 725˚C, for 96 hours (*Mag 1000x*).

4.1.3 Zinc Concentration Gradient

The zinc concentration gradients for the three sample temperatures (400°C, 500°C, and 725°C) were all produced in the same manner, using the SEM procedure previously described in Sections 3.8 and 3.9. All composition analysis was performed on samples that were in an as-polished, unetched state.

Diffusion at 400°C

A concentration gradient produced by the interdiffusion of zinc and iron, measured in one of the samples held at 400°C for 96 hours, is shown in Figure 4.19. The pattern produced by the change of zinc concentration with distance was the standard diffusion S-curve. The concentration started at 68-70 at% zinc (the zinc concentration of Γ phase), then quickly dropped across the narrow, 10 μm thick α-Fe – Γ two-phase region, to 2-3 at% zinc in the solid iron region. The zinc concentration then slowly tapered off to 0 at%, about 25-40 μm into the iron. In addition, from Figure 4.19, the shape of the zinc concentration gradient was asymmetrical. An asymmetrical zinc concentration gradient was found in all samples, for all three temperatures. The asymmetrical gradient does not necessarily mean that the diffusion of zinc into iron varied with zinc concentration. The main cause of the asymmetry could be due to the different diffusion coefficient of zinc through each phase in the iron-zinc diffusion zone (for example: the diffusion coefficient of zinc into ζ phase is 2.6×10^{-13} m^2/s, at 400°C [23]).

The zinc concentration gradient at 400°C was recorded from samples produced by both experimental methods. The results of all samples performed at 400°C for 96 hours are plotted in Figure 4.20. The data on this chart came from both sample methods: the poured liquid metal technique (▲), and the vacuum chamber technique (■). Multiple readings for each sample were also placed on this chart, for example: two poured liquid metal samples were produced, with three readings taken from each sample, therefore six triangles were drawn at each reading distance.

From Figure 4.20, the data was scattered, yet showed a general trend similar to the single concentration gradient shown in Figure 4.19. The difference between the two experiment procedures was also noticeable. The samples made from the vacuum chamber method, on average, had slightly less zinc penetration into the iron than the samples made from the poured liquid metal method. It was decided that the difference was not great and therefore the results for all the experiments conducted at 400°C were simply averaged to obtain a representative concentration – penetration curve. The average zinc concentration gradient formed at 400°C is shown in Figure 4.21.

Diffusion at 500°C and 725°C

Zinc penetration profiles in the iron were also determined for diffusion anneals at temperatures of 500°C and 725°C for 96 hours. A representative profile was calculated for each temperature, and then charted (Figure 4.21). As shown in Figure 4.21, the zinc concentration gradient produced in the iron at 500°C and 725°C was generally the same shape, but much steeper than, the gradient produced in the iron at 400°C.

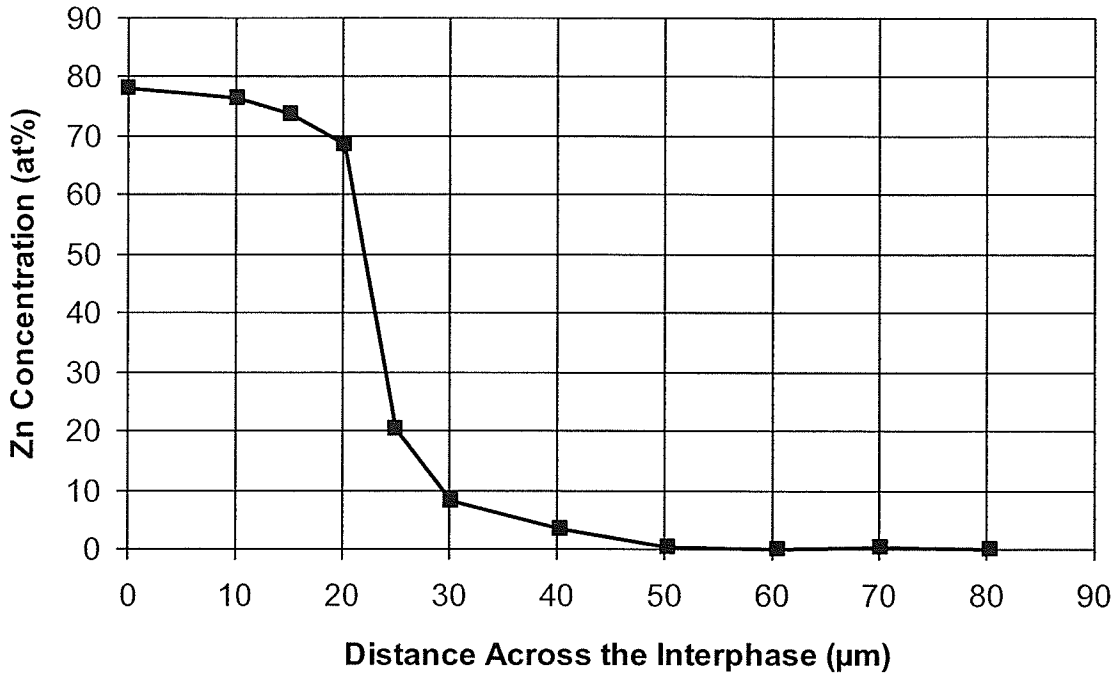

Figure 4.19: Zinc concentration gradient in Sample #81 (400°C for 96 hours).

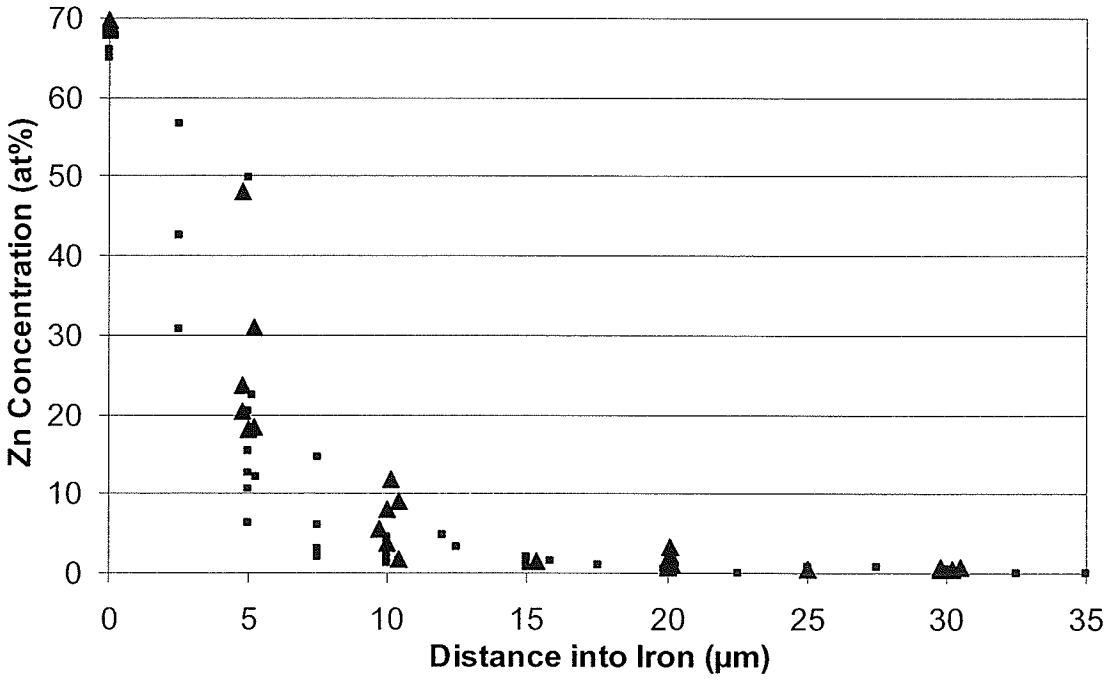

Figure 4.20: Data points of all samples performed at 400°C, for 96 hours.

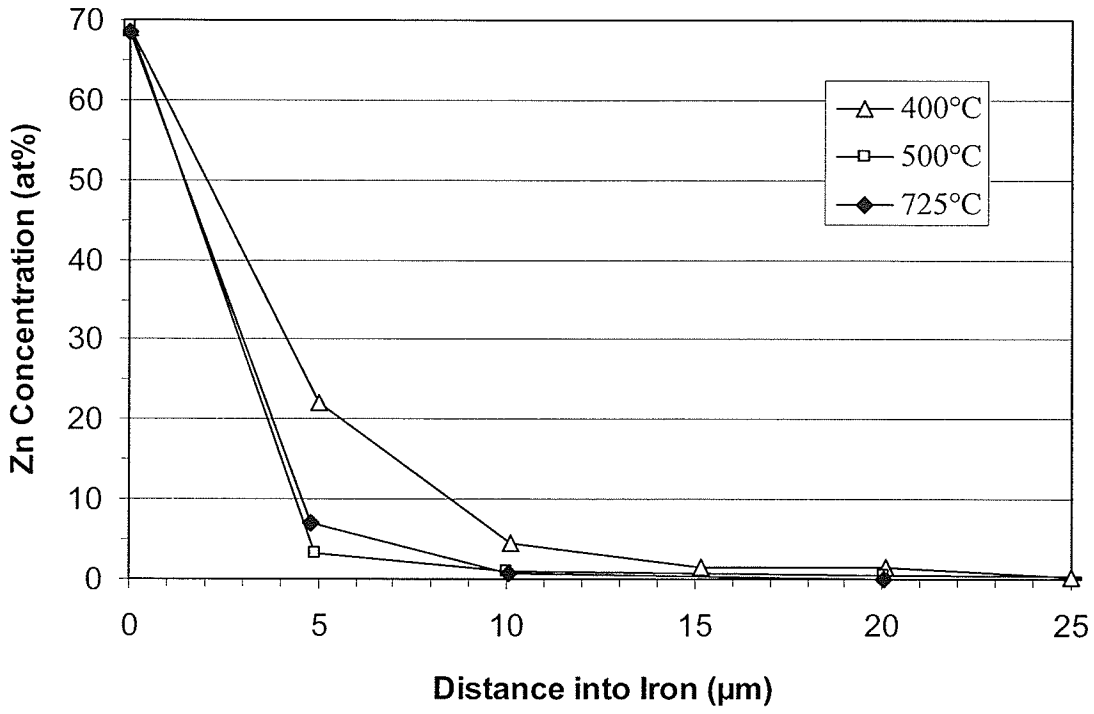

Figure 4.21: Average coarse zinc concentration gradient for 400˚C, 500˚C, and 725˚C.

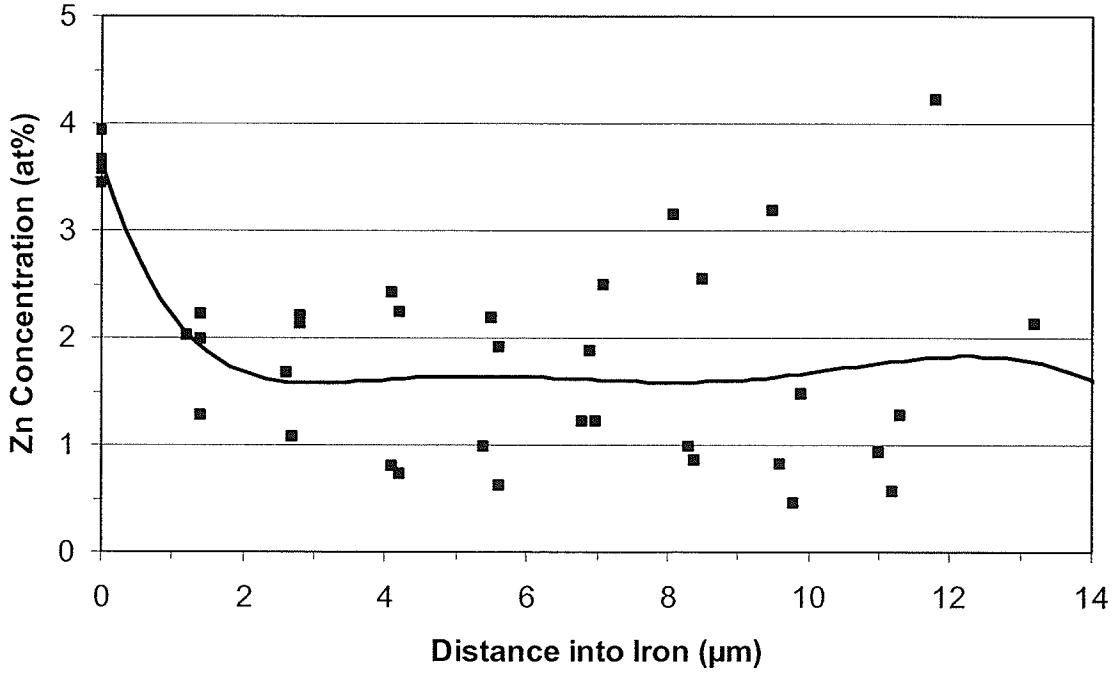

Figure 4.22: Fine zinc concentration gradient for 400˚C.

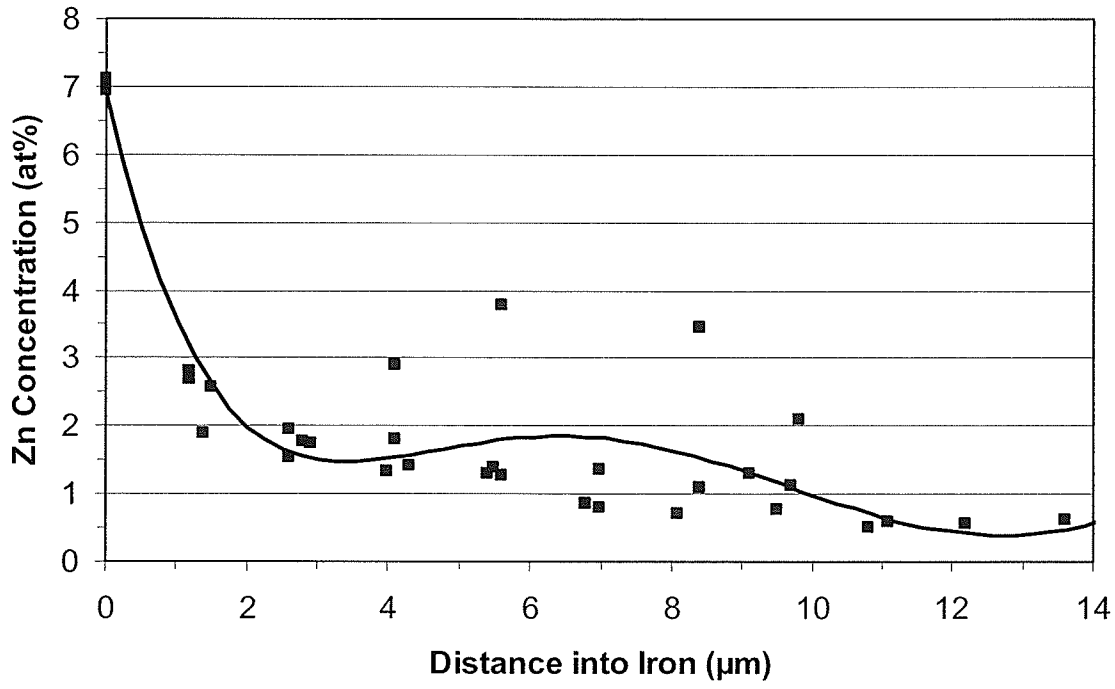

Figure 4.23: Fine zinc concentration gradient for 500˚C.

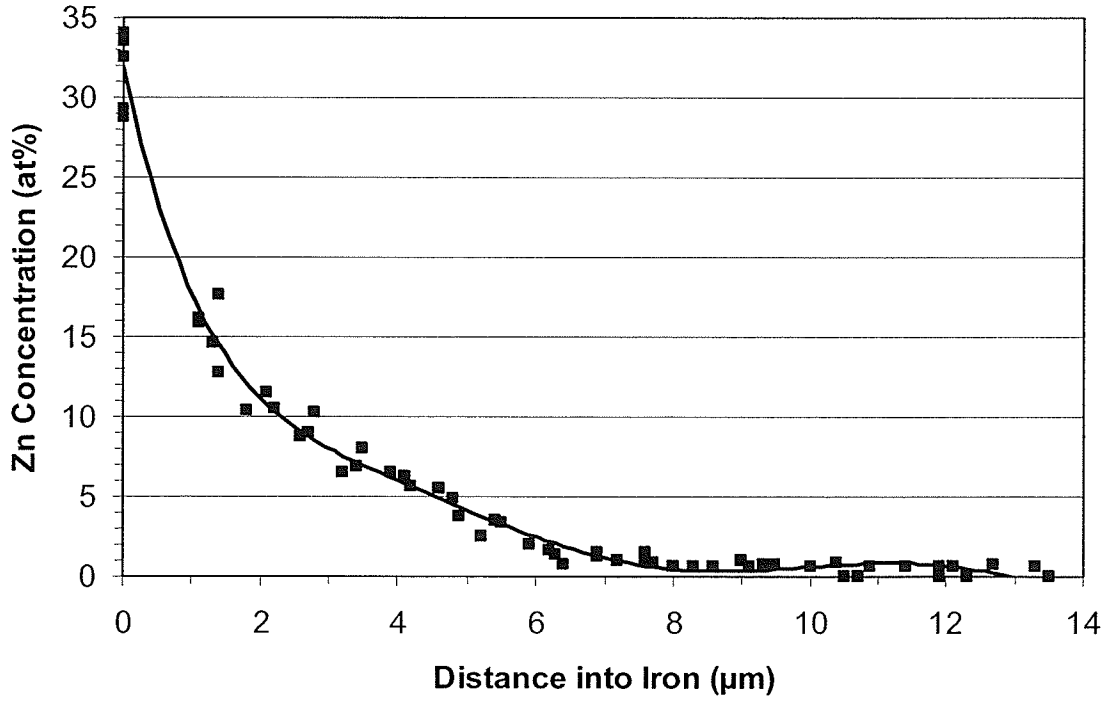

Figure 4.24: Fine zinc concentration gradient for 725˚C.

4.1.4 High Precision Zinc Concentration Gradient

A fine, detailed measurement of the zinc concentration gradient in a sample produced at 400°C is shown in Figure 4.22. The detailed measurement was from a single sample, with four concentration gradients recorded. The fine concentration gradients were measured at a SEM magnification of 2000x, whereas the coarse gradients (averages shown in Figure 4.21) were produced from SEM magnifications of 500-1000x (usually 750x magnification). The fine gradients were produced in a similar manner as the coarse gradients, but with narrow ~1.0 μm by 70.0 μm analyzed sections, and with analyzed sections measured one beneath the other (the section steps were ~1.4 μm). The analyzed section widths/steps are depicted by the black squares (■) in Figure 4.22.

Two locations near the center of the iron rod were chosen as sites to record the fine gradients. From each of the two sites, two gradient recordings were measured – one beside the other. The two recordings at each site effectively formed a gradient that measured ~150 μm wide – similar to the width of an individual recording at 1000x magnification. This method of recording the fine zinc concentration gradients ensured that non-biased measurement was maintained (an adequate sampling of the iron was measured). All four recordings from the sample were charted on Figure 4.22. A 6^{th} order polynomial equation was then plotted through the data points to form a trendline. The 6^{th} order polynomial equation from the data measured at each of the three experiment temperatures is presented in Appendix A.

The method that was used to measure the fine zinc concentration gradient in a sample produced at 400˚C was duplicated for samples produced at 500˚C and 725˚C. A fine measurement of the zinc concentration gradient from a single sample produced at 500˚C is shown in Figure 4.23 (using four gradient recordings), and a fine measurement of the zinc concentration gradient from a single sample produced at 725˚C is shown in Figure 4.24 (using six gradient recordings).

4.1.5 Iron Diffusion

As the zinc diffused into the iron, the iron diffused into the zinc. At certain temperatures, the diffusion of iron atoms will reduce the volume of the iron rod segment; therefore the dimensions of the iron rod will change with time (become smaller). The experiments were designed to restrict zinc diffusion to one direction – into the top of the iron rod. This restriction also limited the direction of the iron diffusion to just from the top of the iron rod. The end result was that any dimensional change in the iron rod would be in only one direction – off the length of the rod.

The decrease in the length of the iron rod after the diffusion anneal was easily determined: the distance of the iron interface shift, ε, was measured from the iron interface to the end of the remnant iron oxide casing found in the diffusion zone (the oxide on the circumference of the iron rod, which was left intact after the pre-heat treatment, formed a tube when the interior iron dissolved away). The iron oxide casing did not dissolve, break away, or move much during the diffusion anneal (as shown in

Figure 4.12 – the iron oxide casing is the black, 50 μm thick, 1 mm long extension on the left side of the micrograph). The iron oxide casing allowed for the original length and position of the iron rod to be observed and measured. Thus the iron oxide that was left on the iron rod after pre-heat treatment served two purposes: to protect the iron from diffusion into the sides of the iron rod, and to serve as a marker for the measurement of the iron interface shift.

The amount of iron dissolution, or the distance of movement of the iron interface, found at each temperature was as follows.

400°C:	50 μm
500°C:	500 μm
725°C:	7000 μm

The movement of the iron interface, or rapid movement in the case of 725°C, may explain why less Γ phase was found at the iron interface at 500°C and 725°C, than at 400°C. Subsequently, it may be the reason why not much Γ phase was found in the grain boundaries at 500°C, and that no Γ phase was found in the boundaries at 725°C. The rapid movement of the iron interface, due to the rapid rate of diffusion of iron in liquid zinc, was the reason for the large amounts of δ and ζ phases found at far distances in the zinc in the samples produced at 725°C.

Although not the primary focus of the research, the iron diffusion into the zinc (or iron dissolution) was an important by-product of the pure metal iron-zinc reaction. The diffusion of iron into the zinc depended largely on the temperature, and subsequently

the state of the metals, in the experiment. Iron diffusion was also dependent on the quantity of the diffusing media. Iron diffusion was shunted in couples containing low volumes of zinc, but had free reign in relatively large pools of zinc (>40g).

4.1.6 Diffusion Coefficients

The diffusion coefficient for zinc into iron was calculated at all three temperatures (400°C, 500°C, and 725°C). The diffusion coefficients were derived from using the following partial differential equation.

(4.1) $$\frac{\partial c}{\partial t} = D\frac{\partial^2 c}{\partial x^2} + V\frac{\partial c}{\partial x}$$

The first two components of Eq. (4.1) come from Fick's second law of diffusion, assuming the diffusion coefficient, D, is constant with position (concentration). The last component of Eq. (4.1) is the term for the boundary movement. The boundary movement is derived from the shift in the position of the iron interface after the diffusion time. The position of the iron interface, ε, is given by:

(4.2) $$\varepsilon = K\sqrt{(D*t)}$$

The values used for ε come from Section 4.1.5. Differentiating Eq. (4.2) with respect to time gives the velocity of the iron interface:

(4.3) $$V = \frac{\partial \varepsilon}{\partial t} = \frac{K\sqrt{D}}{2\sqrt{t}}$$

Solving Eq. (4.2) for K, and substituting into Eq. (4.3) gives:

(4.4) $$V = \frac{\varepsilon}{2t}$$

Substituting Eq. (4.4) into Eq. (4.1) gives:

$$\frac{\partial c}{\partial t} = D\frac{\partial^2 c}{\partial x^2} + \frac{\varepsilon}{2t}\frac{\partial c}{\partial x} \tag{4.5}$$

The boundary movement term can be neglected, since numerical calculations showed that it would require ε to be 200 000 μm to make a small difference in the zinc concentration gradient. An ε of 7000 μm, as found in the samples held at 725°C, had a small, negligible effect on the zinc concentration gradient in the iron. Thus, Eq. (4.5) becomes:

$$\frac{\partial c}{\partial t} = D\frac{\partial^2 c}{\partial x^2} \tag{4.6}$$

Solving Eq. (4.6) using the boundary point $C = C_0$, for $x = 0$ at $t > 0$ (infinite system, constant surface concentration) gives:

$$C(x, t) = (C_0)^*[1 - \text{erf}(x / 2\sqrt{(D^*t)})] \tag{4.7}$$ [17]

Where: C_0 = concentration of solute (Zn) at the surface.
x = the depth into the iron (μm).
t = 345 600 s (96 h diffusion time).
D = diffusion coefficient (m^2/s).

The equation used for modelling the diffusion behaviour thus took the form of the error function. The function derived, Eq. (4.7), was for constant surface concentration in the solvent (the iron), which was assumed from the diffused structure of the experiments. This can be assumed since Γ phase formation occurs relatively quickly (30 s) [7], and the Γ phase remained for the entire diffusion duration, at all three temperatures. Since the Γ phase existed, then the maximum zinc concentration in the iron will be the value found in the α-Fe region, at the respective experiment temperature. The surface of the iron

(iron interface) will have this zinc concentration for the entire diffusion time. The value for C_0 used in Eq. (4.7) was the following.

400°C:	3.66 at% Zn
500°C:	7.05 at% Zn
725°C:	33.5 at% Zn

The time variable, t, in Eq. (4.7) was always 345 600 s (96 h diffusion time). The depth into the iron, x, used an array of values starting from 0 μm, and then increased in increments of 1.25 μm. The diffusion coefficient, D (or D_{Zn}), was then arbitrarily set, and the resultant gradient was plotted over the experimental zinc concentration gradient. The position of the numerical model gradient was shifted on the plot (using an offset on the x-axis) so that C_0 (the starting point) was approximately equal to the corresponding position on the experimental gradient (Figure 4.25). The value of the diffusion coefficient was then varied until the plotted numerical function fit the experimentally derived zinc concentration gradient (Figure 4.25). Once the optimum was achieved, the diffusion coefficient was recorded.

The diffusion coefficients calculated for zinc diffusion into solid 99.95% iron, at each experimental temperature, are shown in Table 4.1. As shown in Table 4.1, two methods of calculating the zinc diffusion coefficient were used. One method of determining the coefficient was by comparing the numerical model to the average zinc concentration gradient of all the results, at a given temperature. The values calculated by this method are presented in the second column of Table 4.1.

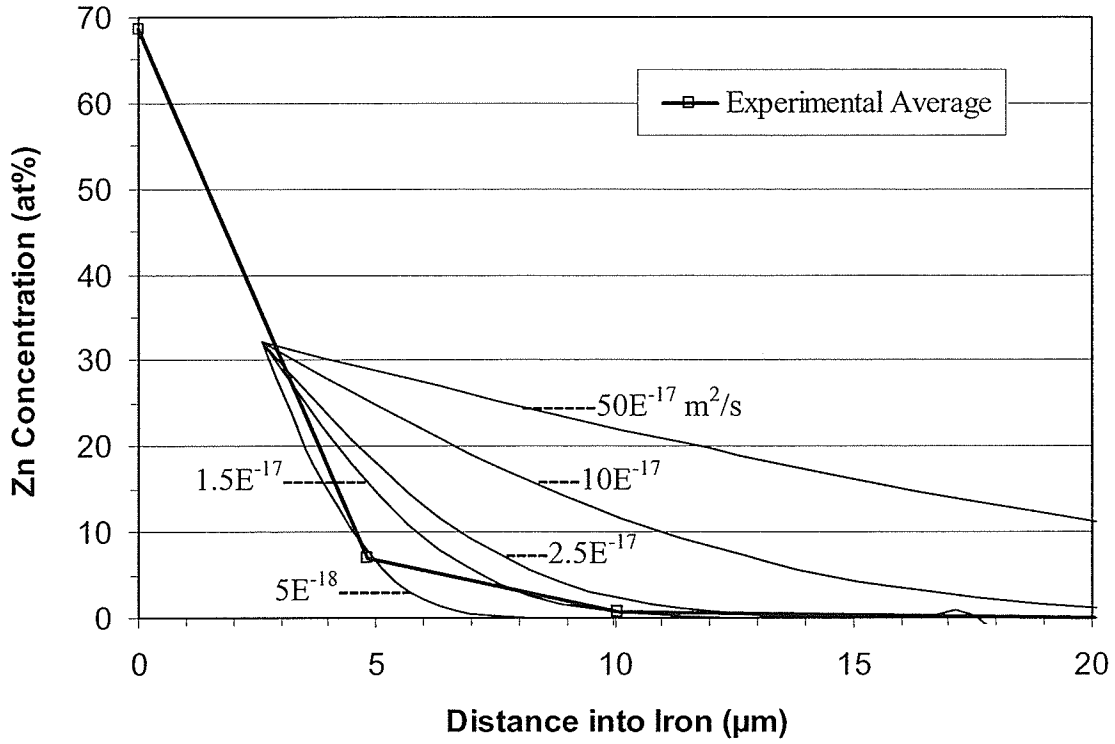

Figure 4.25: Coarse zinc concentration gradient for 725°C, showing derivation of D_{Zn}.

Table 4.1: Zinc Diffusion Coefficients in Iron

Temperature (°C)	From average sample gradient (m^2/s)	Average of the D_{Zn} from each sample gradient (m^2/s)	From the fine zinc concentration gradient (m^2/s)
400	1-3 x 10^{-17}	2.13-3.13 x 10^{-17}	1.5 x 10^{-17}
500	1.25-1.5 x 10^{-17}	1.17 x 10^{-17}	1.6 x 10^{-17}
725	1.5 x 10^{-17}	1.55 x 10^{-17}	1.7 x 10^{-17}

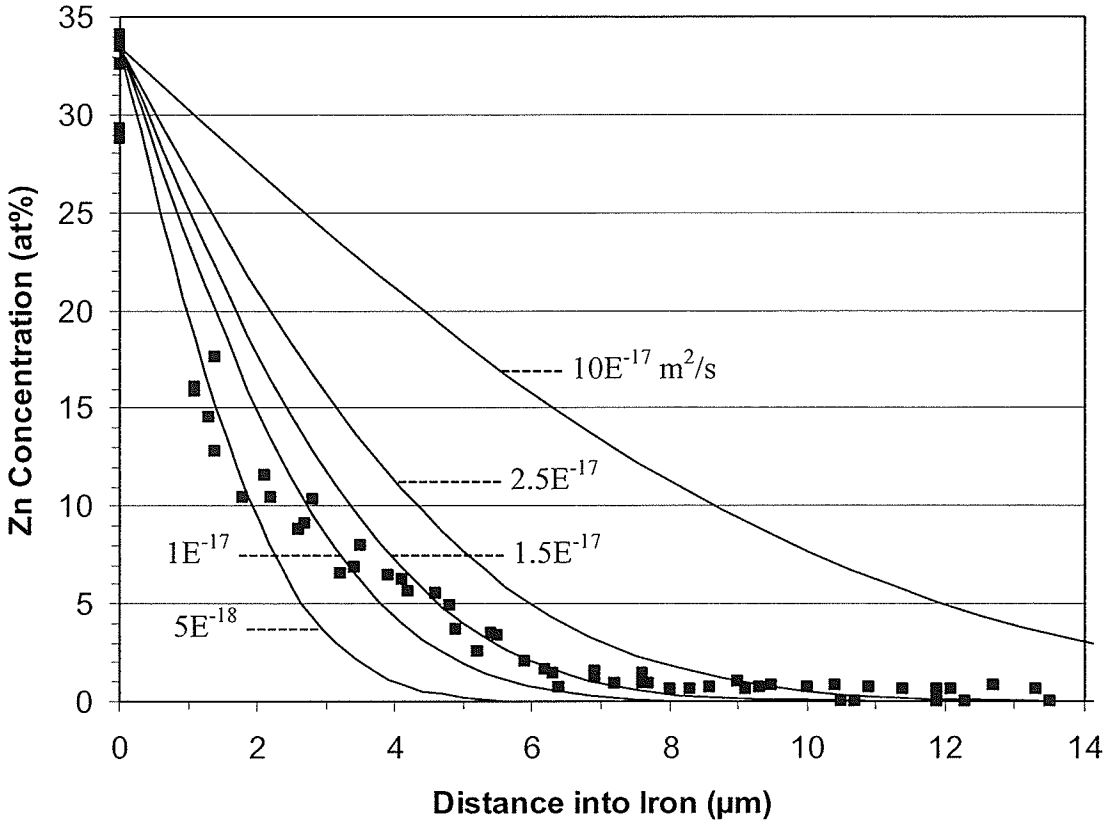

Figure 4.26: Fine zinc concentration gradient for 725˚C, showing derivation of D_{Zn}.

Another method of deriving the diffusion coefficient involved fitting the error function to each individual sample concentration gradient. The diffusion coefficient was obtained from each sample gradient, and then the diffusion coefficients were averaged for the respective temperatures. The diffusion coefficients calculated by this method are presented in the third column of Table 4.1. Comparing the values of the derived zinc diffusion coefficients in Table 4.1, the two methods of averaging the diffusion coefficient were in good agreement.

4.1.7 High Precision Zinc Diffusion Coefficients

The initial zinc diffusion coefficients (the values shown in Table 4.1) were calculated from coarse zinc concentration gradients. While the initial results were satisfactory, conclusive values required higher precision measurements. After the initial values were obtained from the coarse zinc concentration gradient, a single iron-zinc diffusion sample from each of the experiment temperatures was re-analyzed on the SEM and EDS. A fine, more precise zinc concentration gradient in the iron was measured from the selected samples, with the results shown in Figures 4.22, 4.23, and 4.24.

The concentration gradient from the numerical model, Eq. (4.7), was then plotted over the fine experimental zinc concentration gradient data points, and the high precision diffusion coefficient of zinc in iron (D_{Zn}) was recorded. The data for Eq. (4.7), and the method used to derive the zinc diffusion coefficient, were the same as used on the coarse zinc concentration gradients. An example of this method is shown in Figure 4.26, which

is the fine data points for a sample produced at 725°C, showing a variation in the numerical zinc diffusion coefficient, D_{Zn} (the optimum was determined to be 1.7×10^{-17} m^2/s). A summary of the high precision zinc diffusion coefficients derived from the fine zinc concentration gradients is found in Table 4.1.

Variable zinc diffusion coefficients

From the fine zinc concentration gradient measured in the sample produced at 725°C (Figure 4.26), it was determined that the zinc diffusion coefficient derived from Eq. (4.7) was not a good enough fit (the 2nd, 3rd, and most of the 4th points from all six gradient recordings were a much less zinc concentration than calculated with the numerical model with the optimum D_{Zn} of 1.7×10^{-17} m^2/s). It was determined that to provide a better fit to the data points, the value of the zinc diffusion coefficient must vary with zinc concentration. A finite difference program developed by Cahoon et al. [24] was used for this calculation. Shown in Figure 4.27, the numerical model with varying D_{Zn} fits better to the data points, than the numerical model with constant D_{Zn}. The variation of the zinc diffusion coefficient versus zinc concentration at 725°C is shown in Figure 4.28.

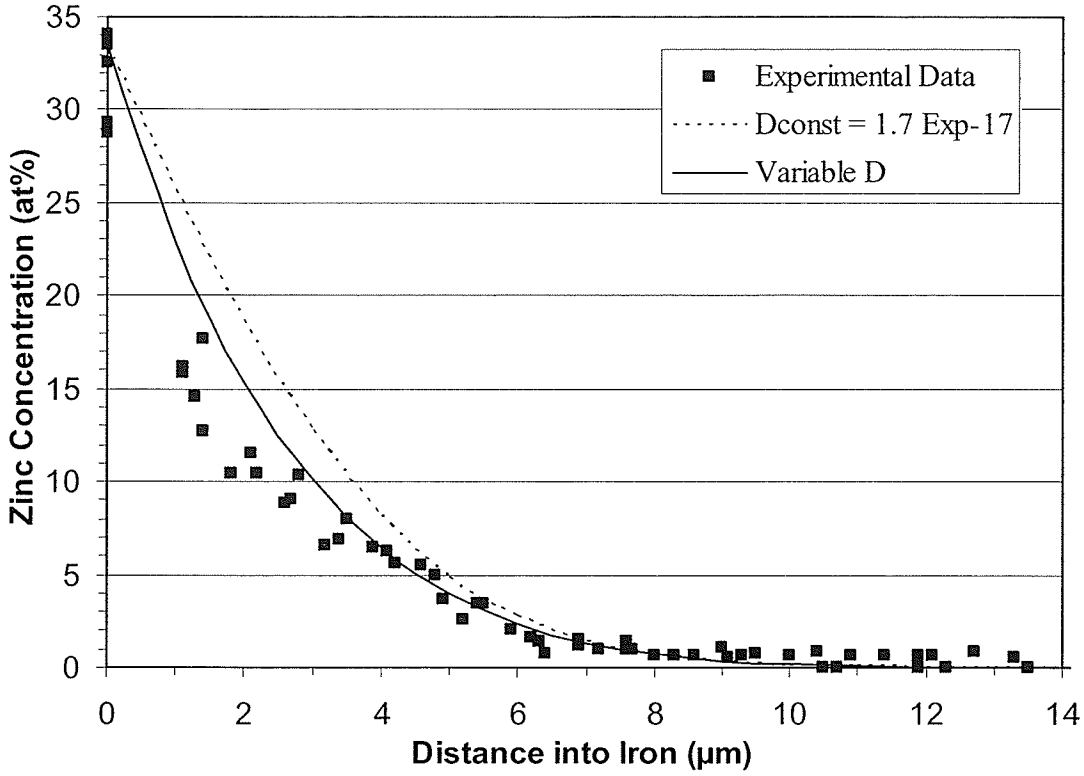

Figure 4.27: Fine zinc concentration gradient for 725°C, with varying D_{Zn}.

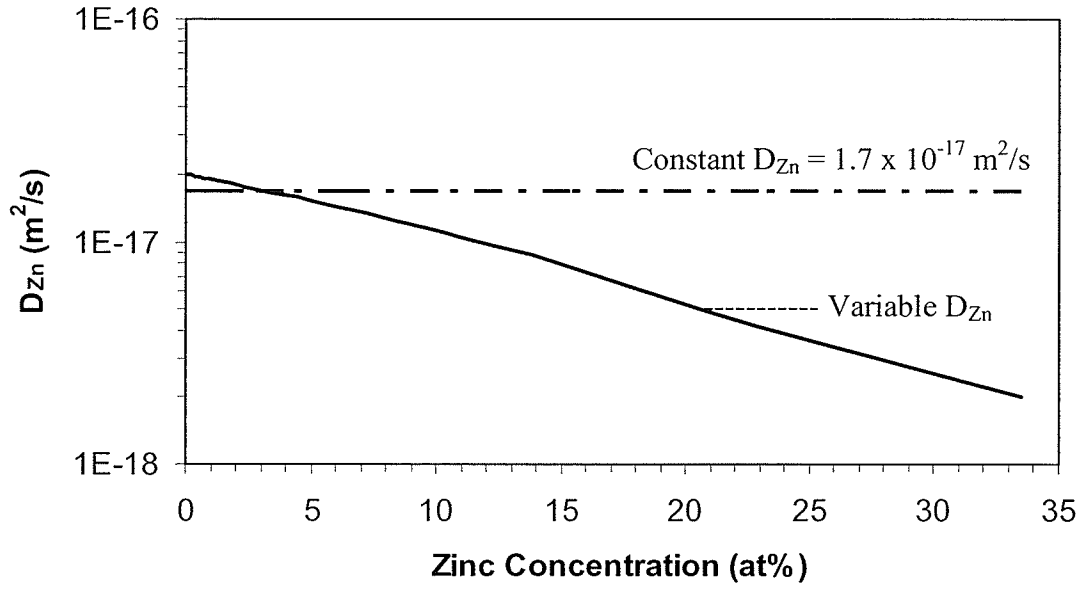

Figure 4.28: Variation of D_{Zn} with zinc concentration in iron, for 725°C.

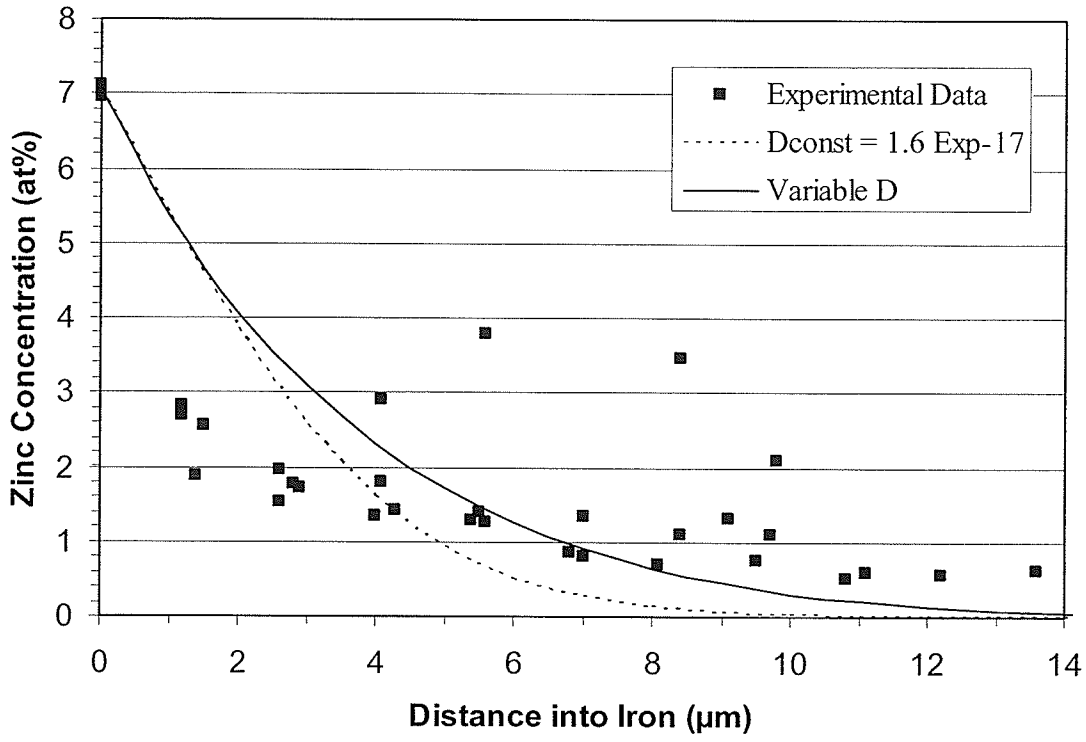

Figure 4.29: Fine zinc concentration gradient for 500°C, with varying D_{Zn}.

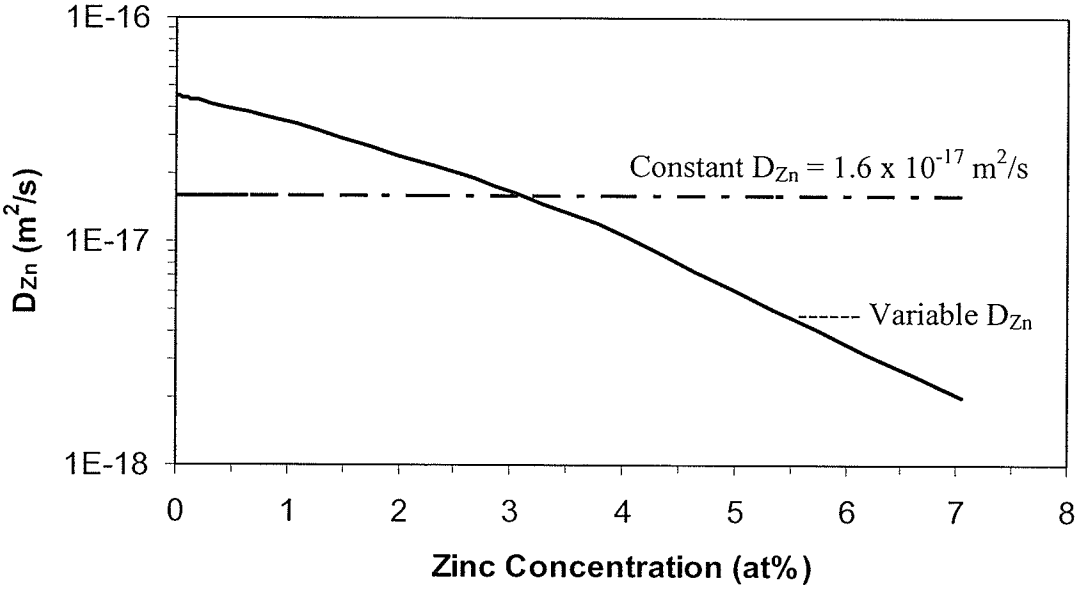

Figure 4.30: Variation of D_{Zn} with zinc concentration in iron, for 500°C.

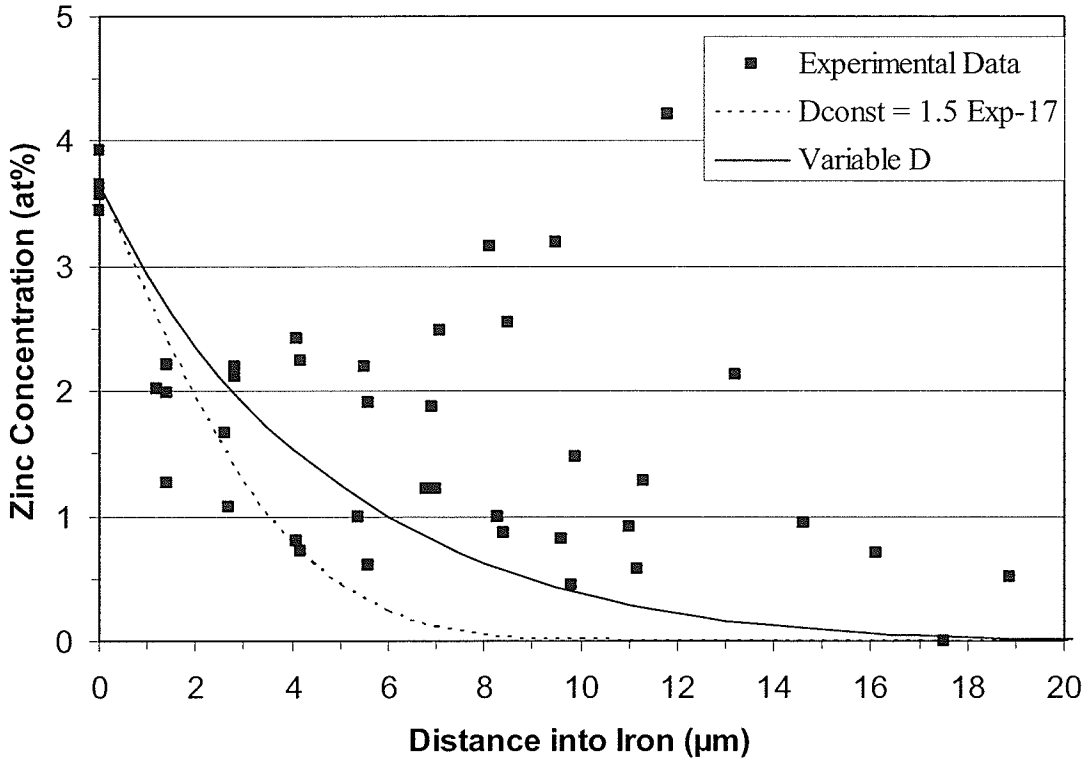

Figure 4.31: Fine zinc concentration gradient for 400°C, with varying D_{Zn}.

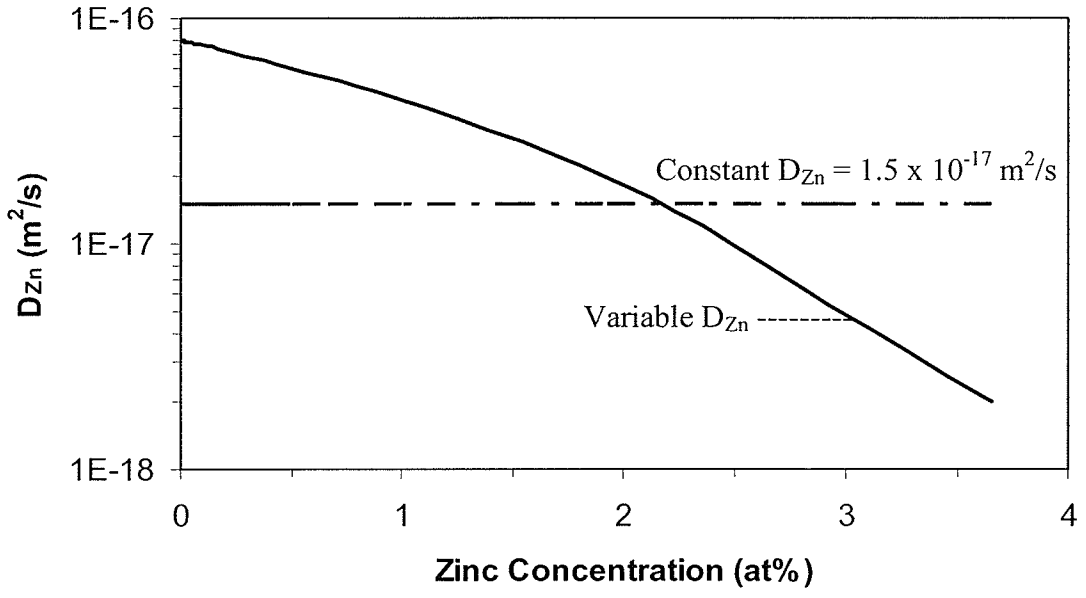

Figure 4.32: Variation of D_{Zn} with zinc concentration in iron, for 400°C.

The calculated zinc penetration curve for diffusion at 500°C using a varying diffusivity is compared to the experimental data points in Figure 4.29, and the variation of diffusivity with zinc concentration is shown in Figure 4.30. The equivalent plots for zinc diffusion at 400°C are given in Figure 4.31 and Figure 4.32, respectively. The constant D_{Zn} values used for the calculations in Figures 4.27, 4.29, and 4.31 were reasonable intermediate values, and are shown in Figures 4.28, 4.30, and 4.32.

It is clear from Figures 4.28, 4.30, and 4.32 that the zinc diffusion coefficient increases greatly (factors of 10 or more) with a decrease in zinc concentration. This is consistent with the combined effects of bulk and grain boundary diffusion. Near the α-Fe interface, bulk diffusion predominates and the diffusion coefficient is low. As the distance from the α-Fe interface increases, grain boundary diffusion becomes dominant. The zinc diffusion coefficient determined at each temperature in this investigation is therefore a combination of both bulk and grain boundary diffusion, and is thus an "apparent" diffusion coefficient.

4.2 Heat Treated Galvanized Steel

4.2.1 As-Polished Microstructure

The diffused structure produced in the heat treated galvanized steel was similar to the structure produced in the pure metal experiments. Major differences existed however.

1) There was always an outer layer of zinc oxide (ZnO) on the heat treated galvanized steel. The tool steel wrap reduced, but did not eliminate, the oxide scale. The oxygen consumed some of the zinc that was coated on the steel. Sealing the strips of galvanized steel in Vycor with an argon atmosphere might have reduced the amount of oxide, but this was not performed due to the time consuming procedure of sealing Vycor. The objective of the heat treated galvanized steel was not important enough, and the results obtained were good enough, to warrant a more sophisticated, and lengthy, experiment procedure.
2) Due to the limited amount of zinc involved, only the iron-rich phases were found on the galvanized steel after the diffusion anneal. This was different than the diffused pure metal structure, but it does foreshadow what would occur in the pure metal samples (400°C and 500°C) if they were held at the temperature for a longer time than 96 hours.
3) Outbursts of intermetallic compounds were found. The intermetallic compound outbursts were caused by aluminum intermetallic inhibition layer breakdown [7]. Readings of 0.55 at% aluminum were found in the bulk of the zinc layer in the

as-received galvanized steel, while at the iron-zinc interface, readings of as high as 5.15 at% aluminum were found. The higher aluminum concentration at the iron-zinc interface indicates that a thin layer of $Fe_2Al_5Zn_X$ was present in the galvanized steel prior to heat treatment. The heat treatment process broke this layer down and caused the outbursts, similar to what was reported by Marder [7].

As with all samples, the galvanized steel samples were analyzed first in an unetched, as-polished state.

Diffusion at 400°C

The interphase created by heat treating galvanized steel at 400°C for 96 hours consisted of the following layers (from Figure 4.33).

From the steel to the zinc oxide:

1) Steel with equiaxed grains of ~5 μm size (Figure 4.33 – the dark layer at the bottom of the micrograph).
2) A two-phase region consisting of iron grains and Γ phase. The Γ phase is depicted as the light grey colour in Figure 4.33, which can be seen penetrating the grain boundaries of the first 3-4 grain layers of the steel. Figure 4.33 displays one of the outburst areas formed as a result of the heat treatment of the galvanized steel. In the outburst areas: towards the steel, thick bands of Γ phase in the grain boundaries; away from the steel, the grains were completely surrounded by Γ phase (Figure 4.33). Away from the outburst areas: long, thick, jagged bands of

Γ phase formed in the grain boundaries, under the first layer of iron grains (Figure 4.34 – the Γ is dark grey and the iron light grey, with the iron interface at the top of the micrograph). Due to the way the Γ phase grew, whole lengths of steel grains were isolated from the rest of the steel.

3) A thin discontinuous layer of Γ phase. Cracks were found running through the Γ phase layer, perpendicular to the iron interface (shown in Figures 4.33 and 4.34). The cracks would have formed in the δ phase, when it existed. The δ phase was eventually transformed into Γ phase, but the cracks remained.
4) A thicker continuous, two-phased layer of Γ and Γ_1 (Figure 4.33).
5) A continuous, two-phased layer of Γ_1 and δ.
6) A thin discontinuous layer of δ phase.
7) A spongy δ phase layer interspersed with ZnO.
8) A spongy ZnO layer (top layer of the micrograph in Figure 4.33).

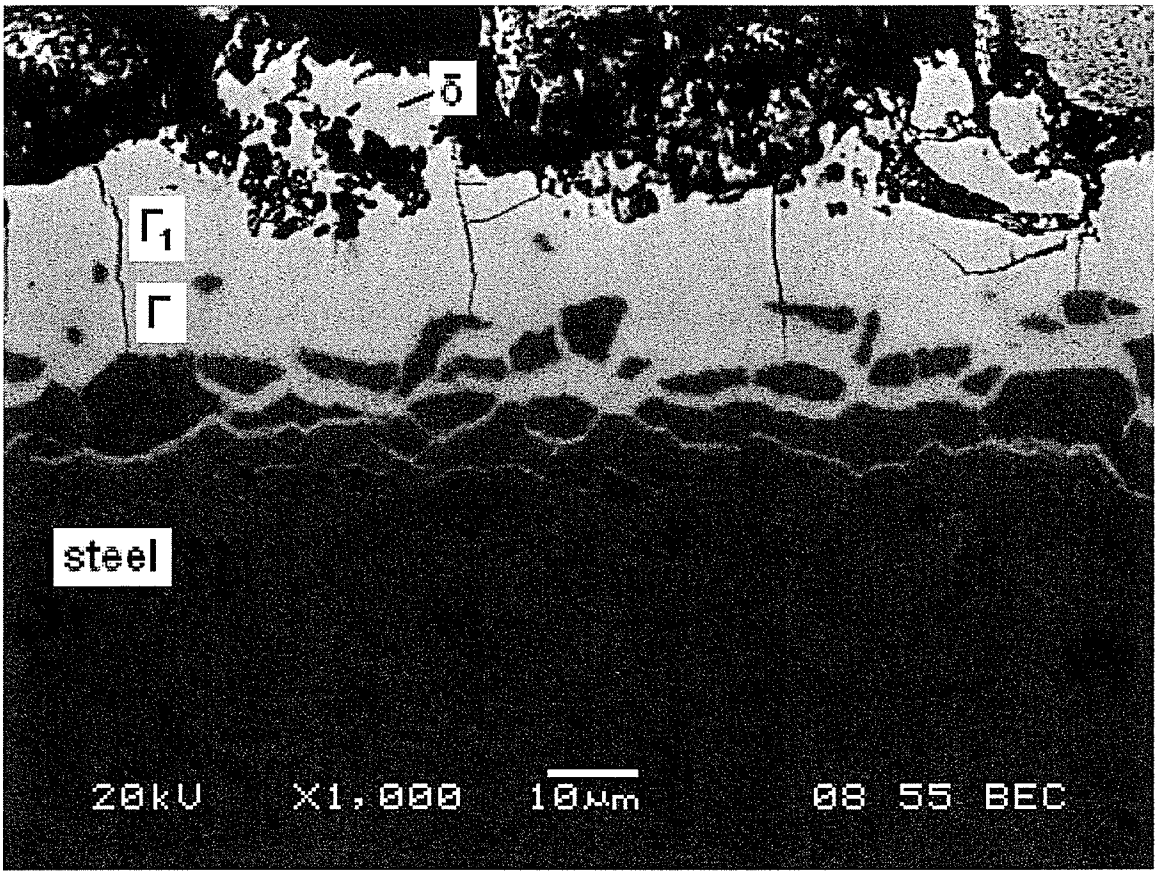

Figure 4.33: Galvanized steel structure, formed at 400˚C, for 96 hours (*Mag 1000x*).

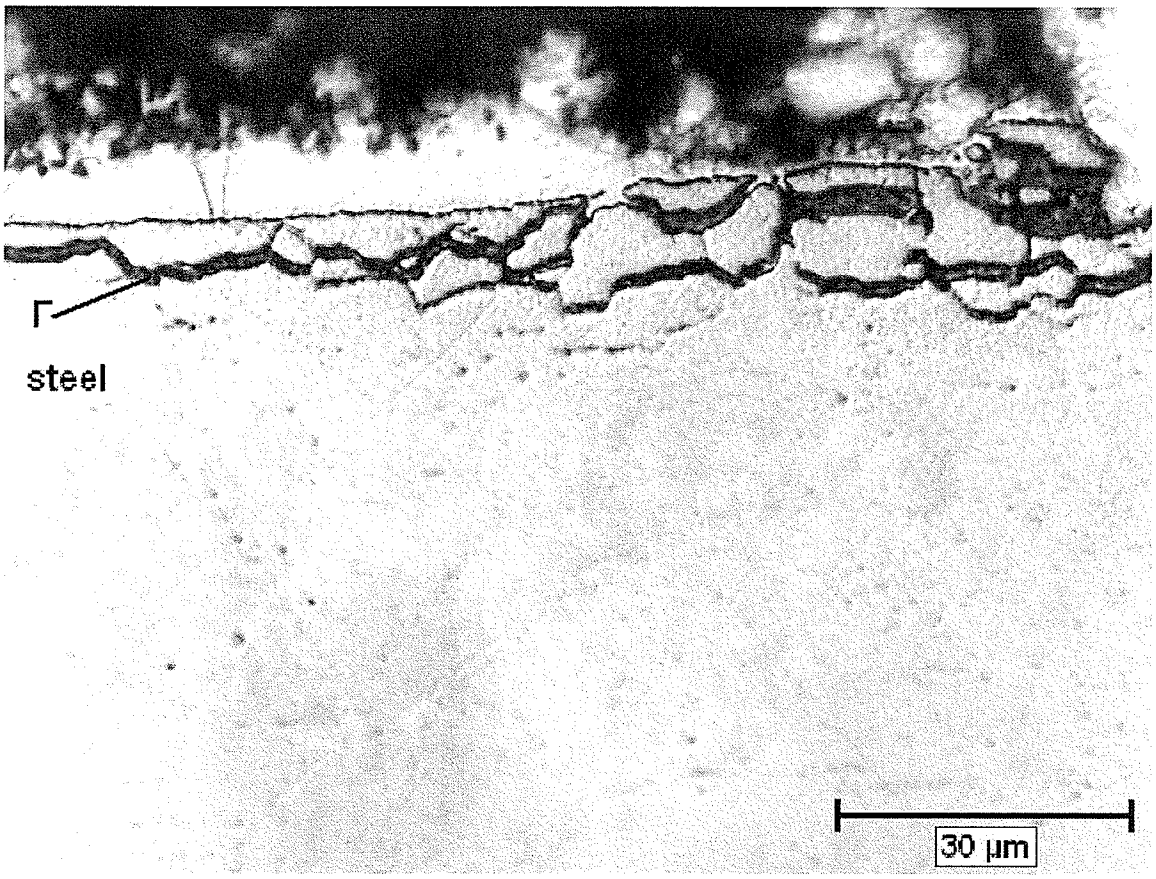

Figure 4.34: Γ phase formation under the first layer of grains in galvanized steel, formed at 400˚C, for 96 hours (*Mag 1000x*).

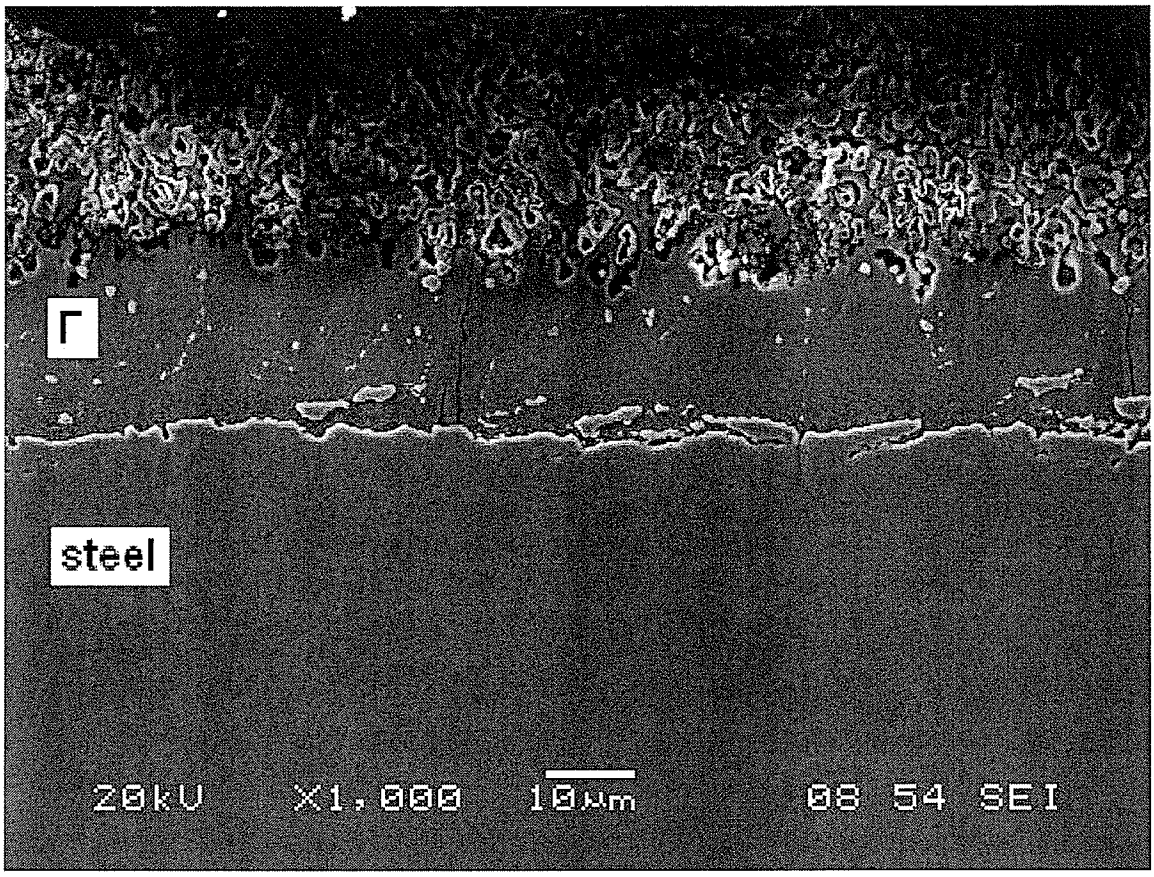

Figure 4.35: Galvanized steel structure, formed at 500˚C, for 96 hours (*Mag 1000x*).

Diffusion at 500°C

The interphase formed in galvanized steel, heat treated at 500°C for 96 hours, consisted of the following layers (from Figure 4.35).

From the steel to the zinc oxide:

1) Steel with equiaxed grains of ~5 μm in size (the solid layer on the bottom half of the micrograph in Figure 4.35).
2) A two-phase region consisting of iron grains and Γ phase in the grain boundaries.
3) A relatively thick, continuous layer of Γ phase (20-25 μm thick). Similar to galvanized steel heat treated at 400°C, cracks can be seen propagating through this layer, perpendicular to the iron interface. Again, this was a remnant of the δ phase layer.
4) A spongy Γ phase layer interspersed with ZnO.
5) A spongy ZnO layer (the top of the micrograph in Figure 4.35).

The only iron-zinc phase found in the samples of galvanized steel heat treated at 500°C for 96 hours was Γ phase. Due to the higher temperature, and the long diffusion anneal, all of the other intermetallic phases were eventually transformed into Γ phase.

4.2.2 Etched Microstructure

As in the pure metal samples, the etched iron microstructure developed from the interior of the steel to the outer areas, due to the galvanic effect. Again, the iron-zinc intermetallic layer on the steel was severely corroded as a result of the etching process. Another problem was that although an excellent etched microstructure of the steel was easy to produce, watermarks always ended up covering at least 90% of the steel-interfacial area.

For most of the watermarked area, the steel interfacial microstructure could still be observed using the various microscopes. The problem was that micrographs of these areas could not be produced due to the altered contrast caused by the watermark. As a result, the representative micrographs presented in the following pages were all taken from the few areas that were not watermarked. The features shown in these micrographs were all observed underneath the watermarks.

Diffusion at 400°C

When strips of commercial galvanized steel were heat treated at 400°C for 96 hours, there was a large number of small particles and ribbons of Γ phase found in the grain boundaries of the steel (Figure 4.36). In Figure 4.36, the steel interface was located at the top of the micrograph, and the Γ phase was the dark grey/black objects in the grain boundaries of the steel. There was a large number of Γ phase artifacts found in the grain boundaries, and they could be found to a depth of 40-80 μm into the steel.

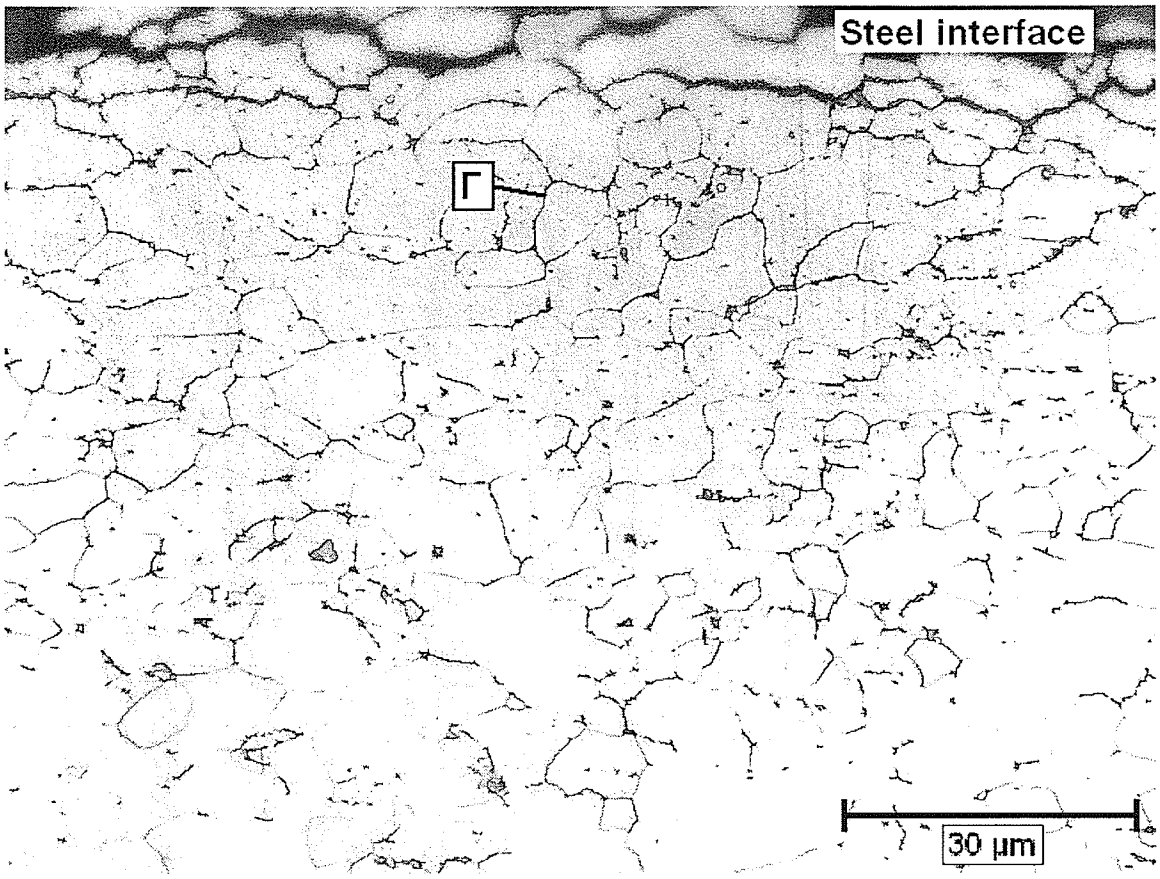

Figure 4.36: Etched galvanized steel microstructure, formed at 400˚C (*Mag 1000x*).

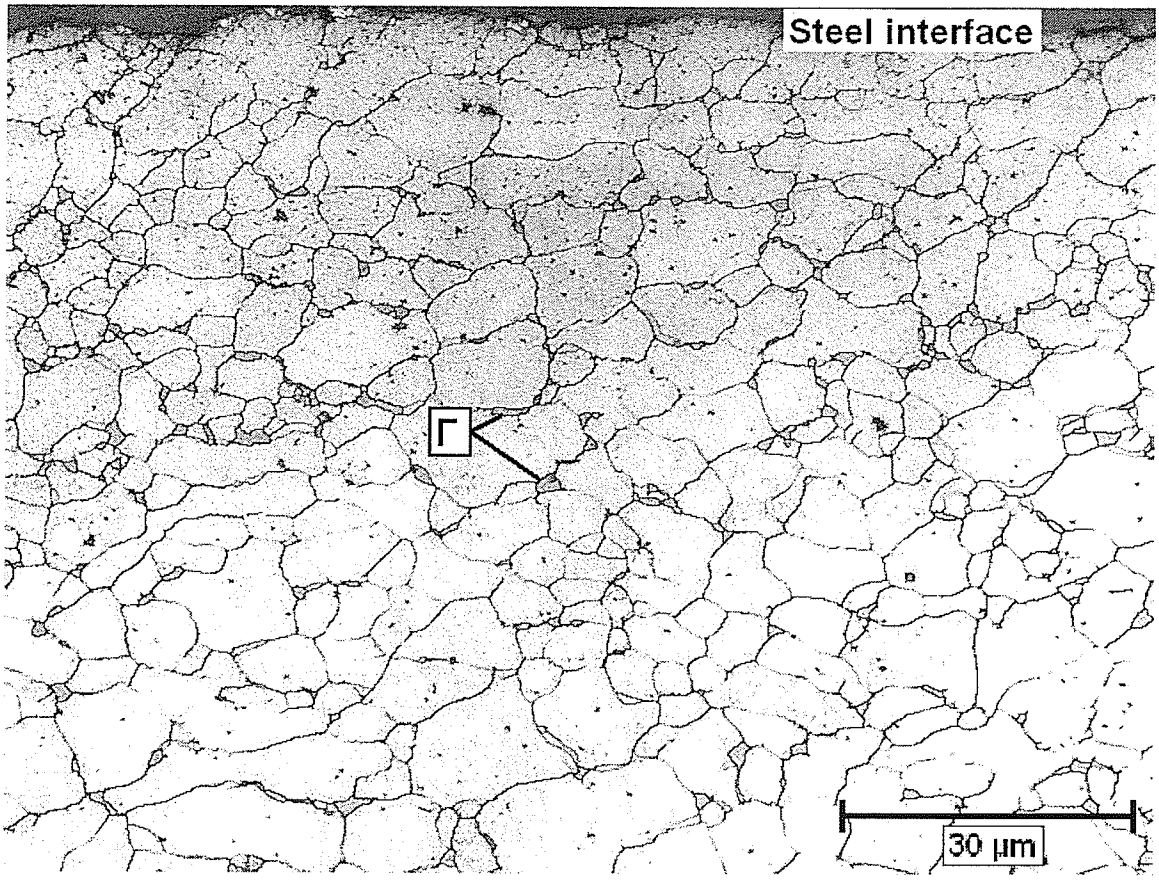

Figure 4.37: Etched galvanized steel microstructure, formed at 500˚C (*Mag 1000x*).

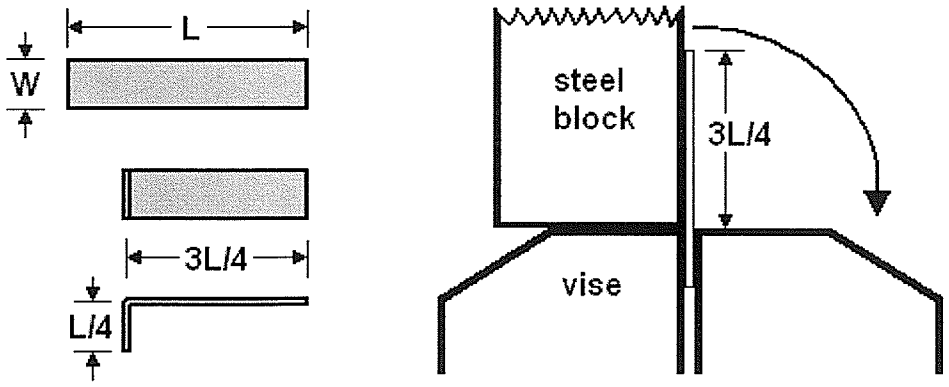

(a) (b)

Figure 4.38: (a) Schematics of non-bent and bent galvanized steel strip, (b) Diagram of bending apparatus.

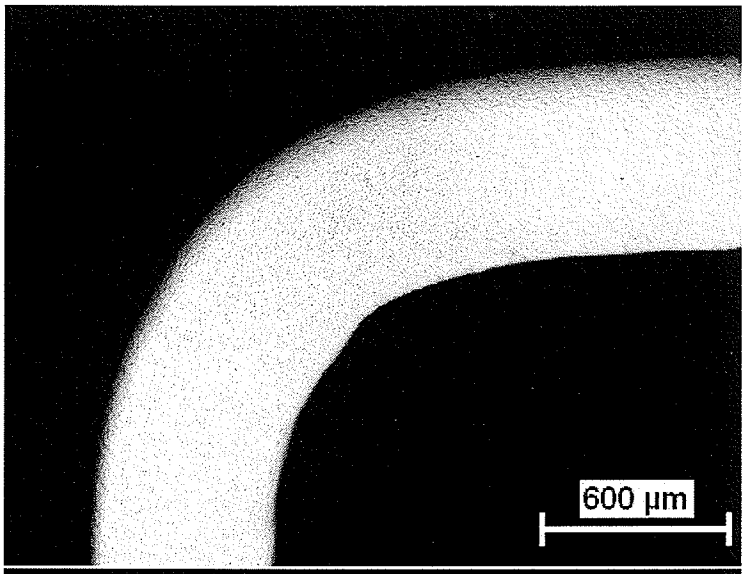

Figure 4.39:

Bent galvanized steel, as received (*Mag 50x*).

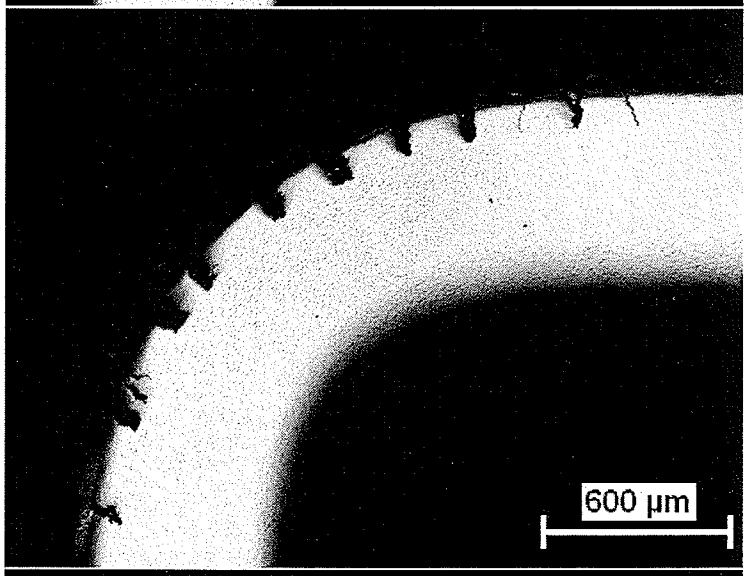

Figure 4.40:

Bent galvanized steel, heat treated at 400˚C, for 96 h (*Mag 50x*).

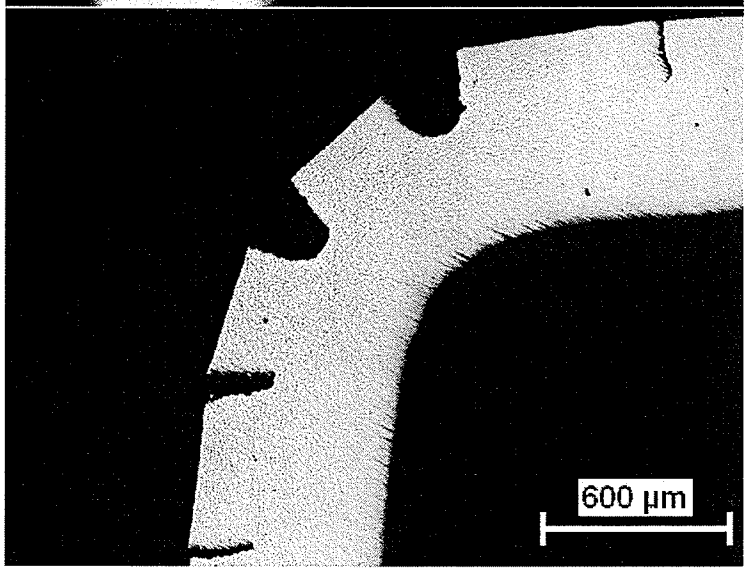

Figure 4.41:

Bent galvanized steel, heat treated at 500˚C, for 96 h (*Mag 50x*).

Diffusion at 500°C

Strips of commercial galvanized steel, heat treated at 500°C for 96 hours, had large particles of Γ phase in the grain boundaries (Figure 4.37). The steel interface was at the top of the micrograph in Figure 4.37, and the particles of Γ phase in the grain boundaries are clearly defined by the darker grey colour. The Γ phase particles were mostly globular in shape, and were as large as 3 μm in size. The grain boundaries contained a large number of Γ phase artifacts, and large particles of Γ phase were found as deep as 50-100 μm into the steel.

4.2.3 Cracking

Embrittlement cracking was found in the heat treated galvanized steel samples. This unexpected result occurred as a by-product of preparing the samples for mounting. For the earlier galvanized steel samples, a 90° bend was used to hold the galvanized steel upright while the bakelite mount was formed (later samples were held upright by a plastic clip). Cracks were discovered in the heat treated galvanized steel samples, in the area of the bend.

The bend was placed roughly at 1/4 the length of the galvanized steel strip (Figure 4.38a). The strip was bent in a vise, by hand, with the aid of a relatively large, flat surfaced, steel block (Figure 4.38b). The block kept the long leg of the L-bent sample straight, which was required for correct analysis of the diffusion zone. Since the galvanized steel strip was restricted so it wouldn't flex, and the load then couldn't be distributed, all of the

force was directed to the bending joint. The small bending radius also magnified the stress in the area. Due to these two effects, a concentrated pure bend was formed in the galvanized steel strips.

Crack morphology

Normal, un-heat treated galvanized steel bent without cracking. The polished cross-section of the bent, as-received, galvanized steel is shown in Figure 4.39. Galvanized steel strips, heat treated at 400˚C for 96 hours, cracked when bent (Figure 4.40). The large, open cracks formed on the outer edge of the bend. A large number of cracks were found (14), and they increased in length and width towards the fulcrum of the bend, where the deepest and widest cracks were found (~85 μm wide, ~120 μm deep). Galvanized steel strips, heat treated at 500˚C for 96 hours, also cracked when they were bent (Figure 4.41). In the case of 500˚C, the samples had a less number of cracks (7), but the cracks were more severe. The cracks were deeper and wider: ~250 μm wide and ~250 μm deep. Again, the deepest and widest cracks were found near the fulcrum, where the maximum stress was located.

Chapter 5

DISCUSSION

This chapter begins with a review of the diffusion coefficients determined in this work, and then describes the differences in the structures formed by diffusion between the experiment temperatures of 400°C, 500°C, and 725°C. Different diffusion mechanisms were involved between the pure iron and zinc for each of the three experiment temperatures. The effects of zinc diffusion, through the embrittlement of iron and steel, are presented.

5.1 Comparison of the Diffusion Coefficients

5.1.1 Coarse and Fine Zinc Concentration Gradients

In general, the zinc diffusion coefficient in iron obtained from the fine zinc concentration gradients were consistent with the zinc diffusion coefficients obtained from the coarse zinc concentration gradients (comparing the data in Table 4.1). For the sample produced at 725°C, the constant zinc diffusion coefficients obtained from both the fine and coarse zinc concentration gradients were almost identical, and the variation in diffusivity from 2.0×10^{-18} m^2/s to 2.0×10^{-17} m^2/s was consistent with the "average" value of 1.7×10^{-17} m^2/s.

5.1.2 Temperature comparison

The diffusion coefficients of zinc into iron that were calculated in Section 4.1.6 are shown in Table 5.1. Comparing the values in Table 5.1 respective to one-another, the zinc diffusion coefficients should have increased exponentially with temperature, much more than the ~12% increase in value found between 400°C and 725°C. The zinc diffusion coefficients found in this investigation remained nearly constant, irrespective of the temperature. Comparison of these diffusion coefficients to others found in the literature [9, 25] will explain this contradiction.

5.1.3 Literature comparison

Numerical

There were no zinc diffusion coefficients in iron found in the literature reviewed at the corresponding experiment temperatures, or derived by using bulk amounts of diffusion material. The only diffusion coefficients found were those produced by Richter et al. [9]. Their work consisted of using α-Fe single crystals and a zinc vapour source, at diffusion runs between 575°C and 896°C. Since Richter et al. derived a zinc diffusion coefficient in iron that varied with zinc concentration, only the lowest value at each temperature was used as a comparison to the values determined in this investigation. The zinc diffusion coefficients in Table 5.1 from Richter et al. were taken as, or extrapolated from, their value of the zinc diffusion coefficient at 0 % zinc concentration in the iron. Values of the diffusion coefficient of zinc into iron for the temperatures of 400°C, 500°C, and 725°C,

calculated by using the Arrhenius equation (Section 2.4.1), are also listed in Table 5.1. For zinc tracer diffusion in paramagnetic iron, the frequency factor (D_0) was 2.03×10^{-4} m^2/s and the activation energy (Q) was 231.4 kJ/mol [25].

When comparing the diffusion coefficient of zinc into iron between the three sources found in Table 5.1, there are orders of magnitude of difference in value between the zinc diffusion coefficient found in this investigation, and that extrapolated from data in the literature, for the temperatures of 400°C and 500°C. The difference in value of the zinc diffusion coefficient was less at 725°C, only a magnitude of difference separated the values between the three sources. The differences in the values of the zinc diffusion coefficients according to temperature are depicted in Figure 5.1, which is a graphical comparison of the zinc diffusion coefficient in iron between the three sources.

In Figure 5.1, the Arrhenius equation forms the typical linear relationship between the logarithmic of the zinc diffusion coefficient (log D_{Zn}) versus the inverse of the temperature (in K^{-1}, and multiplied by 10^4). The data points from Richter et al. (▲) were similar to the values calculated by the tracer diffusion results, and fit well in the paramagnetic region above 770°C ($10^4/T < 9.58$). The data points at the lower temperatures were similar to the tracer diffusion data, but with Arrhenius equation variables calculated to be $D_0 = 400$ m^2/s and $Q = 361.4$ kJ/mol (as derived from Figure 5.1). The data from the two sources were similar, since they both were concerned with lattice diffusion.

Table 5.1: Comparison of the Zinc Diffusion Coefficients

Temperature (°C)	Zinc Diffusion Coefficient (m^2/s)		
	This Investigation (apparent)	Richter et al. (0% Zn) [9]	Tracer Diffusion (Arrhenius) [25]
400	1.5×10^{-17}	3.6×10^{-25}	2.2×10^{-22}
500	1.6×10^{-17}	5.2×10^{-22}	4.7×10^{-20}
725	1.7×10^{-17}	4.5×10^{-17}	1.6×10^{-16}

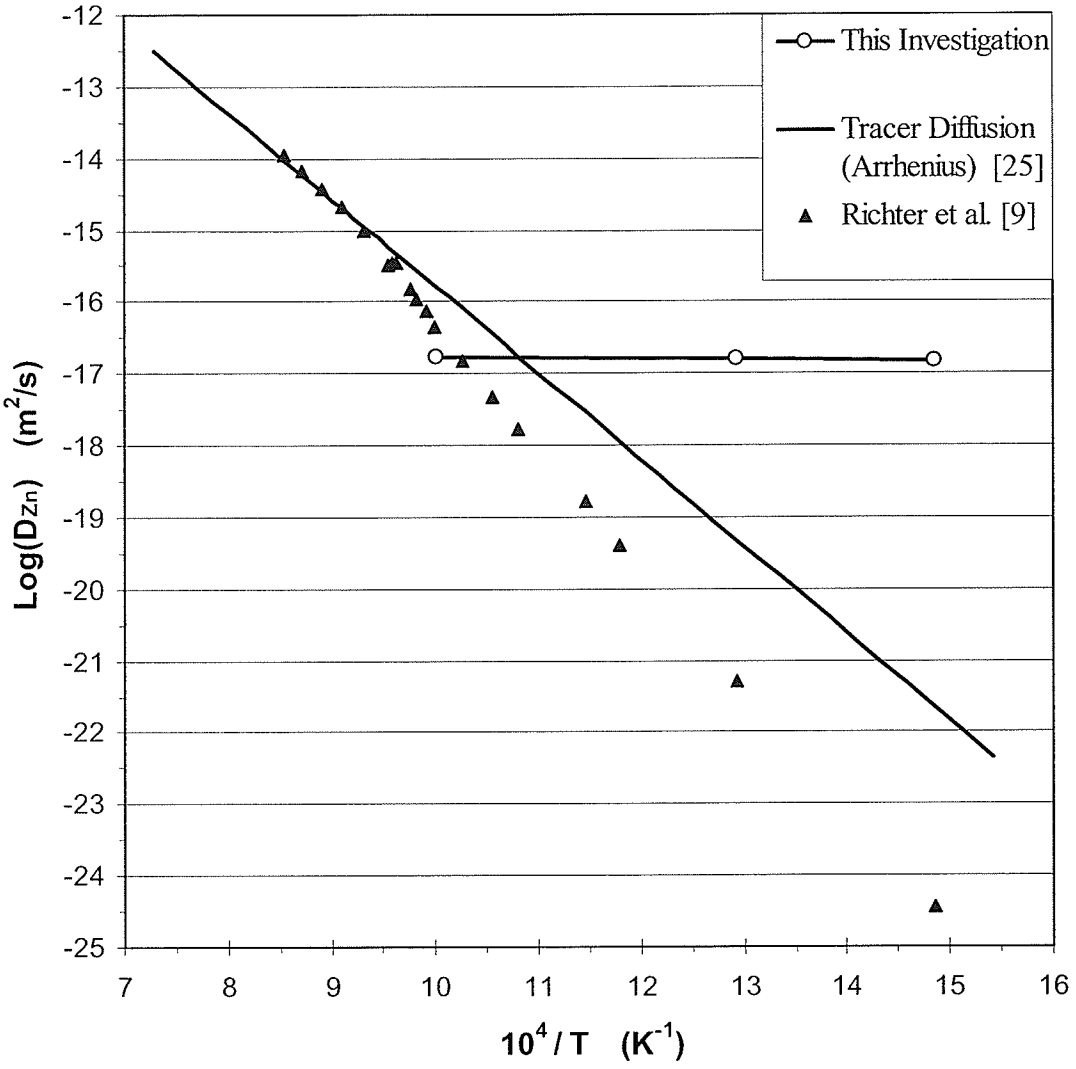

Figure 5.1: Graphical comparison of the zinc diffusion coefficients in iron (D_{Zn}) versus the inverse of temperature (1/T).

The difference between the values of the zinc diffusion coefficient obtained in this work and those of the two sources is depicted in Figure 5.1. In Figure 5.1, the value at 725°C fits reasonably well (within an order of magnitude), and the large differences at 400°C and 500°C are clearly depicted. The value at 500°C is ~2.5 x 10^4 times greater than the data point extrapolated from the work by Richter et al. The difference in the zinc diffusion coefficient is greater at 400°C: ~2.5 x 10^7 times greater than the extrapolated data point from Richter et al. The result of these differences is shown in Figure 5.1; the data points of the values of D_{Zn} obtained in this work are nearly constant in the temperature region between 400°C and 725°C, whereas the values from bulk diffusion in single crystals are much lower in this region. The high values of the zinc diffusion coefficient into polycrystalline iron at 400°C and 500°C were caused by rapid grain boundary diffusion of the zinc into the iron, which was determined by comparing the result in Figure 5.1 to Figure 2.5.

Due to the near constant D_{Zn} found in this work, the trendline of the experimental data intersects the trendlines for the other data sets at large angles (Figure 5.1). The large change in the slope of the trendline for the experimental data would require that D_0 and Q must be different. From Figure 5.1, the D_0 was calculated to be 2.2 x 10^{-17} m^2/s, and the Q was 2.1 kJ/mol (assuming the experimental data follows the Arrhenius equation). When compared to the values from the sources, the values calculated for D_0 and Q are extremely low (Table 5.2).

Table 5.2: Summary of Activation Energies and Frequency Factors

	Frequency Factor, D_0 (m^2/s)	Activation Energy, Q (kJ/mol)
Tracer Diffusion [25]	2.03×10^{-4}	231.4
Derived from Richter et al. [9]	400.0	361.4
This Investigation (Regime 1 of Figure 5.2)	2.2×10^{-17}	2.1
Regime 3 of Figure 5.2	3.34×10^{-3}	257.0

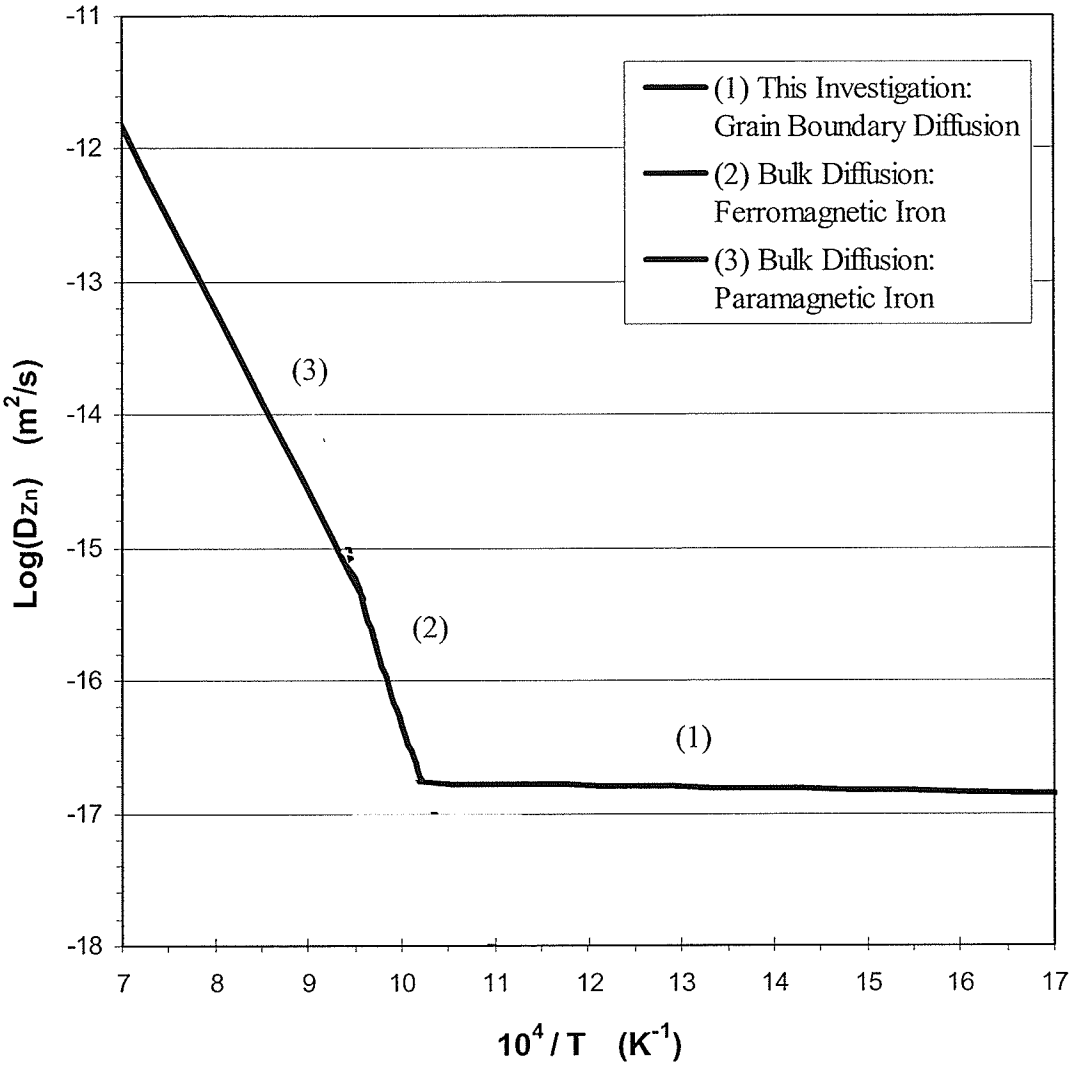

Figure 5.2: Predicted relationship between the zinc diffusion coefficient (D_{Zn}) and the inverse of temperature (1/T) for polycrystalline iron.

Using the data from Figure 5.1, the relationship between the zinc diffusion coefficient (D_{Zn}) and the inverse of temperature for polycrystalline pure iron was drawn, as shown in Figure 5.2. According to Figure 5.2, three behaviour regimes occur in the diffusion of zinc in polycrystalline iron with temperature, they are the following.

Regime 1 – Grain Boundary Diffusion

At lower temperatures ($T < 700^{\circ}C$) the D_{Zn} is very high respective to the temperature, due to the rapid grain boundary diffusion that occurs in the iron. This regime has been drawn linearly in Figure 5.2, following the Arrhenius equation with a D_0 of 2.2×10^{-17} m^2/s and a Q of 2.1 kJ/mol. The exact shape and lower temperature threshold of this line is unknown, as there is no experimental data for temperatures below 400°C.

Regime 2 – Bulk Diffusion in Ferromagnetic Iron

At 700°C, the diffusion of zinc in iron changes from grain boundary diffusion dominated behaviour to lattice diffusion dominated behaviour. For $T > 700^{\circ}C$, this regime resembles the Arrhenius equation with a $D_0 = 400$ m^2/s and $Q = 361.4$ kJ/mol (which were calculated from Figure 5.1). As found by Richter et al. [9], and as shown in Figure 5.1, there is a slight upwards curvature of the data points. It was derived from Figure 5.1 that the curvature of the data points followed a cubic equation up to 770°C:

(5.1) $$y = -0.4299x^3 + 13.507x^2 - 143.2x + 494.88$$

Where: $x = 10^4/T$ (K^{-1}) for: $700^{\circ}C < T < 770^{\circ}C$
$y = \log(D_{Zn})$ (m^2/s)

Regime 2 in Figure 5.2 was drawn with using Eq. (5.1): from 700°C to 770°C.

Regime 3 – Bulk Diffusion in Paramagnetic Iron

The diffusion of zinc in iron follows the curvature of Eq. (5.1) up to 770°C. At 770°C, the iron undergoes a paramagnetic transformation, which subsequently changes the diffusion behaviour. This regime was drawn linearly in Figure 5.2, following the Arrhenius equation, with a $D_0 = 3.34 \times 10^{-3}$ m^2/s and $Q = 257$ kJ/mol. The values for D_0 and Q are different than found by Oikawa (charted in Figure 5.1, and listed in Table 5.2), but the change was required in order to fit the Arrhenius equation to the data from Richter et al., and to the paramagnetic transformation temperature of 770°C. Exact definition of Regime 3, regarding D_0, Q, and curvature, would require further experimentation for confirmation.

Structural

The main reason for the magnitude of difference in values between this experimental investigation and the literary sources is that the experiment materials and procedure were different. Since α-Fe single crystals were used by Richter et al., the zinc could only enter the iron via slow lattice diffusion, and not by rapid grain boundary diffusion. Similarly, the data given by Oikawa was for solute tracer lattice diffusion.

The reason the diffusion coefficient measured at 400°C was many times larger than the value in the literature was because grain boundary diffusion in the multi-crystalline pure iron was dominant at this temperature. The diffusion of zinc at 400°C was primarily and rapidly transported into the iron through the grain boundaries. This was the same reason for the many times larger diffusion coefficient derived from samples heated at 500°C.

The magnitude of the difference was less at 500°C, due to the increased lattice diffusion that occurred. The difference in the diffusion coefficient measured at 725°C was only an order of magnitude, because at this temperature lattice diffusion was the dominant transportation mechanism. The values were similar because it did not matter if the diffusing material had grain boundaries or not, the grain boundary diffusion was overshadowed by the lattice diffusion.

The large difference in the zinc diffusion coefficient in iron was also found by Shewmon et al. [1]. Their work consisted of measuring the zinc diffusion coefficient in heat treated galvanized steel. At the temperatures of 450°C and 550°C, they found that the zinc diffusion coefficient was up to 10^4 times larger than the lattice diffusivity values measured by Richter et al. [9]. This was similar to what was found in this investigation. Shewmon et al. concluded that the increased zinc penetration was caused by diffusion induced grain boundary migration (DIGM).

DIGM may occur in thin metal such as sheet galvanized steel (0.6 mm thick – as used by Shewmon et al.), but DIGM cannot occur in thick metal such as the iron used in this investigation (as discussed in Section 2.4.3). Since DIGM could not have accounted for the high zinc penetration in samples heated at 400°C and 500°C, the only transport method that could have caused the high penetration is rapid grain boundary diffusion. Perhaps this also occurred in the heat treated galvanized steel samples produced by Shewmon et al.

In summary, it appears that diffusion of zinc into polycrystalline iron is not at all anomalous (as suggested by Shewmon et al. [1]). At 725°C, diffusion is controlled by lattice diffusion, while at 400°C and 500°C diffusion of zinc is simply controlled by grain boundary diffusion in the iron. This is normal behaviour for diffusion in polycrystalline metals.

5.1.4 Diffusion at 725°C

At 725°C, it is possible that the zinc diffusion coefficient in iron is not constant with zinc concentration. From Figure 4.27, the numerical model with varying D_{Zn} fits much better to the data points than the numerical model with constant D_{Zn} (as explained in Section 4.1.7, with the values of the D_{Zn} listed in Table 4.1). Further proof of the variation in D_{Zn} with zinc concentration in the iron can be found in Figure 4.26.

In Figure 4.26, the data points from ~1.5 μm depth in the iron were similar to the numerical model with a constant D_{Zn} set at 5×10^{-18} m^2/s. Likewise, the data points at ~3 μm depth in the iron were similar to the numerical model with a constant D_{Zn} of 1×10^{-17} m^2/s. The rest of the data points in Figure 4.26 (depths >4 μm) followed the trendline for a D_{Zn} of 1.7×10^{-17} m^2/s, which is the constant D_{Zn} value reported in Table 4.1. The fact that the data points at shallow depths in the iron (<4 μm) follow trendlines from the numerical model with gradually decreasing D_{Zn} indicates that the diffusion coefficient of zinc in iron varies with zinc concentration in the iron at 725°C, and that the D_{Zn} decreases with increasing zinc concentration.

There was another contradiction found between the literature and the experimental results produced at 725°C. As shown in Figure 4.27, and stated in Section 4.1.7, the zinc diffusion coefficient likely varied with zinc concentration in the iron, at 725°C. It was determined that at 725°C the zinc diffusion coefficient is higher at lower zinc concentration (2.0×10^{-17} m^2/s), and lower at higher zinc concentration (2.0×10^{-18} m^2/s). This result is in direct opposition to the trend found by Richter et al. [9], where it was found that the zinc diffusion coefficient increased exponentially with increasing zinc concentration (Figure 2.3).

The most likely reason for this contradiction is the result of the multicrystalline iron used in this investigation, as compared to the single crystals of iron used by Richter et al. There could have been some effect of grain boundary diffusion in the zinc concentration gradient in the iron, and subsequently the derived zinc diffusion coefficients. On the contrary, the grain boundaries could not have played a major role, as it has been stated previously that the diffusion mode is lattice dominant at 725°C, and that no Γ phase particles formed in the grain boundaries of the iron at 725°C. Another possible reason for the contradiction could be that the iron diffusion (the movement of the iron interface) had a greater effect on zinc diffusion in the iron than what was assumed, but this would mean that the partial differential equation derived for the effect of boundary movement on diffusion, Eq. (4.1), would be incorrect. Another likely reason for the contradiction is from the sample materials that were used: Richter et al. used a zinc vapour source, while a liquid pool of zinc was used in this investigation.

Diffusion of zinc in iron at 725˚C was further complicated by the Curie temperature. At high zinc concentration (above 12 at% zinc), diffusion occurred in the paramagnetic region; while at lower zinc concentrations, diffusion occurred in the ferromagnetic region (Figure 2.1). Since diffusion is slower in the ferromagnetic region, the diffusion coefficient at lower zinc concentrations (ferromagnetic region) should be lower than those at higher zinc concentrations (paramagnetic region). This behaviour is opposite to that observed in this investigation. While it is possible that some grain boundary diffusion occurred at the lower zinc concentrations in the specimens annealed at 725˚C, it is difficult to envision the diffusion coefficient at higher zinc concentrations being nearly 2 orders of magnitude greater than those at lower zinc concentrations (as reported by Richter et al. – Figure 2.3).

5.1.5 Diffusion at 400˚C and 500˚C

From the experimental data measured in the pure iron-zinc diffusion couples heated at 500˚C and charted in Figure 4.29, the interface reading caused a strange initial point in the zinc concentration gradient in the iron. Without the first data point (~7.05 at % Zn), the zinc concentration curve would be much different (the zinc concentration gradient appears that it should have started at a lower concentration: such as 3.5 at% Zn). A number of reasons validate / explain the zinc concentration gradient measurement depicted in Figure 4.29, they are the following.

1) The solid solubility of zinc in iron was determined from the iron-zinc phase diagram to be 7.05 at% Zn.

2) The four fine gradient measurements all had interface readings of ~7 at% Zn.

3) As previously mentioned, the D_{Zn} determined in this investigation were "apparent" diffusion coefficients – they were a combination of both lattice diffusion and grain boundary diffusion of zinc in the iron. Figure 4.29 is evidence of both types of diffusion: the lattice diffusion zinc concentration curve, which begins at ~7 at% Zn and drops to 0% Zn within 0.25 μm depth in the iron, and the grain boundary diffusion zinc concentration curve, which has no set starting value but drops from ~3 at% Zn to ~0.5 at% Zn across a relatively large depth in the iron (~15-30 μm).

4) The erratic zinc concentration readings in Figure 4.29, caused by the reading of Γ phase particles in the grain boundaries of the iron, increase the average zinc concentration gradient in the iron. The erratic readings were not erroneous; they were a true representation of the diffusion of zinc in iron. Due to the Γ phase particles in the grain boundaries, the zinc concentration gradient formed in iron heated at 500°C should have a zinc concentration ~0.5-1 at% Zn higher than the "intuitive" average zinc concentration gradient shown in Figure 4.29.

Points 1 to 4 are also valid for the zinc concentration gradient formed in iron heated at 400°C for 96 hours, shown in Figure 4.31 (with the respective zinc concentrations changed accordingly).

The erratic zinc concentrations found in the fine gradient readings of the 400°C and 500°C samples is understandable, considering the number, shape, and depth of the Γ phase particles that formed within the iron in these samples (Figures 4.14 and 4.17),

and given the high magnification used to measure the fine gradients. Due to the large amount of Γ phase particles that formed in the grain boundaries of the iron in samples produced at 400°C, and the low zinc solubility of the iron at this temperature (3.66 at% Zn), it was impossible to generate a reasonable fine zinc concentration gradient (as shown in Figure 4.22), and to derive the zinc diffusion coefficient.

All of the diffusion coefficients (Table 4.1 and Figure 4.32) derived from the fine zinc concentration gradient (Figure 4.22) were all wide estimates. The values determined from the coarse concentration gradient at 400°C were just as accurate as the values determined from the fine gradient. Only the variable zinc diffusion coefficient at low concentrations in samples at 400°C and 500°C are relatively accurate. Due to the Γ phase particles in the grain boundaries of the iron, the values of D_{Zn} at low concentrations are greater at 400°C and 500°C, than at 725°C. The higher zinc diffusion coefficients that were determined at the low zinc concentrations should be expected because of the rapid grain boundary diffusion that occurred at the lower temperatures.

5.1.6 Iron Dissolution

The rate of iron dissolution by zinc was significantly lower at 400°C than at 500°C. At 725°C, the rate of iron dissolution was rapid. Evidence of the rate of iron diffusion comes from the iron interface shift (ε) measured in the samples, which was presented in Section 4.1.5. Since the iron diffusion / dissolution at 500°C and 725°C was probably aided by convective mixing, a portion of the measured interface shift would have been

attributed to this effect. The convective mixing that occurred at 500°C and 725°C was caused by the density and thermal gradients that existed between the iron and the molten zinc pool, and was aided by the sample design. The end of the iron rod was protruded out into the large zinc pool – these were perfect conditions for convective mixing.

Though conditions were ideal for convective mixing to occur, and it was most likely that it was present during the diffusion anneal, it would have made no difference to the zinc concentration gradient in the iron. It was discussed in Section 4.1.5 that the iron interface shift was neglected from the zinc diffusion coefficient calculation because it had no effect. It was numerically tested and proven that the interface shift, even up to 200 mm, had no influence on the diffusion of zinc into iron. It is from this information that the convective mixing in the samples can be neglected for zinc diffusion into solid iron. Even if the convective mixing accounted for the whole interface shift, which is impossible, it would have made no difference to the zinc concentration gradient in the iron, and the diffusion coefficient of zinc into solid iron.

In summary, some convective mixing occurred within the iron-zinc diffusion couple. The convective mixing was enhanced by the large molten zinc pool, and the protruded iron rod. It was numerically proven that the interface shift, and therefore the convective mixing, had no influence on the zinc concentration gradient in the iron rod. Subsequently, there would be no convective mixing component of the diffusion coefficient of zinc in solid iron.

5.2 Phase Formation at 400°C

The compositions of the phases found in the samples agreed with the corresponding compositions of the phases presented in the iron-zinc phase diagram [6], as discussed in Section 2.2.1. All iron-zinc phases were found, and in some cases, all were found in the same sample. The range of composition of the phases found in the samples had similar compositions as found in the phase diagram. The atomic formulae of the phases are agreeable, except Γ_1 phase. It seems gratuitous to designate the Γ_1 phase $Fe_{11}Zn_{40}$, when the simple $FeZn_4$ would suffice.

5.2.1 Phase Formation away from the Iron Interface

The primary stage of development of the intermetallic phases, between pure iron and pure zinc heated at 400°C, was probably the same as reported in the literature [7, 8, 10, 12, 16]. The first intermetallic phase to form probably was ζ, followed by δ phase, then Γ phase, and then Γ_1 phase. In the bulk pure metal samples, all of the phases continued to grow, or shift towards the η-Zn and α-Fe, as time progressed. The δ phase grew more rapidly than the other phases.

At some point in time, the ζ phase started to decrease in thickness, due to transformation into δ phase. The decrease in ζ phase layer thickness could be due to either the ζ phase growth slowed down, allowing it to be consumed by the growing δ phase, or a blockage to ζ phase growth occurred, such as the formation of a crack in the ζ – η-Zn interface

(no conclusive evidence of a crack was found in this work). For either case, at the end of the diffusion heat treatment (96 hours), the pure metal samples were found to have maybe only a thin, discontinuous layer of ζ phase remaining (probably no ζ phase), due to the transformation into δ phase. While ζ phase was transformed into δ, δ also consumed Γ_1, and the Γ_1 phase consumed the Γ phase. This explains the narrow pillar-like structure of the Γ phase, as shown in Figure 4.1.

The porosity found at the top of the δ phase layer (Figure 4.2) was caused by the transformation of ζ phase into δ phase. The density (D) of δ phase is greater than ζ phase ($\Delta D/D \approx 7\%$) [14], so shrinkage voids were produced by the transformation of ζ phase to δ phase. The start of the porosity was the point where the δ phase started to consume the rest of the ζ phase – as shown in Figure 4.2, there was a definite line where the porosity began. The pores then became smaller and more numerous towards the ζ – η-Zn interface, until the number of pores was so great that the interface was illegible (Figure 4.3). With all the porosity at the interface, it was impossible to conclude that the ζ – η-Zn interface was cracked.

The transformation of ζ phase to δ phase would be the start of the second stage of interphase development. This stage of development consisted of the transformation of the less iron-rich intermetallic phases into a more iron-rich intermetallic phase. The first phase transformation would be ζ into δ phase, then the δ phase would transform to Γ_1, and finally the Γ_1 phase would transform to Γ phase. The start of the transformation of δ phase into Γ_1 and Γ phases was shown in Figure 4.2. After 96 hours at 400°C, the pure

metal samples had a thick Γ_1 and Γ phase, as these phases were starting to consume the δ phase. If this had not been the case, then the thicknesses of these two phases would have been much smaller (similar to the samples produced at 500°C: Γ_1 = 5-10 μm, Γ = 1-5 μm).

If the pure metal samples were held at 400°C for a longer time than 96 hours, the Γ_1 and Γ phases would have entirely consumed the δ phase. Evidence of this was shown in Figure 4.33, from a sample of galvanized steel heat treated at 400°C for 96 hours. In Figure 4.33, the ζ phase was totally consumed, the δ phase nearly consumed, and the Γ_1 and Γ phases dominated the interphase. If the pure metal samples were held at 400°C for an even longer time, the interphase would have been wholly Γ phase, similar to the structure formed in the galvanized steel samples heat treated at 500°C for 96 hours (Figure 4.35). This intermetallic phase structure would be the final structure to form in bulk pure metal samples heated at 400°C. At this stage, the grain boundaries of the iron would probably contain large amounts of Γ phase particles, similar to what was shown in Figure 4.37. To obtain this structure, the pure metal samples would need to be held at 400°C for very long times (probably 15-25 days).

5.2.2 Phase Formation at the Iron Interface

In the pure metal samples heated at 400°C for 96 hours, the Γ phase had grown so thick that it enveloped the top layers of iron grains. In Figure 4.1, it appeared that the grains were being peeled away from the solid iron. The movement of the grains may have been

caused by the influx of zinc atoms in the grain boundaries of the iron, and subsequent formation of Γ phase. In order for the grains to move, the density of Γ phase must be less than pure iron. The volume change, attributed to the change in density, would have caused the iron grains to rise away from the rest of the rod. This was shown in the micrograph in Figure 4.1, evident by the small remnants of two iron grains that were lifted clear from the rest of the iron. One such iron grain was located at the far left of Figure 4.1, the other at right of center of the micrograph.

Another scenario may be that this illusion was created by the transformation of the iron into Γ and Γ_1 phases. As zinc atoms diffuse into the grain boundary, they also diffuse into the crystal lattice of the iron grains. The inward diffusion of the zinc atoms was met by an outward diffusion of iron atoms coming from the grain. When the conditions were right (when the right mix of atoms were contained in a region), the Γ phase then formed. As the diffusion continued, the Γ phase bands in the grain boundaries of the iron would have got thicker, eventually enveloping the iron grain, as shown in Figure 4.1. The Γ phase in turn would be transformed to Γ_1 phase, and then to δ phase. With this phase growth mechanism, the iron grains were transformed to one phase, then to another, thus giving the appearance that the grains were dissolving away.

Physically forcing the grains from the rest of the iron is hard to imagine, since the material was in a solid solute-solid solvent diffusion couple. The most likely scenario was the latter, in that the iron grains dissolved away into the zinc, through the grain boundaries to the interior of each grain. It is possible that there was some wedging action

from the Γ phase formation, which would have then helped the iron grains to dissolve away. It may be that both wedging and dissolving actions were at work.

The thick bands of Γ phase in the grain boundaries of the top iron grains, and the thin ribbons in the grain boundaries in the 3-5 grains below this area (Figure 4.14), were a clear indication of the rapid grain boundary diffusion of zinc into iron that occurred at 400°C. The large amount of zinc grain boundary diffusion into the iron, which caused the α-Fe – Γ two-phase region, made a large impression on the concentration gradient. Large readings of zinc were found across the two-phase region, due to the large bands of Γ phase in the iron grain boundaries. The width of the α-Fe – Γ two-phase region was relatively thick due to the transformation of the top layers of iron grains. These structures accounted for the softer zinc concentration gradient shown in the samples produced at 400°C (Figure 4.21). The ribbons of Γ phase also had a major effect on the fine zinc concentration gradient (Figure 4.22), and the derived zinc diffusion coefficient.

Evidence of rapid grain boundary diffusion of zinc in iron was also shown in Figure 4.16. The thin black ribbons of Γ phase followed the parallel grain boundaries of the non-pre-heat treated iron, to a depth that was greater than the pre-heat treated iron (>100 μm versus 40-80 μm). In the case of the non-pre-heat treated iron, the linear orientation of the grain boundaries allowed zinc to diffuse further into the iron.

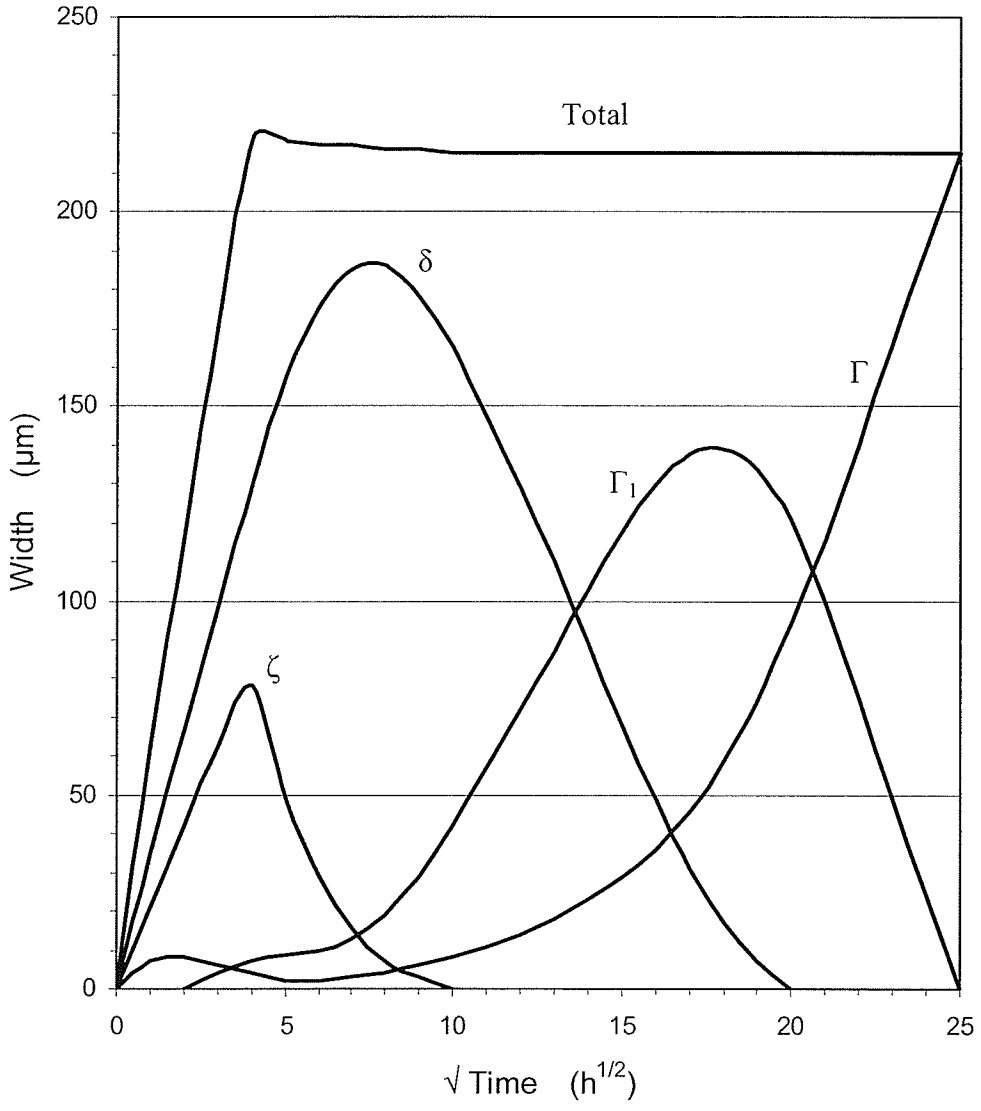

Figure 5.3: Predicted iron-zinc phase growth at 400°C.

5.2.3 Iron – Zinc Phase Growth at 400°C

The predicted iron-zinc phase growth at 400°C is shown by the chart in Figure 5.3. This growth was derived from the results of the bulk pure iron-zinc diffusion couples, and it is due to the quantity and form of the sample materials that make this chart different than Figure 2.2 (Figure 2.2 was derived from samples of heat treated, 700 μm thick electro-deposited zinc-iron couples [12]). The phase growth modelled in Figure 5.3 is similar to the phase growth found in heat treated galvanized steel (the shape and sequence of growth is the same, but the thicknesses and times are different). The hypothetical data points used to create Figure 5.3 can be found in Table B.1. The following facts and evidence were used to construct Figure 5.3.

1) The total thickness of the interphase at 96 hours was ~215 μm, as measured from Figure 4.2.
2) The maximum total thickness of the interphase would be about 3-5 μm larger than the total thickness found at 96 hours. The interphase contracted, pulling away from the zinc, during the diffusion anneal. The void (gap) between the interphase and the zinc was estimated to be 3-5 μm, as measured from Figure 4.3. At some time before 96 hours, the interphase would have reached its maximum thickness, and slowly receded to the thickness found at 96 hours.
3) The contraction of the interphase was caused by the volume change as ζ phase was transformed to δ phase (the density of ζ phase is less than δ phase).
4) The change in density from the phase transformation also created the voids found in the interphase (Figure 4.2). This is due to the fact that in Figure 4.2 the voids

began at the same distance from the iron interface. From this evidence, the thickness of the layer of voids in Figure 4.2 is the maximum thickness of the ζ phase layer. The void layer varies in thickness from 65-95 μm, with the average thickness being 80 μm (as used in Figure 5.3).

5) The maximum thickness of the interphase occurred when the ζ phase was at its maximum thickness.

6) At 96 hours, the thicknesses of the phases were: ζ (0-10 μm), δ (165-195 μm), Γ_1 (~35 μm), Γ (~6 μm), and total thickness = 215 μm. These values were measured from Figures 4.1 and 4.2.

7) When diffusion begins (time = 0), the ζ and δ phase form immediately, the Γ phase after 30 seconds, and the Γ_1 phase forms after a delay [7].

8) The total thickness of the Γ and Γ_1 phases was ~10 μm, for most of the diffusion time prior to 96 hours [12].

9) At some time between 2 and 7 hours annealing time, the Γ phase layer separates into Γ and Γ_1 layers [10]. When this occurs, the Γ_1 layer grows at the expense of the Γ layer.

10) The interphase will consist of only Γ phase at long diffusion times. This was concluded from the interphase that was found in the galvanized steel samples heat treated at 500°C for 96 hours (Figure 4.35).

11) At some time after 96 hours of diffusion, the proportions of the phases between the iron and the zinc will be: Γ (1/5), Γ_1 (3/5), and δ (1/5). These proportions of the interphase were measured from the galvanized steel samples heated at 400°C for 96 hours (Figure 4.33).

12) At ~96 hours of diffusion, the Γ and Γ_1 phases are beginning to thicken (from transforming the δ phase).

13) The maximum thickness of the δ phase would occur at just before 96 hours. This is due to: the total (or near total) consumption of the ζ phase that has occurred at this time, and the start of the thickening of the Γ and Γ_1 phases.

14) Since no extra zinc is added to the interphase (due to the contraction gap that forms as a result of the ζ to δ phase transformation), the total thickness will not increase as the Γ and Γ_1 phases consume the δ phase, for time greater than 96 hours.

15) There may be slight changes in the total thickness of the interphase due to further phase transformations (density changes). This was not depicted in Figure 5.3 since the densities of the Γ and Γ_1 phases are unknown. It is very likely that the densities of these phases are greater than δ phase, which would mean that the interphase will further contract as the δ phase is transformed to Γ and Γ_1 phases.

16) The δ, Γ_1 and Γ phase growth were modelled after 6^{th} order polynomial equations (the equations for growth are found in Appendix B). The 6^{th} order polynomial equations were used since no data could be found for the δ, Γ_1 and Γ phase growth, and it was concluded that the growth should follow some sort of numerical function, rather than just loosely assigning positions for the growth. There is no scientific basis for using the 6^{th} order polynomial equations to model the iron-zinc phase growth – the equations were used in a hypothetical manner. It would require experimental testing to prove if the growth is correct, and if the growth follows the equations presented in Appendix B.

The way Figure 5.3 was designed, it turned out that the time for homogenization of the interphase (transformation to all Γ phase) was 25 √h or 625 hours (26 days). This was in agreement with the prediction as stated in Section 5.2.1: the time for complete transformation of the iron-zinc interphase to Γ phase would take 15-25 days at 400°C. The other important detail about the chart was that there was no point of inflection in the δ phase growth (as there was an inflection point in Figure 2.2, at approximately 6 √h or 36 hours).

The reason for the absence of the inflection point was that the δ phase could not grow thick enough in the bulk pure metal samples to promote the fast growing palisade δ phase. From Figure 2.2, rapid growth of the palisade δ phase occurs when the total δ phase layer is 200 μm thick – which is slightly under the maximum thickness of the interphase developed in the pure metal samples (220 μm). Lastly, the reason for the elimination of the inflection point was that no palisade δ phase was found in the interphase shown in Figures 4.1, 4.2, and 4.3. Palisade δ phase did not grow in the bulk pure metal samples at 400°C, therefore no point of inflection for δ phase growth was drawn in Figure 5.3.

Aside from the finding that the Γ layer separates into Γ and Γ_1 layers at 2 to 7 hours diffusion time (point 9), Bastin et al. also found that once the Γ_1 layer began to grow, the ζ – η-Zn interface usually cracked because of gap formation due to the Kirkendall effect [10]. At this point, they found that when the remaining Fe-δ couple was further heat treated, the Γ and Γ_1 phase layers grew at the expense of the ζ phase layer. From this

information, it may be that the growth of the Γ_1 phase and the maximum thickness of the ζ phase are related (this relationship was loosely drawn into Figure 5.3). More importantly, the work by Bastin et al. verifies the fact that when the interphase is restricted (or when a semi-infinite diffusion couple becomes a finite diffusion couple), the iron-rich phases start to consume the lesser iron-rich phases. This process was the foundation used to construct Figures 5.3 and 5.4.

The cracking and gap formation found by Bastin et al. in their iron-zinc diffusion couples might be related to the gap and voids that were found at the ζ – η-Zn interface in the samples heat treated at 400°C (Figure 4.3). From the structure in Figure 4.3, it is possible that gap formation due to the Kirkendall effect caused a crack, and the subsequent separation of the ζ phase and the η-Zn. Though the structures were similar, further diffusion tests at different temperatures and times would be required to prove if the same gap formation mechanism occurred in the bulk pure metal samples.

5.3 Phase Formation at 500°C

5.3.1 The Effect of ζ Phase

The pure metal diffusion materials at 500°C were in different physical states than the samples at 400°C. At 500°C, the solid iron was diffusing with a molten zinc pool. The materials in the pure metal samples at 500°C did not remain in these states for the whole 96 hour diffusion time. In the first seconds of the heat treatment the δ phase solidified out of the zinc pool. From this, the diffusion situation of the materials at 500°C was: diffusion between solid iron and solid δ phase, and diffusion between solid δ phase and liquid zinc.

From the iron-zinc phase diagram (Figure 2.1), the maximum melting point of δ phase is 665°C. There is also a wide region of iron concentration that forms δ phase and melts above 500°C (~5 at% iron). For diffusion at 500°C, a solid mass of δ phase grew between the iron and the molten zinc pool (as shown in Figure 4.6). The whole thickness of the δ phase layer may not have formed after 96 hours diffusion at 500°C, some of the thickness of the δ phase layer may be attributed to growth while cooling [13]. If the δ phase layer grew during cooling, then it would indicate that the growth of the interphase was unrestricted. This would be a major difference between bulk pure metal diffusion at 400°C and 500°C.

The unrestricted interface growth in the pure metal diffusion couple at 500°C was caused by the absence of ζ phase formation. The ζ phase could not form at 500°C since: the maximum melting point of this phase was just above the experiment temperature (530°C), the region of iron concentration that could have formed ζ phase was very thin (~0.25 at% iron), and the difference of enthalpy and free energy of formation between the δ and ζ phases was very low (from Table 2.1: ΔH = -0.2 kJ/mol, ΔG = 0.7 kJ/mol). This data, coupled with the fact that iron diffusion / dissolution was much more rapid at 500°C, and that once δ phase forms it grows more rapidly than ζ phase, were the reasons no ζ phase layer was found on the iron rod. If ζ phase did form, it would have been in the first instances of diffusion, and it would have been quickly overtaken and transformed to δ phase. Some small free particles of ζ phase were found in the η-Zn, near the δ – η-Zn interface (Figures 4.7 and 4.8). These particles most likely precipitated out of the η-Zn as the sample was solidifying and cooling, and were not remnants of any pre-formed ζ phase layer.

There was a large effect on the diffusion structure in the pure metal samples when no ζ phase formed at 500°C. By eliminating the ζ phase, the boundary that limited the interphase growth in the pure metal samples was also eliminated. The δ phase was then given unlimited growth in samples heated at 500°C, with the only mechanism that controlled the growth being the diffusion of iron and zinc. This unlimited growth was evident in Figure 4.6 – the intermetallic layer formed at 500°C was ~100 μm thicker than the intermetallic layer formed at 400°C.

Other structures that were affected by the absence of ζ phase were the porosity and the cracks in the δ phase. The porosity in the top portion of the δ phase layer, especially at the δ – η-Zn interface, did not form at all (Figure 4.6). As mentioned previously in Section 5.2.1, the voids might have been caused by the transformation of ζ phase into δ phase. The fact that no ζ phase formed at 500˚C, as well as no void formation in the intermetallic layer, is further evidence of this claim. Without the porosity, it was easy to observe that the δ – η-Zn interface was not cracked. The other effect was the growth stress cracks that formed in the δ phase propagated from the δ – η-Zn interface to the Γ phase. If ζ phase had formed in the samples at 500˚C, the cracks would have stopped before they reached the η-Zn (the ζ phase arrests the cracks, as was shown in Figures 4.2 and 4.4).

The elimination of the ζ phase also reduced the amount of Γ and Γ_1 phase in the intermetallic layer. Since there was no limitation to δ phase growth, the iron was not concentrated in the interphase, and therefore the δ phase could not transform into Γ and Γ_1 phases. The thicknesses of the Γ and Γ_1 phases that formed at 500˚C were less than the thicknesses of these phases that formed at 400˚C. Whereas the Γ and Γ_1 phases were visible at low magnification in samples heated at 400˚C (Figure 4.2), they were barely legible at higher magnification in samples heated at 500˚C (Figures 4.5 and 4.6). The effect of this was that no α-Fe – Γ two-phase region formed, and there was very little Γ phase formation in the grain boundaries of the iron. This was also the reason why there was a steeper zinc concentration gradient at 500˚C than at 400˚C, as shown in Figure 4.21.

5.3.2 Comparison to Galvanized Steel

The structure of the pure metal samples heated at 500°C was much different than the structure formed in heat treated galvanized steel. For the pure metal samples: there was a thick δ phase layer, very little Γ_1 and Γ phases, no α-Fe – Γ two-phase region, and there was very little Γ phase in the grain boundaries of the iron (Figures 4.6 and 4.17). In contrast, the galvanized steel samples had a solid, >20 μm thick layer of Γ phase, on an α-Fe – Γ two-phase region (Figure 4.35), and there was an abundant amount of Γ phase in the grain boundaries of the steel (Figure 4.37). This was the largest disagreement of results in this work.

There were some similarities between the results of the pure metal samples and the galvanized steel samples, for instance: the maximum size of the Γ phase particles in the grain boundaries of the pure iron and steel were nearly the same. If the Γ phase particles in the grain boundaries were able to grow to the same size between the two sample methods, then the only difference was the amount of Γ phase. It is likely that if the δ phase growth was restricted in the pure metal samples (by lowering the amount of zinc), then they would begin to form the other phases and structures found in the galvanized steel samples heat treated at 500°C. Simple experiments could prove this development mechanism.

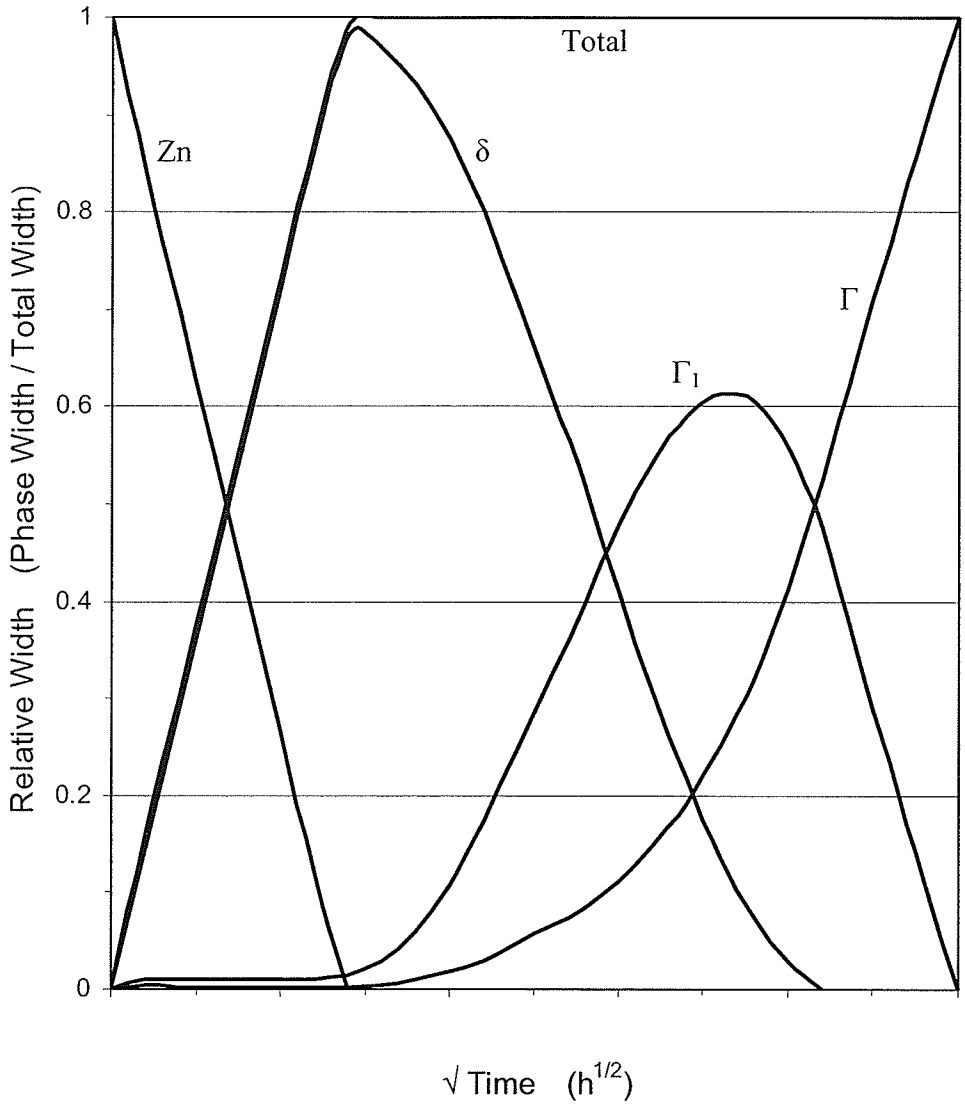

Figure 5.4: Predicted iron-zinc phase growth at 500°C.

5.3.3 Iron – Zinc Phase Growth at 500˚C

The predicted iron-zinc phase growth at 500˚C is shown by the chart in Figure 5.4. This chart was produced from the diffusion of bulk pure metal iron-zinc couples, and is similar to the phase growth that occurs in heat treated galvanized steel. The following facts and evidence found in this work were used to construct Figure 5.4.

1) Due to the absence of ζ phase formation at 500˚C, the only limitation to the interphase growth is the amount of zinc in the diffusion couple. Since the thickness of the interphase is related to the amount of zinc in the diffusion couple, Figure 5.4 depicts the relative phase growth against the square root of time. The growth shown in Figure 5.4 could then be applied to any iron-zinc couple, regardless of the amount of zinc in the couple. The only change would be the time scale on the x-axis.
2) The thicknesses of the Γ and Γ_1 phases are constant at 1-5 μm and 5-10 μm, respectively, while the δ phase is growing. This was measured from Figure 4.5.
3) At long durations at 500˚C, the interphase will eventually comprise of only Γ phase. This was evident by the interphase that formed in the heat treated galvanized steel samples (Figure 4.35).

5.4 Phase Formation in the 725°C Samples

5.4.1 Phase Formation away from the Iron Interface

Since the iron diffused in large amounts and at great distances into the zinc, the structure shown at room temperature in Figure 4.11 would have only formed while solidifying. This was the reason for:

1) The large ζ phase particles found within large homogeneous η-Zn regions (Figure 4.13).
2) The transition of large ζ phase particles to large δ phase particles, in the η-Zn matrix (Figure 4.12).
3) The transition of few large δ phase particles to many small δ phase particles (top to bottom of Figure 4.11).
4) The formation of the thin intermetallic layer on the iron (shown in Figure 4.10). The Γ_1 and δ phases probably precipitated out of the Γ phase layer, as shown by the crystalline-shaped δ phase in the intermetallic layer in Figure 4.10, and the blotched areas in Figure 4.9. The blotches were perhaps caused by changes in volume due to the formation of phases with different densities. The blotches were found to have a variation in zinc concentration, due to the mix of δ and Γ_1, and Γ_1 and Γ phases.

Points 1 to 4 represent a continuous iron gradient in the zinc that was broken down by the precipitation of the intermetallic phases upon cooling. The iron concentration gradient was absorbed by the different iron concentration phases, when the right amount of solute was in a given area. The large particles that formed far away from the iron interface were created from iron gathered from the surrounding liquid iron-zinc.

5.4.2 Phase Formation at the Iron Interface

For pure metal samples heated at 725°C, there was a much greater rate of iron diffusion/dissolution, and the iron rapidly diffused throughout the molten zinc pool. At the 725°C temperature, the phases that existed were pure solid iron, a thin layer of Γ phase (probably 20-40 μm thick), and liquid zinc. During the 96 hour diffusion period, the ζ, δ, or Γ_1 phase could not form while the pure metal samples were at 725°C. The reasons for this phase growth were as follows.

1) The temperature was too high for ζ, δ, or Γ_1 phases to form. The maximum melting points of these phases were all less than 725°C (Figure 2.1).
2) The concentration of the iron in the zinc pool was too low for Γ phase to form.

No α-Fe – Γ two-phase region could exist (grain boundary diffusion is required to form this structure), and therefore was the reason why there was a steeper zinc concentration gradient at 725°C than at 400°C, as shown in Figure 4.21. At 725°C, lattice diffusion was dominant, with perhaps some small Γ phase forming in the grain boundaries of the iron (which could have occurred while cooling). Since there was no evidence found of

precipitated Γ phase, it could not have existed in the molten zinc after 96 hours of diffusion. The only structures of Γ phase found were small, scattered Γ phase particles that appeared at the iron interface in the pure metal samples (Figure 4.9). There was probably a solid layer of Γ phase that would have formed on the iron rod while at 725˚C, but it converted to other phases upon solidification and cooling. The thickness of the mixed-phase intermetallic layer found in the samples was probably proportional to the thickness of the Γ phase layer at 725˚C, before it was transformed.

5.5 Effect of Zinc Diffusion on Iron and Steel

5.5.1 Zinc Embrittlement of Pure Iron

It was shown in Figures 4.14 and 4.17 that Γ phase formed in the grain boundaries of the pure iron in diffusion couples at 400°C and 500°C. There was more Γ phase in the iron grain boundaries in samples heated at 400°C. Already mentioned earlier in Section 5.2.2, Γ phase formation in the grain boundaries of the interfacial iron grains might cause the grains to move. In order for this mechanism to work, the density of the Γ phase must be less than that of pure iron.

At 400°C, since the pure metal diffusion couple was in a solid solute-solid solvent condition, it would be difficult for the affected grains to move. Material would have to diffuse around the grain in order for it to easily move. If the grain was restricted to movement, which was most likely the case, then the volume change from the α-Fe to Γ phase transformation would lead to a stress build-up in the grain boundaries. Grain movement could be restricted by the solid intermetallic layers, or by other iron grains. Since other iron grains restrict the movement of the affected iron grains, stresses could be built up deep inside the iron/steel. The internal stress build-up in turn would cause the iron to become embrittled.

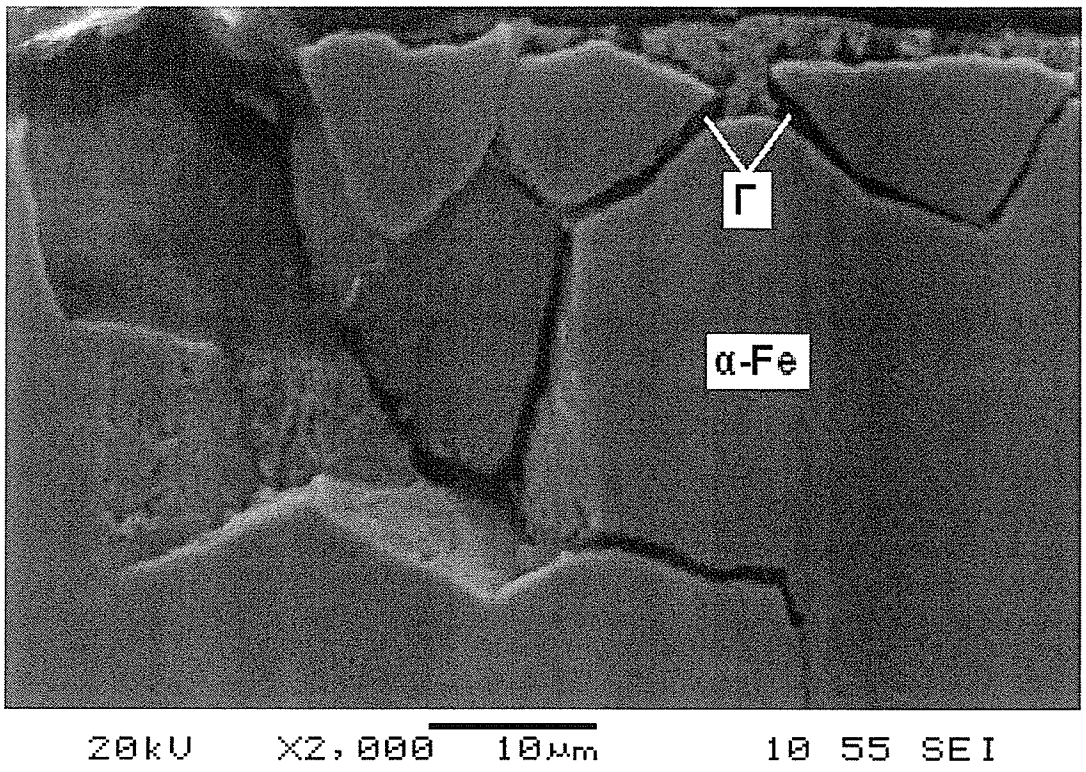

Figure 5.5: Whole grains broken out of the polished face of the α-Fe – Γ interface, in iron embrittled at 400˚C (*Mag 2000x*).

Evidence of such stress build-up causing embrittlement is shown in Figure 5.5. In this micrograph, three iron grains have broken out of the polished face of a pure metal sample that was heated at 400°C for 96 hours. The removal of these grains left jagged pits, respective to the shape of each extracted grain, in the area where they were once located – near the iron interface of the sample (at the top of Figure 5.5). The darker coloured Γ phase can be seen in amongst the grain boundaries of the interfacial iron grains. A dark coloured ribbon of Γ phase formed deep within the sample (30 μm depth), and some of this ribbon can be seen extruding out into the cavity of one of the removed grains. The Γ phase in the grain boundaries allowed whole grains to be easily removed from the iron. This would not have occurred if the iron was in a normal, un-embrittled state.

5.5.2 Cracking in Heat Treated Galvanized Steel

The galvanized steel samples were also embrittled by the zinc diffusion, most likely due to the same mechanism as found in the pure metal samples. The galvanized steel samples should be more embrittled than the pure metal samples, due to the larger amounts of Γ phase found in the grain boundaries of samples heat treated at 400°C and 500°C (Figures 4.36 and 4.37). This was the case, as shown by the large cracks in the embrittled galvanized steel in Figures 4.40 and 4.41.

From Figures 4.40 and 4.41, it was determined that the cracking mode in these samples was intergranular, with the cracks assisted by the brittle Γ phase found in the grain boundaries. Larger cracks found in the samples heated at 500°C were caused by the

larger particles and amount of Γ phase in the grain boundaries of the steel. The Γ phase was also detected to a greater depth in the steel, than the samples heat treated at 400°C (50-100 μm vs. 40-80 μm).

By itself, the detected Γ phase would have created a deeper crack in the samples heated at 500°C. The full length of the crack must be attributed to undetected Γ phase along the grain boundaries deeper within the galvanized steel. For the samples heat treated at 500°C, it was possible that the Γ phase, located in the grain boundaries, existed throughout the entire cross-section of the steel strip. The cracks may have initiated in the brittle iron-zinc intermetallic phase layer, but this was inconclusive. It could be possible that the cracks in the steel were extensions of the cracks formed in the δ phase layer, when it existed in the interphase. Cracks were found in the interphase layer of the galvanized steel samples heat treated at 400°C and 500°C (Figures 4.33 and 4.35). More time could have been spent to assess the cracking, but this was not a priority of this research. Only topical analysis was performed.

Inducing stress to cause cracks was not an objective of this research, but it was an important and significant result nonetheless. The cracks were large and deep, they were created in a formerly ductile and tough material, and were produced by a rudimentary, low stress-inducing 90° bend. This surprise result had to be documented. Related to the objective, it illustrated the effect of zinc diffusion into iron.

Chapter 6

CONCLUSIONS

From the results and discussion in this work, the following conclusions can be made.

Pure metal diffusion couples

- The diffusion coefficient for zinc into iron, with using bulk amounts of pure metal, was determined to be: 1.5×10^{-17} m^2/s at 400°C, 1.6×10^{-17} m^2/s at 500°C, and 1.7×10^{-17} m^2/s at 725°C.
- The numerical model with the zinc diffusion coefficient that varied with zinc concentration in the iron modelled the measured zinc concentration gradient in the iron better than the numerical model with the zinc diffusion coefficient that was constant with zinc concentration in the iron. For 400°C, 500°C and 725°C, the zinc diffusion coefficient was found to decrease with increase in zinc concentration in iron. This relationship was due to an increase in the effect of grain boundary diffusion at the lower zinc concentrations.
- The zinc diffusion coefficient measured in this investigation was an "apparent" D_{Zn}. This was due to the combination of lattice diffusion and grain boundary diffusion of zinc into iron that occurred at all three experiment temperatures.
- Γ phase particles formed in the grain boundaries of the iron in pure metal samples at 400°C and 500°C. There were negligible, if any, amounts of Γ phase particles in the grain boundaries of the iron at 725°C.
- Γ is the only iron-zinc phase that forms in the grain boundaries of iron.

- For pure metal samples, more Γ phase particles formed in the grain boundaries of the iron at 400°C than at 500°C.
- Rapid grain boundary diffusion accounted for the Γ phase particles in the iron at temperatures of 400°C and 500°C. The high zinc diffusion coefficient derived at 400°C and 500°C was a result of rapid grain boundary diffusion of zinc into iron.
- At 725°C, lattice diffusion is dominant, while at 400°C and 500°C, grain boundary diffusion in the iron is dominant.

Heat treated galvanized steel

- Γ phase particles were found in the grain boundaries of commercial galvanized steel, when heat treated at 400°C and at 500°C.
- For heat treatment temperatures of 400°C and 500°C, more Γ phase formed in the grain boundaries of galvanized steel, than in pure iron.
- More Γ phase particles formed in the grain boundaries of galvanized steel heat treated at 500°C, than at 400°C.
- The reason for the differences in diffusion structure between the galvanized steel and the pure metal samples was due the amount of zinc available for diffusion: there was a limited amount of zinc in the galvanized steel, whereas there was an semi-infinite amount of zinc in the pure metal samples.
- The pure metal samples, heated at the temperatures of 400°C and 500°C, would have formed the same structure as the galvanized steel samples, if the samples were held at the experiment temperature for a longer time, or if the amount of zinc was reduced.

- The amount of each diffusing material greatly influenced the diffusion behaviour. When less zinc was involved, there was more zinc found in the steel. When a large pool of zinc was used: there was a high amount of iron diffusion (in the samples heated at 500°C and 725°C), and much less Γ phase formation (both as a layer on the iron interface, and as particles in the grain boundaries of the iron).

Effect of zinc diffusion

- Zinc diffusion embrittled both pure iron and commercial steel. The severe reduction in fracture toughness was found in pure metal samples heat treated at 400°C for 96 hours, and galvanized steel samples heat treated at 400°C and 500°C for 96 hours.
- The galvanized steel samples heat treated at 500°C for 96 hours were more embrittled than the samples heat treated at 400°C for 96 hours, due to the larger amount of Γ phase formed in the grain boundaries of the steel at 500°C.
- The size of the cracks that form in zinc diffusion embrittled iron / steel is dependant on the amount of Γ phase in the grain boundaries. The larger the amount and size of the Γ phase particles, the deeper and wider the cracks that will form. The diffusion coefficient of the zinc into the iron, and the transportation mechanism of the zinc atoms, determines the size of the Γ phase particles.
- Fracture in zinc diffusion embrittled iron / steel was by intergranular mode. The cracks were aided by the brittle Γ phase that formed in the grain boundaries of the iron/steel.

6.1 Recommended Work

1) For the pure metal samples: produce more samples at each of the three temperatures, using the poured liquid metal method. This would qualify and verify the average concentration gradients determined in this work. Analysis of these samples should be done using the procedure used to produce a fine zinc concentration gradient (Section 4.1.4).

2) For heat treating galvanized steel: seal the galvanized steel strips in Vycor with an inert atmosphere (argon), instead of wrapping the strips in tool steel. This would reduce the amount of oxide on the samples, thereby freeing more zinc to be used in the diffusion experiments. The results of these experiments can then be compared with the results produced in this work, therefore checking if a more sophisticated experiment procedure would make a difference in the results.

3) Determine the intermetallic phase transition periods for bulk pure metal couples heat treated at 400°C. This would be accomplished by heat treating the bulk pure metal samples for different times, and then measuring the thicknesses of the phases that formed. This experiment could also be done at the temperature of 500°C, which would also prove if δ phase thickness can become so large that the Γ_1 and Γ phases start to thicken. These tests would also verify the intermetallic phase growth predictions made for the interdiffusion of bulk iron and zinc at temperatures of 400°C and 500°C (Figures 5.3 and 5.4).

4) Using the poured liquid metal method: run pure metal samples at 500°C, with decreasing amounts of zinc. The experiments would start at 96 hours with 50 g of molten zinc, with successive trials using 5-10 g less zinc each time. This experiment would find the point where δ phase growth becomes restricted. This would check the assumption that at 500°C the Γ_1 and Γ phases would begin to consume the δ phase, once phase growth is restricted.

5) Using the poured liquid metal method: run pure metal samples at 725°C, with decreasing amounts of zinc. The experiments would start at 96 hours with 100 g of molten zinc, with successive trials using 5-10 g less zinc each time. This experiment would find the point where the zinc becomes saturated with iron, and would thus precipitate Γ phase. The resulting structure would probably resemble the structure formed in the pure metal samples held at 500°C for 96 hours (Figure 4.6), with a large Γ phase structure formed on the iron instead. This experiment would also prove if Γ phase can form in the grain boundaries of the iron at 725°C.

6) Create a thin coat of pure zinc onto pure iron, and then heat treat the samples for 96 hours using the temperatures of 400°C and 500°C. The zinc coated pure iron samples could be created by passing iron rod, or strip, in a pool of pure molten zinc (mimicking the galvanizing process). The zinc on the iron would be solidified, and then the samples heat treated in the same manner as the galvanized steel samples produced in this work.

This experiment would check, or verify, the assumption that the pure iron behaved in the same manner as the heat treated galvanized steel. If the results weren't the same, then something else caused the galvanized steel to pick up zinc and form large amounts of Γ phase in the grain boundaries. This would also explain why more Γ phase formed in the grain boundaries of the galvanized steel at 500°C than at 400°C, when the opposite was found in the bulk pure metal samples.

A different way to check this assumption would be to drop a strip of commercial galvanized steel into a molten pool of pure zinc, solidify the galvanized steel strip within the zinc casting, and then heat treat the ingot at 400°C for 96 hours. Yet another way to check this assumption could be to hold the pure metal diffusion couple for times greater than 96 hours. Diffusion times as long as 10 to 20 days could be performed. The longer diffusion times could also be run for pure metal samples heat treated at 500°C.

7) Using the poured liquid metal method: determine the zinc diffusion coefficient in iron across a range of temperatures, using intervals of 25-50°C, and starting at 300°C. Plot the zinc diffusion coefficients versus the inverse of the temperature (D_{Zn} vs. 1/T – see the example in Figure 5.1). Compare this chart to the predicted chart in Figure 5.2.

8) Determine the change in fracture toughness in the iron-zinc system with change in diffusion temperature and time (use pure metal samples and/or zinc coated steel samples). Determine a numerical model if necessary and/or feasible. This model could then be checked with experimental data from samples of heat treated commercial galvanized steel.

9) A full and complete study of the cracking mode, initiation, and morphology in embrittled heat treated galvanized steel.

Chapter 7

REFERENCES

[1] Shewmon, P.; Abbas, M.; Meyrick, G., "Anomalously Fast Diffusion in the Fe-Zn System", Metallurgical Transactions A, v 17A, 1986, p 1523.

[2] Hillert, M.; Purdy, G., "Chemically Induced Grain Boundary Migration", Acta Metallurgica, v 26, n 2, 1978, p 333.

[3] Chongmo, L.; Hillert, M., "A Metallographic Study of Diffusion-Induced Grain Boundary Migration in the Fe-Zn System", Acta Metallurgica, v 29, n 12, 1981, p 1949.

[4] Yu, Z.; Shewmon, P., "Diffusion Driven Grain Boundary Migration in Iron during Zincification", Metallurgical Transactions A, v 13A, 1982, p 1567.

[5] Raghavan, V., "Fe-Zn (Iron-Zinc)", Journal of Phase Equilibria, v 24, n 6, 2003, p 544.

[6] Burton, B.; Perrot, P., Phase Diagrams of Binary Alloys, ASM International, 1993, p 459.

[7] Marder, A., "The Metallurgy of Zinc-Coated Steel", Progress in Material Science, v 45, 2000, p 191.

[8] Guttmann, M., "Diffusive Phase Transformations in Hot Dip Galvanizing", Materials Science Forum, v 155-5, 1994, p 527.

[9] Richter, I.; Feller-Kniepmeier, M., "Diffusion of Zn in α-Fe Single Crystals", Phys. Stat. Sol., v 68A, 1981, p 289.

[10] Bastin, G.; van Loo, F.; Rieck, G., "A New Compound in the Iron-Zinc System", Zeitschrift fuer Metallkunde, v 65, n 10, 1974, p 656.

[11] Bell, A.; Caplin, A., "Magnetic and Electrical Properties of Very Dilute Zn – 3d Alloys", J. Phys. F: Metal Phys., v 5, 1975, p 143.

[12] Onishi, M.; Wakamatsu, Y.; Miura, H., "Formation and Growth Kinetics of Intermediate Phases in Fe-Zn Diffusion Couples", Journal of the Japan Institute of Metals, v 15, n 5, 1974, p 331.

[13] Borhan-Tavakoli, A., "Formation and Growth of the δ_1 Phase in the Fe-Zn System; Part I", Zeitschrift fuer Metallkunde, v 75, n 5, 1984, p 350.

[14] Borhan-Tavakoli, A., "On the Formation and Growth of the δ_1 Phase in the Fe-Zn System; Part II", Zeitschrift fuer Metallkunde, v 75, n 6, 1984, p 436.

[15] Rigg, G., "The Diffusion of Zinc and Iron at Temperatures below the Melting Point of Zinc", Metal Industry (London), v 44, n 11, 1934, p 301.

[16] Syahbuddin; Munroe, P.; Gleeson, B., "The Development of Fe-Zn Intermetallic Compounds in Solid Fe/Zn and Fe/Zn – Al Diffusion Couples During Short-Term Annealing at 400°C", Materials Science and Engineering A: Structural Materials: Properties, Microstructure and Processing, v 264, n 1, 1999, p 201.

[17] Shewmon, P., Diffusion in Solids, 2nd Edition, TMS, 1989.

[18] Peterson, N., "Grain-Boundary Diffusion in Metals", International Metals Reviews, v 28, n 2, 1983, p 65.

[19] Balluffi, R., "Grain Boundary Diffusion Mechanisms in Metals", Metallurgical Transactions B, v 13B, 1982, p 527.

[20] Shewmon, P., "Diffusion Driven Grain Boundary Migration", Acta Metallurgica, v 29, 1981, p 1567.

[21] Shewmon, P.; Yu, Z., "Size Effect, Internal Stress, and Diffusion Driven Grain Boundary Migration", Metallurgical Transactions A, v 14A, 1983, p 1579.

[22] Iyer, V.; Meyrick, G.; Shewmon, P., "The Reversibility and Reproducibility of Diffusion Induced Grain Boundary Motion in the Fe-Zn System", Scripta Metallurgica, v 19, n 9, 1985, p 1117.

[23] Gellings, P.; de Bree, E.; Gierman, G., "Synthesis and Characterization of Homogeneous Intermetallic Fe-Zn Compounds, Part II: The ζ Phase", Zeitschrift fuer Metallkunde, v 70, n 5, 1979, p 315.

[24] Cahoon, J.; Tandon, K.; Chaturvedi, M., "Ternary Diffusion in Liquid Cd-In-Sn Alloys in Microgravity", paper #IAF-01-J.3.06, proceedings 52nd International Astronautical Conference, Toulouse, France, October 1-5, 2001.

[25] Oikawa, H., The Technology Reports of the Tohoku University, v 47(2), 1982, p 215.

Appendix A

CONCENTRATION GRADIENT TRENDLINE EQUATIONS

The trendlines determined from the spreadsheet (Microsoft Office Excel 2003) for the relationship between the zinc concentration in the iron and the distance into the iron were 6^{th} order polynomial functions. The trendlines were developed from the fine zinc concentration gradient produced at each of the experimental temperatures (400°C – Figure 4.22; 500°C – Figure 4.23; 725°C – Figure 4.24).

Equations for the Trendlines

Where: y = the zinc concentration (at%)
x = the distance into the iron (μm)

400°C:

$$y = 0.00001x^6 - 0.0007x^5 + 0.0149x^4 - 0.1558x^3 + 0.8303x^2 - 2.1253x + 3.6375$$

500°C:

$$y = 0.000005x^6 - 0.0004x^5 + 0.0129x^4 - 0.1937x^3 + 1.4006x^2 - 4.5774x + 6.9116$$

725°C:

$$y = 0.0002x^6 - 0.0087x^5 + 0.162x^4 - 1.4904x^3 + 7.2989x^2 - 20.151x + 31.869$$

Appendix B

PHASE GROWTH CHART DATA

Table B.1: Hypothetical Data Points for Figure 5.3

√ Time (h^1/2)	Phase Thicknesses (μm)				
	Zeta	Delta	Gamma-1	Gamma	Total
0	0	0		0	0
1	21	35		7	63
2	42	67	0	8	117
3	63	99	4	6	172
4	78	130	7	4	219
5	49	158	9	2	218
6	29	176	10	2	217
7	16	185	13	3	217
8	7	186	19	4	216
9	3	178	29	6	216
10	0	165	42	8	215
11		147	57	11	215
12		129	72	14	215
13		110	87	18	215
14		89	103	23	215
15		68	118	29	215
16		49	130	36	215
17		31	138	46	215
18		17	139	59	215
19		7	134	74	215
20		0	121	94	215
21			100	115	215
22			75	140	215
23			49	166	215
24			24	191	215
25			0	215	215

The growth of the δ, Γ_1, and Γ phases followed closely to 6th order polynomial equations. The growth equations were developed by the spreadsheet that was used to construct Figure 5.3 (Microsoft Office Excel 2003). The equations that were derived were as follows.

Equations for Phase Growth at 400°C

Where: y = the width of the phase (μm)
x = the square root of time in hours ($h^{1/2}$)

δ phase:

$$y = 0.00003x^6 - 0.0031x^5 + 0.1029x^4 - 1.5139x^3 + 6.8081x^2 + 23.906x + 1.8517$$

Γ_1 phase:

$$y = 0.00002x^6 - 0.0012x^5 + 0.0091x^4 + 0.2586x^3 - 3.6453x^2 + 17.395x - 22.404$$

Γ phase:

$$y = -0.00003x^6 + 0.0018x^5 - 0.05x^4 + 0.6486x^3 - 3.9068x^2 + 8.9617x + 0.5878$$

When these equations were checked, the values they gave were slightly different for longer lengths of time (15-25 √h). The erroneous values were not plotted on the chart (Figure 5.3), yet the trendline followed the data points in Table B.1. Though the equations for growth were wrong for long periods of time, it can be concluded that the δ, Γ_1, and Γ phase growth might be similar to the equations given above. The error is probably due to rounding the constants in front of each variable in the growth equations.

Appendix C

EXPERIMENT LOG

Experiment Number and Date	Experiment Procedure	Results and Analysis
The first experiments were tests to see if powder metals could be used as the diffusing media. The experiments were mostly a failure, as oxidation would occur throughout the powdered material. The powder metal (P/M) used in these experiments were: *1) Slices from compressed P/M rods. Two compositions were used: 50/50 wt% P/M, and 84/16 wt% Fe.* *2) Pure iron powder mixed with 99.99% pure Zn shot.*		
1	Heat 50/50 P/M at 390°C for 24h in Ar.	Material produced was a brittle agglomeration of metal, oxide, and intermetallic (Fe-Zn) phases.
2	Heat 84/16 P/M at 500°C for 1h in Ar.	Same results as previous experiment.
3	Melt alloy of 6.5 wt% Fe P/M at 800°C.	Ingot was successfully created.
4	Heat slice of ingot from Sample #3 at 400°C, sealed in Pyrex with Ar, for 24h.	The casting turned into a brittle mass.
5	Melt alloy of 6.5 wt% P/M at 700°C.	Cast ingot was successfully created. Analyzed polished sample on the SEM on May 23.
6	Heat ingot section from Sample #5 at 400°C, sealed in Pyrex with Ar, for 18h.	Material produced was a brittle agglomeration of metal, oxide, and intermetallic (Fe-Zn) phases.

7		Melt alloy of 18 wt% Fe P/M, sealed in Pyrex with Ar at 820°C.	Same results as previous experiment.
8	27-May-02	Re-melt material from Sample #7 in an induction furnace at 800°C.	Failure: sample material did not pour, just formed oxidized lumps.

Experiment #9 was the first test of pure metal diffusion in bulk amounts. This experiment consisted of liquid zinc and a 12.7 mm diameter, 6.35 mm tall piece of iron rod contained in a machined graphite crucible. The loaded crucible was placed in a sealed, 31.75 mm diameter stainless steel tube. The tube was evacuated, filled with argon, and clamped into position inside a vertical furnace.

9	28-May	Heat Fe/Zn at 725°C for 48h.	Mounted and polished the sample, diffusion occurred. Analyzed on the SEM on May 31.
10	4-Jun	Heat Fe/Zn at 725°C for 17h.	Mounted and polished the sample, diffusion occurred. Analyzed on the SEM on June 13.
11	12-Jun	Heat Fe/Zn at 725°C for 137h.	Mounted and polished the sample, diffusion occurred. Analyzed on the SEM on June 19.
12	20-Jun	Heat 84/16 P/M at 800°C for 17h.	Failure: crucible broke in the equipment.

Experiment #13 was the first test of heat treated galvanized steel. The 6 x 25 x 0.7 mm thick strips of commercial galvanized steel were wrapped bare in tool steel, and placed in air in a box furnace at the designated temperature.

13	2-Jul	Heat galvanized steel at 400°C for 22h.	Failure: nearly all of the zinc oxidized.

14	15-Jul-02	Heat galvanized steel at 400°C for 23.25h.	Analyzed polished sample on the SEM on July 19. Graphed the zinc concentration gradient.
15	22-Jul	Mount as-received galvanized steel.	Analyzed polished sample on the SEM on July 22. Failure: diffusion contamination found from the aluminum foil backing, and brass clip.
16	23-Jul	Heat galvanized steel at 400°C for 24h.	Analyzed polished sample on the SEM on July 24 and 26. Graphed the zinc concentration gradient.
17	25-Jul	Heat galvanized steel at 400°C for 96h.	Analyzed polished sample on the SEM on July 30. Graphed the zinc concentration gradient. Images of sample used for Figures 4.39 and 4.40.

Prior to Experiment #18, a new diffusion apparatus was constructed. This apparatus was a bigger, and more sophisticated, version of the equipment used for Experiment #9. However, there were at least four major errors with the equipment that were overlooked, when it was put together. These errors were corrected within the experimentation process, and summaries of the corrections can be found in the following pages.

Also, for Experiment #18 and on, alumina crucibles were used to contain the pure metal diffusion samples. These crucibles eliminated the carbon that was diffusing into the sample material from the graphite crucible.

18	8-Aug	Heat Fe/Zn at 725°C for 90h.	Mounted and polished the sample, diffusion occurred. Analyzed on the SEM on August 13. Graphed the zinc concentration gradient, and calculated the diffusion coefficient.
19	23-Aug	Heat Fe/Zn at 700°C for 92.5h.	Mounted and polished the sample, diffusion occurred. Analyzed on the SEM on August 28. Graphed the zinc concentration gradient, and calculated the diffusion coefficient.

20	30-Aug-02	Heat Fe/Zn at 705°C for 94h.	Mounted and polished the sample, diffusion occurred. Analyzed on the SEM on September 3. Graphed the Zn concentration gradient, and calculated the diffusion coefficient.

After Experiment #20, the iron for the samples was provided by pure iron rod (3.175 mm diameter). A 9 mm long segment was cut off the rod stock, using bolt shears. The cold-worked section was ground off, the segment hand polished to 600 grit, and then placed in a pre-drilled machineable ceramic disc (the "iron holder").

The iron holder kept the iron rod segment upright, restricted diffusion along the sides of the iron, and positioned the molten zinc pool above the iron. The iron holder was machined to fit the bottom of the crucible, and was formed prior to use in each experiment. The iron rod was placed in the holder so that it was recessed 2-3 mm down inside the center hole. This cavity would separate the metals while heating up, and it would fill with liquid zinc for contact with the iron.

21	12-Sep	Heat Fe/Zn at 700°C for 91.5h.	Failure: nearly all of the iron dissolved, and most of the zinc vapourized.

Began to use a pipe cutter to cut the iron rod, instead of bolt shears.

22	25-Sep	Heat Fe/Zn at 700°C for 48h.	Mounted and polished the sample, diffusion occurred. Analyzed on the SEM on October 7.
23	10-Oct	Heat Fe/Zn at 700°C for 24h.	Analyzed polished sample on the SEM on October 21. Graphed the zinc concentration gradient.
24	24-Oct	Melt alloy of 7 wt% Fe P/M in crucible at 625°C.	Material produced was a brittle agglomeration of metal, oxide, and intermetallic (Fe-Zn) phases.
25	19-Nov	Heat Fe/Zn at 725°C for 72h.	Mounted and polished the sample, diffusion occurred. Analyzed on the SEM on December 18.

26	10-Jan-03	Heat Fe/Zn at 720°C for 71h.	Failure: most of the zinc vapourized.
27	7-Feb	Heat Fe/Zn at 720°C for 72h.	Oxidation prevented the metals from contacting.

The crucible used since Experiment #18, broke in Experiment #25. As well, the straight-wall crucibles employed in Experiments #26 & #27 had to be broken to retrieve the sample material. New crucibles were ordered, and the first crucible used was TW37. Since this crucible was taller than the previous crucibles, the stainless steel thermocouple tube had to be raised.

As well, started to flush the vacuum chamber 5 times with argon, prior to heating. This was done to minimize contamination and oxidation.

28	6-Jun	Heat Fe/Zn at 710°C for 72h.	Oxidation prevented the metals from contacting.

Water appeared for the first time in the vacuum chamber with Experiment #28. The water formed in beads under the brass cap, which is the coolest part of the chamber. It appeared in the same quantities in Experiments #29, #30, and #31.

If beads of water formed underneath the brass cap at the top of the vacuum chamber, then the rest of the chamber was saturated with water. Along with, or because of, the beads of water, there was also heavy oxide on the sample metals. The oxidation did not allow the two metals to contact, therefore diffusion could not occur. This trend was prevalent in a large portion of the experiments.

The roughing pump that was used since the beginning, burnt out during Experiment #28. A newer, more powerful roughing pump was used as a replacement. However, the pump required a different setup on the vacuum chamber, so the piping was re-designed to accommodate the exchange. Not only was the piping layout changed to adapt to the replacement pump, it was also greatly simplified. The final result was a system that not only had a stronger pump, but had a more efficient piping network, and was less likely to leak.

29	7-Jul	Heat Fe/Zn at 710°C for 72h.	Same results as previous experiment.

Experiment #30 was the first attempt at a solid zinc - iron diffusion sample. Samples were first heated at 725°C for 2 hours to produce a liquid zinc state, then cooled to 400°C for the solid state diffusion.

30	18-Jul-03	Heat Fe/Zn at: 710°C for 2h, 400°C for 70h.	Ceramic holder floated, therefore incomplete/inconsistent diffusion. Analyzed on the SEM on September 3.
31	25-Jul	Heat Fe/Zn at: 710°C for 2h, 400°C for 72h.	Same results as previous experiment.

The last of the TW37 crucibles broke, the replacement crucible chosen was TW36. The stainless steel thermocouple tube was lowered to accommodate the shorter TW36 crucible.

32	30-Jul	Heat Fe/Zn at: 710°C for 2h, 400°C for 72h.	Oxidation prevented the metals from contacting.

With Experiment #32, large beads of water appeared under the brass cap. At this time, it was thought that the water was caused by wet argon.

33	8-Aug	Heat Fe/Zn at: 710°C for 2h, 400°C for 72h.	Ceramic holder floated, therefore incomplete/inconsistent diffusion.

Three of the four previous experiments failed due to the iron holder floating to the top of the molten zinc pool. The cause of the failures was due to inconsistently dimensioned, hand ground iron holders. The misshaped holders allowed liquid zinc to get under them, thus causing them to float. This problem was solved by precision machining the holders on a lathe. When the iron holder was machined to fit the bottom of the crucible, it was impossible for it to float.

34	22-Aug	Heat Fe/Zn at: 710°C for 2h, 400°C for 72h.	Oxidation prevented the metals from contacting.
35	27-Aug	Heat Fe/Zn at: 710°C for 2h, 400°C for 72h.	Same results as previous experiment.

By Experiment #35, the amount of water vapour was so great inside the vacuum chamber that a film of water formed under the brass cap.

36	9-Sep-03	Heat 50/50 P/M at 700°C for 1h.	Analyzed polished sample on the SEM on September 19.
37	10-Sep	Heat 84/16 P/M at 600°C for 1h.	Material produced was a brittle agglomeration of metal, oxide, and intermetallic (Fe-Zn) phases.

As the experimentation continued, the machineable ceramic sleeves within the chamber were found to contain water. Instead of heat treating them to remove the water, they were replaced with stainless steel sleeves for Experiment #38.

38	12-Sep	Heat Fe/Zn at: 720°C for 2h, 400°C for 72h.	Mounted and polished the sample, diffusion occurred. Analyzed on the SEM on September 23 and 24. Graphed the Zn concentration gradient, and calculated the diffusion coefficient.

The beads of water were reduced in size in Experiment #38. Furthermore, the beads gradually got smaller with each passing experiment, until they finally disappeared by attrition in Experiment #47. The experiments were purposely repeated, wiping the water up each time, until finally no more water showed up. Other methods to remove the water vapour were hopeless.

In retrospect, the disappearance of the beads of water may be due to the change of the season into the dry winter. The wet spring may be the reason for the reappearance of the beads of water in Experiment #63.

39	19-Sep	Heat Fe/Zn at: 720°C for 2h, 400°C for 72h.	Oxidation prevented the metals from contacting.
40	29-Sep	Heat Fe/Zn at: 720°C for 2h, 400°C for 72h.	Same results as previous experiment.

41	7-Oct-03	Heat Fe/Zn at: 720°C for 2h, 400°C for 72h.	Same results as previous experiment.

Introduced the second thermocouple into the vacuum chamber apparatus. The temperature was now recorded above and below the crucible. The thermocouple was placed into a position up and underneath the furnace, wedged lengthwise between the bottom of the vacuum chamber and the concrete floor.

42	14-Oct	Heat Fe/Zn at: 720°C for 2h, 400°C for 72h.	Same results as previous experiment.

Began to use iron holders with three blind holes drilled in the top face. These pits would fill with zinc, which would protect the brittle diffusion zone from shear forces inflicted on the sample by the hacksaw during sectioning.

43	20-Oct	Heat Fe/Zn at: 720°C for 2h, 400°C for 72h.	Same results as previous experiment.

To make the pure metal diffusion experiments consistent, began to use 725°C as the melt temperature.

44	27-Oct	Heat Fe/Zn at: 725°C for 2h, 400°C for 72h.	Same results as previous experiment.
45	31-Oct	Heat Fe/Zn at: 725°C for 2h, 400°C for 72h.	Same results as previous experiment.
46	4-Nov	Heat Fe/Zn at: 725°C for 2h, 400°C for 72h.	Mounted and polished the sample, diffusion occurred. Analyzed on the SEM on November 20. Image of sample used for Figure 4.4.
47	10-Nov	Heat Fe/Zn at: 500°C for 0.5h, 725°C for 1.5h, 400°C for 72h.	Oxidation prevented the metals from contacting.

During Experiment #47, one of the wires from the bottom thermocouple broke. Consequently, the bottom thermocouple was rebuilt, with a plastic cover on the plug. After reconstruction, both thermocouples were tested for accuracy, using a box furnace. The repaired bottom thermocouple was accurate to the readings given by the box furnace thermocouple. However, when the top thermocouple was tested, it gave readings of 370°C at 400°C, and 705°C at 725°C. Compensation was made for this error in future experiments.

To prevent future damage to the rebuilt bottom thermocouple, an aluminum stand was built to hold the thermocouple upright and in place.

For Experiment #48 (and all other future heat treated galvanized steel experiments), the metal was placed in a machineable alumina holder to separate the metal from the tool steel.

48	27-Nov-03	Heat galvanized steel at 500°C for 0.25h.	Failure: zinc undercut while polishing.

To prevent the edge of the galvanized steel from undercutting during polishing, started to use blank galvanized steel strips for backing.

49	27-Nov	Heat galvanized steel at 500°C for 24h.	Analyzed polished sample on the SEM on December 3.
50	27-Nov	Heat galvanized steel at 500°C for 96h.	Analyzed polished sample on the SEM on December 17. Image of sample used for Figure 4.41.

Experiment #51 and #53 were tests of an anomaly that occurred when mounting Experiment #15. Experiment #51 used polished blocks of Zn and Al, whereas Experiment #53 used a block of Zn with Al foil.

51	2-Dec	Heat Zn/Al pieces at 100°C for 0.75h.	Analyzed polished sample on the SEM on December 3. No Al found in the Zn.
52	4-Dec	Heat galvanized steel at 400°C for 96h.	Analyzed polished sample on the SEM on December 11 and 17.

53	10-Dec-03	Heat Zn/Al pieces at 100°C for 0.75h.	Analyzed polished sample on the SEM on December 11. No Al found in the Zn.
54	15-Dec	Heat Fe/Zn at: 725°C for 2h, 400°C for 72h.	Oxidation prevented the metals from contacting.

Began to use spark-cut iron rod segments, produced by a Hansvedt Electro-Discharge Machine. This eliminated the cold- work inflicted on the iron rod by the pipe cutter.

55	16-Jan-04	Heat Fe/Zn at: 725°C for 2h, 400°C for 72h.	Ceramic holder floated, therefore incomplete/inconsistent diffusion.

The iron holder floated in Experiment #55 because an old holder was used in the new crucible. However, the casting that was formed gave a good impression of the bottom of the crucible. The casting was then used as a model when machining new iron holders.

Returned to using 96 hours as the duration for solid diffusion. If diffusion occurred, it would be easier to measure on the SEM due to the wider interphase.

56	23-Jan	Heat Fe/Zn at: 725°C for 2h, 400°C for 96h.	Oxidation prevented the metals from contacting.
57	29-Jan	Heat Fe/Zn at: 725°C for 2h, 400°C for 96h.	Oxidation prevented the metals from contacting.

Beads of water were found under the brass cap in Experiment #57.

58	5-Feb	Heat galvanized steel at 500°C for 96h.	Mounted, polished, and etched the sample. Analyzed on the SEM on February 17 and 18.
59	6-Feb	Heat Fe/Zn at: 725°C for 2h, 400°C for 96h.	Zinc didn't contact the iron.

Tapered the lip of the centre hole leading to the iron in the holder, beginning with Experiment #60. This was done in an effort to coax the zinc down to contact the iron. As the experiments progressed, and kept failing, the taper became more pronounced. By Experiment #64, the taper had grown into a 60° angle, and started 0.5 mm above the iron.

60	12-Feb-04	Heat Fe/Zn at: 725°C for 2h, 400°C for 96h.	Failure: zinc vapourized, due to running the vacuum while the zinc was molten.
61	12-Feb	Heat galvanized steel at 400°C for 96h.	Mounted, polished, and etched the sample. Analyzed on the SEM on April 28, and May 6. Image of sample used for Figure 4.34.
62	11-Mar	Heat Fe/Zn at: 725°C for 2h, 400°C for 96h.	Zinc didn't contact the iron.

For Experiment # 63, started to flush the vacuum chamber 10 times with argon, prior to heating up.

63	22-Mar	Heat Fe/Zn at: 725°C for 2h, 400°C for 96h.	Zn didn't contact the iron (< 1 mm gap).

Large water beads were found under the brass cap in Experiment #63, and in Experiments #64 and #65 as well.

For Experiment #64, started to use a 3 hour duration at the liquid temperature (725°C). This would provide a greater chance for metal contact, and hopefully remove the iron oxide.

64	1-Apr	Heat Fe/Zn at: 725°C for 3h, 400°C for 96h.	Zinc didn't contact the iron (< 0.5 mm gap).

For Experiment #65 and on, the iron was protruded about 1 mm above the top of the iron holder. This would promote metal contact.

65	8-Apr-04	Heat Fe/Zn at: 725°C for 2.5h, 400°C for 96h.	Oxidation prevented the metals from contacting.

With Experiment #66, started to flush the vacuum chamber with argon while heating up. This was done in hope of reducing the amount of water vapour in the vacuum chamber.

66	27-Apr	Heat Fe/Zn at: 725°C for 3h, 400°C for 96h.	Zn didn't contact the iron (0.5 mm gap).

Again, large beads of water were found with Experiment #66, but in less amount than the previous three experiments.

With Experiment #67, a major leak was discovered in the diffusion apparatus. The leak was detected by using undiluted liquid soap, applied at the joints of the equipment with a toothbrush.

67	4-May	Heat Fe/Zn at: 725°C for 3h, 400°C for 96h.	Diffusion occurred, however, oxide/void was found 2-3 mm above the iron interface. Analyzed polished sample on the SEM on May 14. Graphed the Zn concentration gradient, and calculated the diffusion coefficient.

Took apart the diffusion equipment, found damaged o-rings around the thermocouple tube, replaced them. Small leaks were still found in the repaired area, so low vapour pressure epoxy was used to permanently seal up the area. That solved the leaks in that location.

The vacuum chamber o-ring was also replaced. A crack was found in the splice joint in the o-ring, as well, it was determined that it was an improper o-ring for the contact area (it didn't fit). A thicker o-ring was used as the replacement.

The vacuum chamber performed excellently after these repairs. The water vapour in the chamber, and the oxidation in the samples, was greatly reduced. Only very small beads of water were found in the next five experiments. Thus began a string of successful experiments.

68	13-May-04	Heat Fe/Zn at: 725°C for 3h, 400°C for 96h.	Diffusion occurred, however, oxide/void was found 2-3 mm above the iron interface. Analyzed polished sample on the SEM on May 21. Graphed the Zn concentration gradient, and calculated the diffusion coefficient. Image of sample used for Figure 3.10.
69	21-May	Heat Fe/Zn at: 725°C for 3h, 400°C for 96h.	Diffusion occurred, however, iron oxide was found 2-3 mm above the iron interface. The oxide was in a smaller amount than in Sample #68. Analyzed polished sample on the SEM on May 28. Graphed the Zn concentration gradient, and calculated the diffusion coefficient.
70	26-May	Heat Fe/Zn at: 725°C for 3h, 400°C for 96h.	Diffusion occurred, however, iron oxide was found 2-3 mm above the iron interface. The oxide was in a smaller amount than in Sample #69. Analyzed polished sample on the SEM on June 4. Graphed the Zn concentration gradient, and calculated the diffusion coefficient. Image of sample used for Figure 4.15.

Experiment #71 was a check of the effect of the liquid diffusion component of the experimental procedure.

71	2-Jun	Heat Fe/Zn at 725°C for 3h.	Oxide found within the diffusion zone. Analyzed polished sample on the SEM on June 7. Graphed the zinc concentration gradient, and calculated the diffusion coefficient.

When filling the crucible with zinc shot for Experiment #72, the bottom layer of shot, closest to the iron, was arranged so that a void was formed around the iron. This would reduce zinc oxide in the vicinity of the iron, allowing liquid zinc to have better contact with the iron.

72	3-Jun-04	Heat Fe/Zn at: 725°C for 3h, 400°C for 96h.	Less oxide found within the diffusion zone. Analyzed polished sample on the SEM on June 8. Graphed the zinc concentration gradient, and calculated the diffusion coefficient. Images of sample used for Figures 4.14 and 5.5.

Sample #72 was the best pure metal solid diffusion sample to date.

Since iron and zinc oxide were still found in the interphase, a quick run, 3 hour experiment (#73) was performed with a piece of machineable ceramic on top of the iron holder, just above the iron rod. The idea was to separate the iron from the zinc shot, while heating up to the melt temperature. Once molten, the zinc would run down and around the machineable ceramic piece, thus causing it to float away from the iron.

Due to this action, no zinc oxide would contact the iron oxide, and therefore no voids would form above the iron. It was assumed that the zinc would then penetrate through the iron oxide, contact the iron, and then diffusion products would lift off the remainder of the iron oxide. The iron oxide would then float away from the diffusion zone. No voids, no oxide, just pure metal contact would be the result.

The machineable ceramic piece that would sit on top of the iron holder was called "the floater".

73	8-Jun	Heat Fe/Zn at 725°C for 3h.	Floater worked, diffusion occurred.

The sample crucible had to be broken to remove Sample #73. A zinc casting was then created from the replacement sample crucible for iron holder production. A good impression was needed from the casting, in order to make a representative model. Therefore, scrap chunks of zinc were melted in one crucible, and then the liquid zinc was poured clean into the pre-heated sample crucible, for casting. This step removed the oxide that formed on the crucible wall when the zinc was melted down, therefore producing a better quality casting.

74	15-Jun	Melt down scrap Zn. Pour liquid Zn into sample crucible.	Casting successfully created.

Experiment #75 was the preliminary poured liquid zinc technique sample. This new procedure was a culmination of the previous three experiments.

75	16-Jun-04	Poured liquid Zn, heat at 725°C for 1h.	Diffusion occurred, no oxides found in the interphase.

The poured liquid metal experiments were performed in an open-top pot furnace. Using this method, the samples were quicker to do, less complicated to produce, and the results were better. As well, using a second furnace for the 96h anneal, samples could be produced concurrently. The vacuum chamber samples could only be produced one at a time.

The following were the first, full-run, poured liquid zinc samples. The crucible used for these experiments was CL30, as the last of the TW36 crucibles broke in Experiment #75. A new iron holder design was used for these experiments.

76	21-Jun	Poured liquid Zn, heat Fe/Zn at: 725°C for 1h, 400°C for 96h.	Ceramic holder floated, therefore incomplete/inconsistent diffusion.

A second CL30 crucible was utilized so that samples could be run concurrently. This would speed up the experimentation process.

77	22-Jun	Poured liquid Zn, heat Fe/Zn at: 725°C for 1h, 400°C for 96h.	Same results as previous experiment.

The holder floated at 725°C, due to the decreased viscosity of the liquid zinc (the zinc got under the holder). To make sure the holder didn't float, heated only to 525°C. As well, to reduce the liquid diffusion effects, held at 525°C for only a short time.

78	26-Jun	Poured liquid Zn, heat Fe/Zn at: 525°C for 0.25h, 400°C for 96h.	Analyzed polished sample on the SEM on July 6. The iron didn't recrystallize (columnar grains survived). Graphed the zinc concentration gradient, and calculated the diffusion coefficient. Image of sample used for Figure 4.16.

The iron microstructure was not consistent with prior samples, therefore the iron needed to be pre-heat treated before being used. The heat treatment used for the iron was 725°C for 1.5 hours, placed in an alumina holder, and wrapped in tool steel. The heat treated microstructure was checked and confirmed with previous samples. Experiment #79 was the first to use the pre-heat treated iron.

79	8-Jul-04	Poured liquid Zn, heat Fe/Zn at: 525°C for 0.25h, 400°C for 96h.	Analyzed polished sample on the SEM on July 13. Graphed the zinc concentration gradient, and calculated the diffusion coefficient.

Sample #79 was "the perfect sample". Took 26 months to achieve this feat.

The last experiments performed were definitive tests, duplicates, and checks on other phenomena.

80	9-Jul	Heat galvanized steel at 400°C for 96h.	Analyzed polished sample on the SEM on July 23. Images of sample used for Figure 4.33 and Figure 4.36.
81	15-Jul	Poured liquid Zn, heat Fe/Zn at: 525°C for 0.25h, 400°C for 96h.	Analyzed polished sample on the SEM on July 22. Graphed the zinc concentration gradient, and calculated the diffusion coefficient. Images of sample used for Figures 4.1, 4.2, 4.3, and 4.19.
82	15-Jul	Heat galvanized steel at 500°C for 96h.	Analyzed polished sample on the SEM on July 23. Images of sample used for Figure 4.35 and Figure 4.37.
83	16-Jul	Poured liquid Zn, heat Fe/Zn at 500°C for 96h.	Analyzed polished sample on the SEM on July 21. Graphed the zinc concentration gradient, and calculated the diffusion coefficient. Images of sample used for Figures 4.6 and 4.17.

84	22-Jul-04	Poured liquid Zn, heat Fe/Zn at 500°C for 96h.	Analyzed polished sample on the SEM on August 5. Graphed the zinc concentration gradient, and calculated the diffusion coefficient. Image of sample used for Figures 4.5, 4.7, and 4.8.

In Experiment #85, a machineable ceramic peg was used to pin down the iron holder. This peg was inserted into one of the pits in the iron holder. A counterweight was then set on top of the peg to hold everything down and in place.

85	26-Jul	Poured liquid Zn, heat Fe/Zn at 725°C for 96h.	Peg worked, ceramic holder didn't float. Analyzed polished sample on the SEM on August 6. Graphed the zinc concentration gradient, and calculated the diffusion coefficient. Images of sample used for Figures 4.9, 4.10, 4.11, 4.12, 4.13, and 4.18.

The first CL30 crucible broke while cooling Experiment #83, and the second CL30 crucible broke while cooling Experiment #85. While the crucibles perform perfectly for experiments at 400°C, experiments at 500°C and 725°C will cause the crucible to break. It is assumed that the crucible will fracture for any temperature above the melting point of zinc, for 96h diffusion experiments. The exact reason for this is uncertain, but it may have to do with the machineable ceramic iron holder design.

If these experiments were to be repeated, the poured liquid zinc method should be used, with the iron holder machined to fit the bottom of the crucible. A simpler tapered wall crucible would allow the iron holder to be easier fitted. A fitted iron holder may prevent the crucible from fracturing when cooling samples from 500°C or 725°C.